Effect of biomacromolecules on calcium carbonate formation and sand solidification induced by urease-based mineralization

A dissertation submitted in partial fulfillment of the requirements

for the degree of Doctorate of Engineering

By

THILOTHTHAMA HIRANYA KUMARI NAWARATHNA

Laboratory of Biotechnology for Resources Engineering,

Division of Sustainable Resources Engineering,

Graduate School of Engineering,

Hokkaido University, Japan

September 2019

Acknowledgement

First and foremost I would like to express my sincere and intense gratitude to my research supervisor **Associate Professor, Kazunori Nakashima**, laboratory of biotechnology for resources engineering, Division of sustainable Resources Engineering, Hokkaido University, for his continuous encourage, perfect guidance, friendly cooperation and patience throughout my research. I cannot imagine myself obtaining a PhD without his encouragement and obtaining a PhD would have been only a dream without his great support.

Besides my supervisor, I would like to convey my heartfelt gratitude towards **Professor, Satoru Kawasaki** for his valuable guidance, encouragement and support during these 3 years. Further, my thanks go to **Assistant Professor, Masaji Kato** for his friendly cooperation. I would like to express my gratitude towards **Mrs. Hitomi Tada** for her friendly cooperation and unlimited support throughout this time period. And my heartfelt gratitude towards the Japanese government for selecting me as MEXT scholar.

I like to thank my lab mates, Ms. Momoko Takatsu, Mr. Masahiro Fujita, Mr. Wilson Mwandira and all past and present lab mates for their invaluable support, guidance and stimulating discussions. Further, my thanks go to Ms. Nadeeka Dilrukshi, Mrs. Nirmali Amarakoon, Mr. Gowthaman Shivakumar and all of my Sri Lankan friends for their friendly support and staying with me during my hard times.

In addition, I would like to express my heartfelt gratitude to **Dr. L.I.N. De Silva**, Senior Lecturer, Department of Civil Engineering, University of Moratuwa, Sri Lanka, for encouraging me for pursuing PhD and showing me the correct path.

Last but not least, my thanks go to my dear mother, father and sister for their invaluable support throughout my life.

TABLE OF CONTENTS

LIST OF FIGURES vii

LIST OF TABLES ix

CHAPTER 1. INTRODUCTION 1

1.1. Back ground 1

1.2. Literature Review 3

1.2.1. Biomineralization 3

1.2.1.1. Formation of biominerals 3

1.2.1.2. Calcium carbonate biomineralization 4

1.2.2. Microbial Induced Carbonate Precipitation (MICP) 6

1.2.2.1. Engineering applications of MICP 8

1.2.2.2. Drawbacks of the MICP 9

1.2.2.3. Polymer modified MICP process 9

1.2.2.4. Polymer modified EICP process 11

1.3. Scope of the thesis 13

1.4. Originality and the usefulness of the study 14

References 15

CHAPTER 2. EFFECT OF THE SYNTHETIC POLY PEPTIDES ON THE $CaCO_3$ CRYSTALIZATION AND SAND DENSIFICATION USING MICP METHOD 23

2.1. Introduction 23

2.2. Objectives 25

2.3. Materials and methods 25

2.3.1. Preparation of bacterial cell culture 25

2.3.2. Precipitation of $CaCO_3$ by ureolytic bacteria 26

2.3.3. Precipitation of $CaCO_3$ by urease enzyme 26

2.3.4. Analysis of precipitate 27

2.3.5. Toxicity of the poly-L-lysine 27

2.3.6. Sand solidification in syringe....28
2.3.7. Determination of the amount of $CaCO_3$....31
2.4. Results and Discussion....32
2.4.1. Effect of the synthetic polypeptides on the $CaCO_3$ Crystallization....32
2.4.1.1. Effect of poly-L-lysine on the $CaCO_3$ Crystallization by using bacterial urease. 32
2.4.1.1.1. Effects of poly-L-lysine concentration on $CaCO_3$ crystallization 37
2.4.1.1.2. Time course of precipitation with and without poly-L-lysine 40
2.4.1.1.3. Cytotoxicity of poly-L-lysine on the *Pararhodobactor* sp. 42
2.4.1.1.4. Effect of poly-L-lysine on the $CaCO_3$ Crystallization by using urease enzyme 44
2.4.1.2. Effect of poly-glutamate on the $CaCO_3$ Crystallization by using bacterial urease 45
2.4.1.2.1. Effect of poly-glutamate on the $CaCO_3$ Crystallization by using urease enzyme 49
2.4.2. Effect of the synthetic polypeptides on the sand densification....49
2.4.2.1. Sand solidification for Mikawa sand....50
2.4.2.2. Sand solidification for Toyoura sand 57
2.4.2.3. Control experiments 59
2.4.2.4. Fixation of bacteria on the sand surface in the presence of poly-L-lysine....60
2.5. Conclusion....61
References....62
CHAPTER 3. EFFECT OF THE NATURAL BIOPOLYMER ON THE $CaCO_3$ CRYSTALLIZATION AND THE SAND SOLIDIFICATION BY USING MICP METHOD 66
3.1. Introduction 66
3.2. Objectives....68
3.3. Materials and methods 68

3.3.1. Preparation of bacterial cell culture 68
3.3.2. Preparation of chitosan solution 68
3.3.3. Precipitation of $CaCO_3$ 69
3.3.4. Precipitation of $CaCO_3$ by urease enzyme 69
3.3.5. X-ray diffraction and scanning electron microscopy analyses 69
3.3.6. Sand solidification in syringe 69
3.4. Results and Discussion 71
3.4.1. Effect of chitosan on the $CaCO_3$ Crystallization 71
3.4.1.1. Effect of chitosan on the $CaCO_3$ Crystallization by using bacterial urease 71
3.4.1.1.1. Rate of precipitation 75
3.4.1.1.2. Effect of the chitosan concentration 77
3.4.1.1.3. Control experiment without bacteria 79
3.4.1.2. Effect of chitosan on the $CaCO_3$ Crystallization by using extracted urease enzyme 80
3.4.2. Effect of chitosan on sand solidification 81
3.5. Conclusion 85
References 87
CHAPTER 4. DEVELOP A NOVEL FUSION PROTEIN TO FACILITATE ORGANIC-INORGANIC HYBRID MATERIAL FORMATION 91
4.1. Introduction 91
4.1.1. Chitin binding domain 93
4.1.2. Calcium binding peptides 94
4.2. Objectives 95
4.3. Materials and methods 96
4.3.1. Investigate the performance of Fusion protein 96
4.3.1.1. Construction of the target gene 96
4.3.1.2. Transformation of the target gene into E.coli 97
4.3.1.3. Expression of the target protein 98

4.3.1.4. Purification and dialysis of the protein 98
4.3.1.5. Chitin binding assay 99
4.3.1.6. Calcium binding assay 99
4.3.2. Investigate the performance of chitin binding domain (ChBD) 100
4.3.2.1. Construction of the target gene 100
4.3.2.2. Chitin binding assay 100
4.3.3. Investigate the performance of Calcium Binding Peptide (CaBP) 101
4.3.3.1. Preparation of the stock solution of ChBD 101
4.3.4. $CaCO_3$ precipitation experiment 101
4.4. Results and discussion 103
4.4.1. Construction of the CaBP-ChBD 103
4.4.1.1. Expression of the CaBP-ChBD 104
4.4.1.2. Chitin binding assay 105
4.4.1.3. Calcium binding assay 106
4.4.2. Construction of the ChBD 107
4.4.2.1. Expression of the ChBD 108
4.4.2.2. Chitin binding assay 109
4.4.3. $CaCO_3$ precipitation experiment 110
4.5. Conclusion 119
References 121
CHAPTER 5. CONCLUSIONS AND FUTURE PROSPECTS 127
Appendix A 131
Appendix B 135
Appendix C 138

LIST OF FIGURES

Fig. 3-4 Variation of the pH of the reaction mixture with time in the presence and absence of the chitosan 72
Fig. 3-5 SEM images of $CaCO_3$ precipitates at various bacterial concentrations with chitosan (0.03 %) (a) OD_{600} = 0.01, (b) OD_{600} = 0.05, (c-1) OD_{600} = 0.1 and (c-2) spherical vaterite crystals 73
Fig. 3-6 XRD pattern of $CaCO_3$ precipitates with chitosan 75
Fig. 3-7 Rate of precipitation with and without chitosan 76
Fig. 3-8 SEM images of the precipitate with chitosan at different time intervals (a) 0 h (b) 2 h (c) 4 h (d) 6 h (e)8 h (f) 10 h 76
Fig. 3-9 Variation of the amount of precipitate with the chitosan concentration 77
Fig. 3-10 SEM images of precipitated by bacteria (OD_{600} = 0.1) at different chitosan concentrations: (a) 0.003%, (b) 0.03% and (c) 0.15%. 78
Fig. 3-11 Variation of the amount of precipitate with the chitosan concentration without bacteria 79
Fig. 3-12 SEM images of the precipitate with chitosan without bacteria 80
Fig. 3-13 Variation of the pH in the reaction mixture with and without chitosan under extracted urease enzyme 81
Fig. 3-14 Estimated UCS values of solidified sand specimens with and without chitosan. 82
Fig. 3-15 Amount of precipitated $CaCO_3$ with the UCS value along the length of the sample (a) S2 (b) S5 (c) S3 (d) S6 (e) Comparison between all the samples 84
Fig. 3-16 SEM images of the cemented sand specimens: (a) without chitosan (b) with chitosan (0.3%). 85
Fig. 4-1 Internal structure of the exoskeleton of the cray fish 93
Fig. 4-2 Schematic ribbon drawing of the chitin binding domain of chitinase A1 94
Fig. 4-3 Schematic of precipitation of $CaCO_3$ directed by CaBP-ChBD on the surface of chitin. 95
Fig. 4-4 Schematic design of the target gene 97
Fig. 4-5 Amplified Fragment for CaBP-ChBD 103
Fig. 4-6 Transformation of pET 22b(+) with target gene into E.Coli DH5α (a-1,2) Colonies of E.Coli DH5α containing target gene (b) Confirmation of E.Coli DH5α with pET 22b(+)-CaBP-ChBD 103

Fig. 4-7 Transformation of plasmid into E.Coli BL21(DE3) (a) Colonies of E.Coli BL21(DE3) with pET 22b(+)-CaBP-ChBD (b) Confirmation of E.Coli BL21(DE3) with pET 22b(+)-CaBP-ChBD.....104
Fig. 4-8 SDS-page analysis to confirm the expression of CaBP-ChBD (a) Expression of the CaBP-ChBD with in 24 h (b) Protein purification and dialysis; M – Protein marker, 1-Sample after 24 h, 2- Wash 1, 3-Wash 2, 4- Elution, 5- Flow through, 6- After dialysis. 105
Fig. 4-9 Chitin binding assay (a) Time courses of binding of CaBP-ChBD into insoluble chitin (b) Variation of the protein concentration in the reaction mixture with time.....106
Fig. 4-10 Variation of the concentration of CaBP-ChBD with time after react with the $CaCO_3$ 107
Fig. 4-11 Amplified fragment of ChBD 107
Fig. 4-12 Transformation of pET 22b(+) with target gene into E.Coli DH5α (a) Colonies of E.Coli DH5α containing target gene (b) Confirmation of E.Coli DH5α with pET 22b(+)-ChBD. 108
Fig. 4-13 Transformation of plasmid into E.Coli BL21(DE3) (a) Colonies of E.Coli BL21(DE3) with pET 22b(+)-ChBD (b) Confirmation of E.Coli BL21(DE3) with pET 22b(+)-ChBD. 108
Fig. 4-14 SDS-page analysis to confirm the expression of ChBD (a) Expression of the ChBD within 24 h (b) Protein purification and dialysis; M – Protein marker, 1- Sample after 24 h, 2- Flow through , 3-Wash 1, 4- Wash 2, 5- Elution, 6- After dialysis. 109
Fig. 4-15 Chitin binding assay (a) Time courses of binding of ChBD into insoluble chitin (b) Variation of the protein concentration in the reaction mixture with time. 110
Fig. 4-16 Amount of precipitate obtained for different test cases with and without chitin ...111
Fig. 4-17 Graphical illustration of the samples.....111
Fig. 4-18 $CaCO_3$ precipitate (1) S1 (2) S2 (3) S4 112
Fig. 4-19 $CaCO_3$ formation efficiency.....112
Fig. 4-20 SEM images of the $CaCO_3$ precipitate (a) S1 (b) S2 (c) S3 (d-1,2) S4 115
Fig. 4-21 SEM images of the $CaCO_3$ precipitate with ChBD (a) S5 (b) S6.....116
Fig. 4-22 SEM images of the $CaCO_3$ precipitate with CaBP (a) S5 (b) S6.....116
Fig. 4-23 SEM images of the $CaCO_3$ precipitate with CaBP & ChBD (a) S9 (b) S10.....118
Fig. 4-24 Amount of precipitate obtained for different test cases with and without chitin or BSA.....119
Fig. 4-25 SEM images of the $CaCO_3$ precipitate with BSA (a) S11 (b) S12 119

LIST OF TABLES

Table 2-1 Physical properties of the Mikawa and Toyoura sands 28
Table 2-2 Experimental conditions for sand solidification with and without poly-L-lysine ... 29
Table 2-3 Experimental conditions for sand solidification without bacteria 30
Table 3-1 Experimental conditions for the sand solidification test with and without chitosan 70
Table 4-1 Amino acid sequence of the ChBD and CaBP 96
Table 4-2 DNA sequence of the forward and reverse primers 96
Table 4-3 Primer design for construction of ChBD 100
Table 4-4 Experimental conditions for $CaCO_3$ precipitation 102
Table 4-5 Experimental conditions for $CaCO_3$ precipitation with and without BSA 102

CHAPTER 1. INTRODUCTION

1.1. Back ground

Today due to the rapid growth of population and the urbanization, suitable lands available for the constructions are getting decreased day by day. Hence, people are moved to use problematic weak grounds for the constructions. Problematic grounds mainly consist with soft organic soil or loose granular soil. It is an engineering challenge to use these problematic grounds for the constructions due to associated excessive settlement and low bearing capacity (Roy, Surendra, 2017). Hence, proper ground improvement is necessary before the constructions to ensure a safe and economical design.

Compare with the organic soft soil, sandy soils poses a larger and rapid settlement due to its naturally shifting characteristics and free draining nature. Another challenge associated with the saturated sandy soil is liquefaction under the seismic activities. Due to the seismic activities, shear strength of the soil tends to decrease as a result of the buildup of pore water pressure. Then this excess pore water pressure is released to the ground surface as sand boiling which causes the settlement of the ground surface (Kenji Ishihara, 1992; Mesri et al., 2018; Yasuyuki Koga, 1990) and damages the buildings by differential settlement, tilting and lateral sliding (Andrus and Chung, 1995; Karimi et al., 2017). In history, Japan has undergone number of liquefaction related disasters which were associated mainly with the well-known massive earthquakes. Kobe earthquake in 1995, is a recent example which damaged the water and gas supply system and transportation system due to liquefaction (Andrus and Chung, 1995). Hence, it is very important to perform suitable and effective ground improvement to prevent this kind of worst disasters and make sure a safe life for the residencies.

Sand densification or solidification is the most efficient way to prevent the liquefaction. Most commonly using techniques for sand densification are vibro compaction, dynamic compaction and sand files. However, compaction methods are associated with the undesirable vibration which can cause some other problems in future (Sarker and Abedin, 2015). Another option is the use of grouting methods, which are widely used to densify the loose sand in order to prevent liquefaction. Among the available grouting techniques cement grouting and chemical grouting are the most common. Compaction methods are mostly effective only for shallow depths (<10 m) and chemical grouts can be injected to deep layers in the soil bed

(Ivanov and Chu, 2008) that is the main advantage of the chemical grout over the compaction methods. Cement, lime, bentonite, sodium silicates, acrylates, acrylamides are the most common types of chemicals which are used for the chemical grouting (Karol, 2010).

Cement is a one of a best engineering material due to its higher strength, durability and workability which makes it more suitable for various applications in ground improvement (Chang et al., 2016). But large amount of CO_2 is released to the environment during the cement production, which is more harmful to the environment. Each one ton of cement emits 0.95 tons of CO_2 during the cement manufacturing and CO_2 emission due to the geotechnical applications is 2% from the total CO_2 from cement (Chang et al., 2016). This makes the use of cement as grouting material is not efficient. On the other hand, most of the chemicals use for the chemical grouting are environmental unfriendly. Specially, the grouts contain acrylamides and polyurethane are toxic and damage to the environment. Use of acrylamide grout has banned in japan after report of several water poisoning cases due to the acrylamide grouts (DeJong et al., 2010; Ivanov and Chu, 2008).

Due to the above-mentioned problems, recent engineers are seeking for a new biological approach which can produce ecofriendly material as an alternative for the cement and chemical grouting. Generally, biological approach involves the network of chemical reactions which are acting within the soil mass through biological activities (Fujita et al., 2008). These bio-geo chemical processes are mainly consisted with the inorganic precipitation, organic precipitation and biogas generations (DeJong et al., 2010). Among them, bio-grout formation is mainly associated with the inorganic precipitation of carbonate minerals, mainly calcium carbonate. Deposition of $CaCO_3$ within the pore spaces between sand particles reduce the permeability and improve the strength and stiffness of the soil. This biogenic $CaCO_3$ act as a more eco-friendly cementing material than the existing cementing materials.

Among the bio-mediated soil improvement methods, Microbial Induced Carbonate Precipitation (MICP) method can be classified as the most efficient and ecofriendly ground improvement technique. In MICP process, biogenic $CaCO_3$ is formed due to the hydrolysis of urea by urease, which is produced by urea-hydrolyzing (ureolytic) bacteria. Number of laboratory (Amarakoon and Kawasaki, 2017; B. M. Montoya, 2015; Chou et al., 2011; Danjo and Kawasaki, 2016a; DeJong et al., 2006; Whiffin et al., 2007) and field (Dejong et al., 2014; Gomez et al., 2014; Martines, 2008; Paassen et al., 2009) studies have been proved that MICP has capability to improve the strength and stiffness of soil effectively.

Now time has arrived to think about the ways to improve the efficiency of the MICP process effectively and sustainably in order to minimize the cost associate with the MICP

process and minimize the formation of hazardous byproducts such as ammonia. In this thesis, attempt has taken to introduce the concept of organic matrix mediated biomineralization into MICP process in order to improve the efficiency of $CaCO_3$ formation and enhance its applicability to soil improvement.

1.2. Literature Review

1.2.1. Biomineralization

Biomineralization, is a process of formation and growth of minerals in biological systems. It is a combined approach of study of the biologically-formed materials and processes that lead to the construction of hierarchically structured composite materials (Estroff et al., 2008; Masica et al., 2010). In detail, it includes uptake of certain ions from the environment and arrange them in to highly ordered structures under the control of biological actions (Stephen Mann, 2001). Generally, formation of biominerals are mainly associated with organic macromolecules like polysaccharides, phospholipids and certain proteins (Kato et al., 2002; L.Addadi, 1985). These organic materials control the nucleation and the growth of the crystals. In addition, polymorphism, morphology of the crystals are also greatly influenced by the organic materials. Organic macromolecules play a significant role to keep distinctive mechanical properties of mature mineralized tissues (Hansma et al., 2005; Stephen Mann, 2001; Stephen and Lia, 1997). These organic-inorganic composite materials are fundamental component of living organisms which provide a protection, structural support, and mechanical strength for the organisms. Hydroxy apatite in bones and teeth of mammals, calcium carbonate in molluscan shells, amorphous silica in marine sponges are some examples available in nature for the bio-mineral formation (Jimenez-Lopez, 2008).

1.2.1.1. Formation of biominerals

Biominerals are formed under ambient temperature and pressure, mainly due to two mechanisms as follows (Beniash, 2012; He et al., 2003; Stephen and Lia, 1997).

- Forming of the biominerals upon the template of organic matrix
- Formation of the mineral phase due to the co-operative interaction between the organic macromolecules

Biominerals are discovered among all kingdoms of life and more than 50 mineral phases that are accompanied with them have been identified. Among them 50 % of minerals are calcium bearing minerals such as calcium containing phosphates, carbonates, oxalate and so on. Also, 25 % of biominerals are amorphous. Amorphous silica and amorphous hydrous iron phosphate are the most abundant amorphous minerals (Weiner and Dove, 2003). Among all of them, calcium carbonate ($CaCO_3$) is the most abundant biomineral available in nature. $CaCO_3$ presence in nature in five different polymorphism and one amorphous phase. Calcite, aragonite and vaterite are the most stable form of polymorphisms and $CaCO_3$ monohydrate, $CaCO_3$ hexahydrates and amorphous $CaCO_3$ are extremely unstable and very rare in non-biological environments (Stephen and Lia, 1997). Evian egg shells mainly consist with calcite crystals and main component of the nacre of the mollusk is aragonite $CaCO_3$ (Jimenez-Lopez, 2008). Vaterite crystals can be found in some ascidian spicules and in variety of gravity receptors (Stephen and Lia, 1997).

1.2.1.2. Calcium carbonate biomineralization

One of the best examples available in nature for $CaCO_3$ biomineralization is a nacre of the mollusk shell. Nacre mainly consists with aragonite form of $CaCO_3$ and certain types of proteins and polysaccharides (Menig et al., 2000). Generally, toughness of the nacre is 3000 times higher than that of pure aragonite. This toughness is mainly due to the layered structure of the nacre (Jackson et al., 1990). Nacre has a brick and motor structure where aragonite crystals are formed with in soft organic materials (Lopez et al., 2010). Organic materials in nacre mainly consist with chitin fibers. Smith et al.(1999) explained that high fracture toughness of the nacre is due to the high energy dissipation and organic materials in nacre contribute significantly for this energy dissipation. Xu and Li (2011) found that biopolymer in the nacre have ability to strength itself during the deformation.

Exoskeleton of the crustacean is another example for the organic inorganic hybrid material formation. As shown in the Fig.1-1, at the molecular level antiparallel arrangement of chitin leads to the formation of chitin crystals. Then chitin nano fibrils are formed due to the wrapping of the long crystalline chitin chains by proteins. Bunching of these chitin fibrils tend to form long chitin protein fibers. This chitin protein fibers form planar and periodically branched network and space between this chitin protein fibers are filled up with crystalline $CaCO_3$. This inorganic-organic composite material give extremely higher strength to the cuticle (Nikolov et al., 2010; Raabe et al., 2005; Vincent, 2002; Vincent and Wegst, 2004).

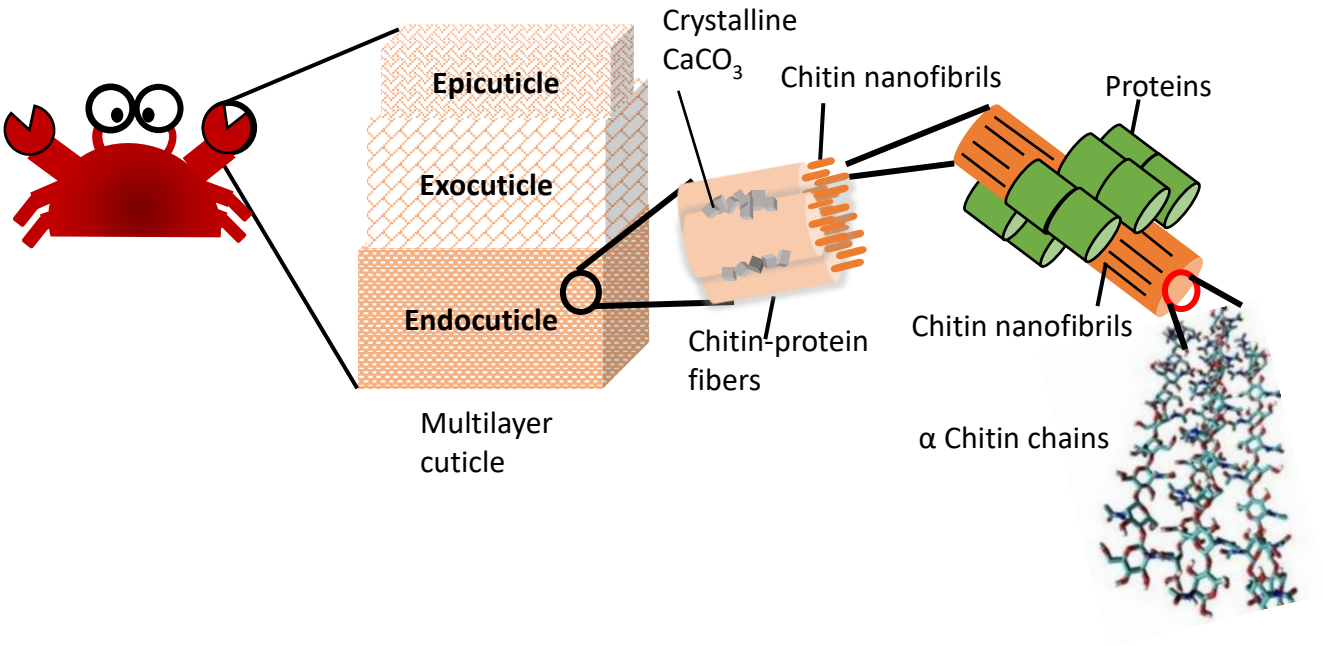

Fig. 1-1 Main structural levels and microstructural elements of the exoskeleton of the crustacean (Regenerated from the original image created by Rabee et al., 2005)

These examples are revealed that organic materials play a significant role in the nucleation and growth of the minerals as well as their mechanical and optical properties. Extreme stiffness, toughness and strength of these organic-inorganic composite materials gained much attention by engineers, researches and scientists. Hence, today researches are trying to mimic this concept of organic-inorganic composite material to produce synthetic organic-inorganic hybrid materials which can be used for number of industrial applications. However, this concept is still new to the civil engineering field and the applications related to the organic-inorganic composite materials are still in the initial stage. Therefore, we tried to fill this space by introducing this amazing concept of organic matrix mediated biomineralization

into the civil engineering applications. We took an attempt to spread this concept throughout this thesis step by step by incorporating with the concept of microbial introduced carbonate precipitation (MICP) which is a novel bio mediated $CaCO_3$ precipitation method.

1.2.2. Microbial Induced Carbonate Precipitation (MICP)

Microbial induced carbonate precipitation is a bio-geochemical process, which is catalyzed by the enzyme urease. Urease is a nickel containing multi subunit enzyme which is belong to the family of amidohydrolases and phosphotriestreases. Existing of the Nickel (Ni (II)) ions in the active site is a unique feature of urease compare with the other enzymes (Holm and Sander, 1997). Urease mainly existing in some kind of bacteria, plants, algae and invertebrates. According to the amino acid sequence and the reaction kinetics, all of these sources form one enzyme with same structure and catalytical mechanism (Krajewska et al., 2003). Urease from the jack bean (*Canavalia ensiformis*) is the very first enzyme identified in crystal form and the same time it is the first nickel containing enzyme (Dixon et al., 1975). Other than that soybean leaf and seeds, pig weeds and mulberry leaf also have been identified as sources of urease enzyme (Sirko and Brodzik, 2000).

Compared with the plant urease, bacterial urease is more convenient for the insitu applications since it can be used as a whole cell without extraction of the enzyme. Number of urease producing bacteria have been identified up-to today. *Sporosarcina pasteurii* (*Basillus pasteurii*) (Bang et al., 2001; Wei et al., 2015), *Bacillus subtilis* (Barabesi et al., 2006), *psychrobacillus* (Gowthaman et al., 2019), B. *megateriumSS3* and *B. thuringiensis* (Kaur et al., 2013) are the extensively examined ureolytic bacteria due to their higher urease activity. Urease enzyme has a capability to hydrolysis urea and produce ammonium and carbarmate ions. Carbarmate ions spontaneously transferred into ammonia and carbonic acid as given in the equation (1-2). Then in the presence of calcium ions (Ca^{2+}), $CaCO_3$ is formed (Amarakoon and Kawasaki, 2017; Danjo and Kawasaki, 2016a; Fujita et al., 2017; Mortensen et al., 2011) as given in the equation (3).

$$CO(NH_2)_2 + H_2O \xrightarrow{\text{Urease}} H_2NCOO^- + NH_4^+ \quad (1)$$

$$H_2NCOO^- + H_2O \rightarrow HCO_3^- + NH_3 \quad (2)$$

$$Ca^{2+} + HCO_3^- + NH_3 \rightarrow CaCO_3 + NH_4^+ \quad (3)$$

In microbially induced carbonate precipitation method, $CaCO_3$ crystals are formed in 3 stages. During the first stage, supersaturation is developed which is favorable for the $CaCO_3$

crystals to nucleate. In the second stage, nucleation is initiated at the critical supersaturation and finally spontaneous crystal growth on the stable nuclei is started (Ferris et al., 2004) . In MICP process, negatively charged bacteria cells, attract in to the calcium ions and act as nucleation sites for $CaCO_3$ crystals to nucleate and growth as shown in the Fig.1-2(a). This amazing technique has been applied successfully in number of applications mainly in geotechnical and geo-environmental engineering for the purpose of producing ecofriendly and sustainable cementing material. The $CaCO_3$ produced by the MICP process act as a cementing material to densify the loose sand by efficient filling of the pore spaces between the soil particles as illustrated in the Fig.1-2(b)

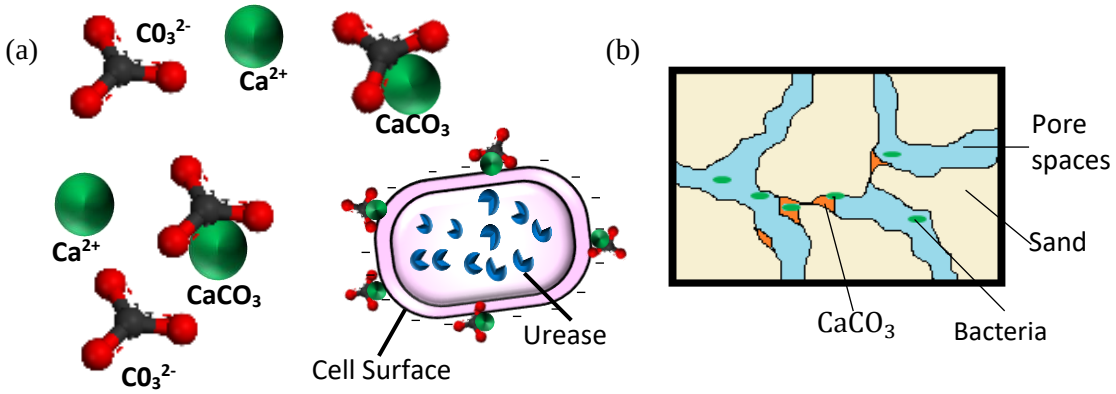

Fig. 1-2 Schematic diagram of MICP (a) Formation of $CaCO_3$ (b) Efficient pore filling by MICP

It has been proven that MICP method has capability to improve the soil properties very effectively and efficiently. Remarkable strength increments have been reported for the bio cemented sand compare with the other geo-materials. Larger increment of the soil friction angle and higher peak shear strength value have been achieved by MICP treated soil than the untreated soils (Chou et al., 2011; Montoya and DeJong, 2015). Increment of shear strength and stiffness has a direct correlation with the amount of the precipitated $CaCO_3$ and significant increment of the cohesion, friction angle and elastic modulus have been reported for the higher $CaCO_3$ content due to the efficient filling of the pore space (Cheng et al., 2013; Montoya and DeJong, 2015). Interestingly, MICP has capability to increase the soil strength while maintaining the sufficient permeability which is required during the bio cementation process. This permeability retention in bio cemented soil samples is higher than the other cementing materials such as cement. Van Paassen (2009) Have obtained 60 % reduction of the

permeability of bio treated soils and 50-99 % permeability reduction have been obtained by Ivanov et al. (2010). In addition, increment of the unconfined compressive strength (UCS) of the MICP treated soil have been reported by the number of researches (Amarakoon and Kawasaki, 2017; Danjo and Kawasaki, 2016a; Whiffin, 2004; Whiffin et al., 2007).

1.2.2.1. Engineering applications of MICP

MICP has gained much attention in number of field as an ecofriendly approach than the available methods. As mentioned earlier, it is widely used as a soil stabilizer as well as produce cementing material to improve the properties of the weak soils. Van Paassen (2009) have successfully implemented microbial grouting technique in large scale (100 m^3) and could be obtained successfully bonded sand body. Gomez et al., (2014) have been conducted a field scale experiments to check the applicability of MICP as a surface stabilizer for prevention of erosion in loose sand. They have reported that they could be achieved improvement to a depth of approximately 28 cm which is near to the target depth of 30 cm. MICP technique has been applied successfully to reduce the permeability of the sandy soil in Rotterdam port area, Holland. Also in 2005, seepage damage happened on the railway subgrade in Amesterdam was successfully controlled by using MICP method (Wang et al., 2017a). In addition, MICP method has been used in oil exploration to reduce the permeability of the sand layer which help to increase the efficiency of the oil recovery (Ferris et al., 1996). Similarly MICP has been successfully applied to repair the surface cracks in the cement-based coatings. Water absorption rate of the cement mortar can be reduced by 10 % using MICP due to the cover of the surface of the cement mortar by micro-organisms (Bachmeier et al., 2002; Wang et al., 2017b).

In addition, MICP has been used to removal of heavy metals and radionuclides. Selection of heavy metal tolerant bacteria with ureolytic capability is very important for this purpose, because heavy metals can be toxic for some bacteria and it can reduce the bacterial and urease activity. Previous researches have been found some heavy metal tolerable ureolytic bacteria and immobilization of the heavy metal mainly lead and cadmium was successfully achieved by using MICP (Kang et al., 2014; Mor et al., 2006). Similarly, MICP can be used to immobilize radionuclides by co-precipitation of the radionuclides as radionuclide carbonate minerals with the $CaCO_3$ (Fujita et al., 2008; Mitchell and Ferris, 2005).

1.2.2.2. Drawbacks of the MICP

Though MICP has recognized as an ecofriendly and sustainable ground improvement technique, some limitations are associated with the MICP process. In the large scale applications, main problem associated with the bio cementation is its homogeneity and durability and at this moment research works related to the detail investigation of the durability of the MICP treated soil couldn't be found. Another negative point is the production of large amount of the ammonia as a byproduct of the MICP process which can be polluted the environment as well as underground water. Removing these kind of toxic byproducts will make the bio-grouting process more complex and reduce the efficiency of the grouting reinforcement (Wang et al., 2017b). Back feeding of the ammonia into the environment as a fertilizer for the plant is also one alternative (Mujah et al., 2017). Use of denitrifying bacteria to produce $CaCO_3$ may be a best alternative and more environmentally friendly method since final product is only nitrogen. However, low activity and the slower growth rate of the denitrifying bacteria make it low efficient for the field applications (Van Paassen et al., 2010).

Also, it is a challenge to use the existing MICP method to improve the soil at target location than the widespread treatment. Specific equipment and long treatment period are required to control the release of water-based cementation solution to obtain the localized treatment. Therefore, it is essential to modify the existing MICP method which can control the transport of cementation solution in highly permeable soil to achieve efficient treatment (Wang and Tao, 2018a).

According to the literature data, MICP has studied so deeply and has been proven as a best alternative for the commonly available environmental unfriendly methods. Hence, now researches are moving to finding out the ways to improve the efficiency of the MICP process to make it more ecofriendly and sustainable. Introduction of the organic materials into the MICP process would be more interesting and it is closely related to the nature. Our study also based on this concept and we took an attempt to modify the MICP process by using organic materials to increase the efficiency of the MICP process through efficient $CaCO_3$ formation.

1.2.2.3. Polymer modified MICP process

Introduction of the organic materials in to the MICP process is closely related to the concept of organic matrix mediated biomineralization. Since the concept is inspired from

nature, it would be an attractive approach to upgrade the efficiency of the MICP process more sustainably and produce more ecofriendly green material. However, several factors must be considered before introducing the organic macromolecules in to the MICP process. Mainly, efficiency of the MICP process depend upon the activity of the urease enzyme. Therefore, organic materials should not interfere with the enzyme activity as well as it should not inhibit the bacterial growth. Also, to success the MICP process it should have capability to produce sufficient amount of $CaCO_3$ with sufficient rate. Hence, introduction of the organic materials should not disturb to the nucleation and growth of the $CaCO_3$.

It is a well-known fact that some organic materials inhibit $CaCO_3$ crystallization and also affect the morphology and polymorphism of the $CaCO_3$ crystals significantly. Therefore, the selection of suitable organic material is highly important. Due to these difficulties, very little number of research works have been carried out earlier to investigate the effect of organic materials, mainly biopolymer on the efficiency of the MICP process.

Previously, Wu and Zeng (2017) have been introduced sodium alginate in to the MICP process for the purpose of immobilization of the bacteria. Sodium alginate is a natural polysaccharide, which has number of industrial applications due to its gelling property and commonly use as an immobilization material (Butler et al., 2006). Wu and his research group could be immobilized the bacteria very successfully on the calcium alginate gel and porosity of the calcium alginate gel has been provided an extra support for the bacteria immobilization. The addition of the sodium alginate has modified the polymorphism and morphology of the $CaCO_3$ crystals significantly with time.

Vaterite crystals with rough surface has been formed after 6 h of reaction and it is converted completely into the dump bell-shaped calcite crystals within 24 h reaction. In addition, sodium alginate concentration affects significantly on the morphology of the crystals and hexagonal, spherical and capsule shaped crystals have been obtained as shown in the Fig.1-3. Formation of the hexagonal crystals was due to the interaction of the ammonium ions with the carbonate ions in the unfavorable (001) plane of vaterite. In contrast, at higher alginate concentrations effect of the ammonium ions can be neglected, due to the more negative charge of the sodium alginate resulting the formation of capsule-shaped crystals.

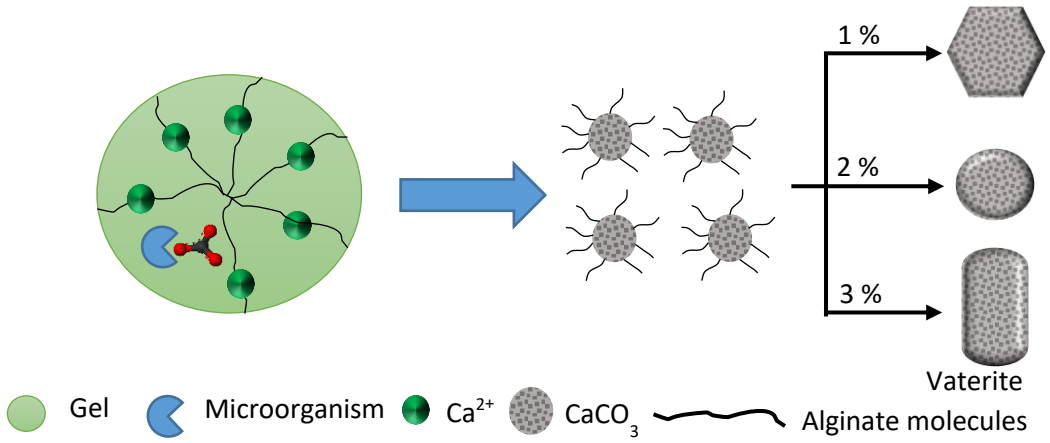

Fig. 1-3 $CaCO_3$ formation in the presence of sodium alginate by using MICP (Modified from the original image generated by Wu and Zeng, 2017)

Wang and Tao (2018b) have been examined the effect of the polyvinyl alcohol (PVA) on the MICP process which is a synthetic polymer with a superb adhesive and emulsifying properties (Alihemati et al., 2017). Higher amount of $CaCO_3$ precipitate was obtained in the case with PVA than the case without adding PVA. PVA modified MICP process formed framboidal shaped vetarite crystals while rhombohedral calcite crystals were dominant in the case of water based MICP approach. Higher unconfined compressive strength has been obtained for the cemented sand samples by using polymer modified cementation solution than the case with water-based cementation solution. Relatively a denser and uniform distribution of vaterite crystals between the sand particles were also reported. The reason behind the formation and stabilization of the vaterite crystal is higher absorption capacity of the PVA (Kim et al., 2005).

1.2.2.4. Polymer modified EICP process

Use of the extracted urease enzyme instead of the whole cell urease for the experimental purposes has become popular recently due to the associated difficulties of using whole cell urease. Urease enzyme extracted from the plant species (Jack bean and soya bean) have been used widely for the research purposes. Several studies can be found in literature regarding the polymer modified EICP.

Hamdan et al. (2016) have been investigated the effect of the xanthan gum on the $CaCO_3$ crystallization and soil stabilization using jack bean urease and found that xanthan gum hydrogel didn't adhere with the enzyme activities and $CaCO_3$ precipitate. Further, xanthan gum modified EICP extended the reaction time and increased the precipitation efficiency. Also, xanthan gum hydrogel has capability to create strong interaction with the water molecules and it hold water molecules tightly and preventing the significant evaporation. Further, Pasillas and research group have been studied the performance of the viscosity enhanced EICP solution for high permeable (Ottawa 20/30) and low permeable (F-85 sand) sand using xanthan gum (Pasillas et al., 2018). Xanthan gum enhanced sand column shows the highest water retaining ability. However, relationship couldn't be found between the level of water retention and the uniformity of the cementation and the unconfined compressive strength.

Zhao et al. (2016) have been synthesized a hyper-branched biomimetic hydrogel network across a soil matrix by using Poly (acrylic) acid to improve the mechanical strength of the loose soil and simultaneously lessen potential contamination due to excessive ammonium. By adding Poly (acrylic) acid Strongly cemented sand specimen have been obtained and it could be sustained even under the pressure high as 4.8 MPa while it is for sand treated by using only EICP was 64 KPa. Porous hydrogel network created by poly (acrylic) acid act as a binder to bind soil grains effectively by forming polymer calcite composite. Also, excellent water retaining capacity of poly (acrylic) acid make it more efficient for $CaCO_3$ precipitation. Most interesting behavior of poly (acrylic) acid is its ability to absorb NH_4^+ ions. It can remove NH_4^+ ions from the reaction system very effectively.

However, in literature it is difficult to a find complete investigation of the effect biomacromolecules on the MICP. Therefore, this research work addresses this issue and detail investigation of the synthetic and natural biomacromolecules on the $CaCO_3$ crystallization and sand solidification was carried out by using the MICP and EICP process.

1.3. Scope of the thesis

Scope of this thesis is investigation of the effect of biomacromolecules on the $CaCO_3$ crystallization and the sand solidification by using the urease based mineralization. Thesis consists with five sections as illustrated in the Fig.1-4.

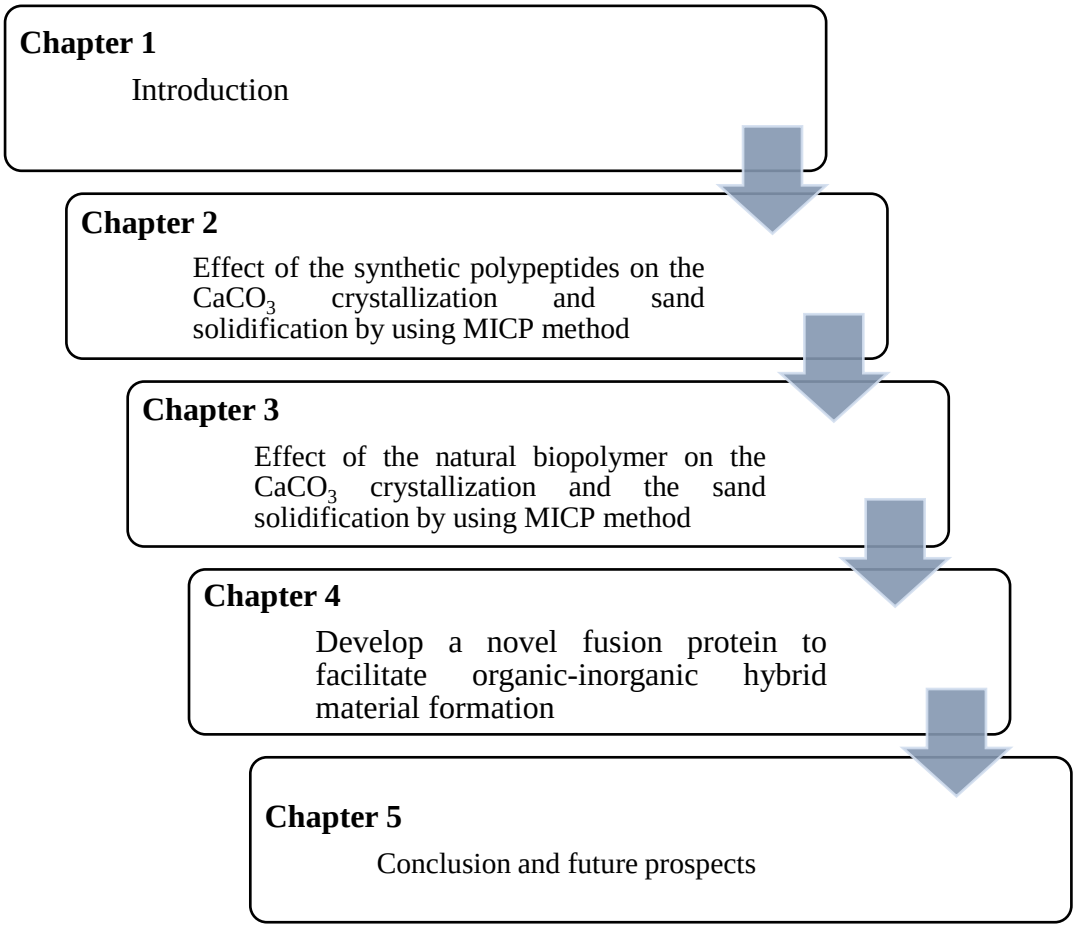

Fig. 1-4 Scope of the Thesis

1.4. Originality and the usefulness of the study

MICP has been recognized as a more ecofriendly ground improvement technique and its capability to stabilize and densify weak soil has been well studied. Hence, researches are moving to finding out novel approaches to enhance the performance of MICP. According to the literature, several attempts have been taken by using additives such as fly ash, fibers and by introducing magnesium.

Introduction of organic biopolymer in to the MICP process is a more interesting approach and we have taken an attempt to initialize this concept. Only few research works have been carried out by addressing the incorporation of organic additives into the MICP process. In this thesis, detail investigation about the incorporation of the biomacromolecules into the MICP process was carried out. As mentioned in the Chapter 2, complete investigation about the effect of cationic as well as anionic synthetic poly peptides on the $CaCO_3$ crystallization and the sand solidification was examined by using MICP method. Effect of these synthetic poly peptides on the crystal morphology and the polymorphism also investigated deeply. Though cationic synthetic poly peptide has positive effect on sand densification and $CaCO_3$ crystallization, associated higher cost make it little inefficient. Therefore, we moved into finding some natural biopolymer which has capability to improve the efficiency of the MICP process by efficient formation of $CaCO_3$. Throughout the Chapter 3, effect of natural polysaccharide, chitosan on the $CaCO_3$ crystallization and the sand solidification have been examined. We found that chitosan has capacity to upgrade MICP process very effectively and sustainably.

Results of the Chapter 2 and Chapter 3 reflect the positive effects of the organic materials on the $CaCO_3$ formation. Therefore, introduction of intermediate protein would be assisted to efficient precipitation of $CaCO_3$ on the organic matrix. To satisfy this purpose novel fusion protein was introduced to effective precipitation of $CaCO_3$ on the chitin matrix. In addition, effect of the fusion protein on the enzyme induced carbonate precipitation (EICP) was studied. We found that, fusion protein has better ability to adsorb into the chitin and it exhibited superior performance in $CaCO_3$ formation. Hence, this novel protein could be used to produce organic-inorganic composite green materials.

References

Alihemati, Z., Navarchian, A.H., 2017. Response Surface Methodology for Investigating the Effects of Hydrolysis Reaction Parameters on Molecular Structure and Performance of Polyvinyl Alcohol as Primary Suspending Agent.Iranian Journal of Chemical Engineering. 14, 52-66.

Amarakoon, G.G.N.N., Kawasaki, S., 2017. Factors Affecting Sand Solidification Using MICP with *Pararhodobacter* sp. Mater. Trans. 59, 72–81. https://doi.org/10.2320/matertrans.m-m2017849

Andrus, R.D., Chung, R.M., 1995. Ground Improvement Techniques for Liquefaction Remediation Near Existing Lifelines. Proc Jt. Meet. Us 1–82.

B. M. Montoya, J.T.D., 2015. Stress-Strain Behavior of Sands Cemented by Microbially Induced Calcite Precipitation. J. Geotech. Geoenvironmental Eng. 141, 04015019–04015029. https://doi.org/10.1061/(ASCE)GT.1943-5606

Bachmeier, K.L., Williams, A.E., Warmington, J.R., Bang, S.S., 2002. Urease activity in microbiologically-induced calcite precipitation. J. Biotechnol. 93, 171–181. https://doi.org/10.1016/S0168-1656(01)00393-5

Bang, S.S., Galinat, J.K., Ramakrishnan, V., 2001. Calcite precipitation induced by polyurethane-immobilized Bacillus pasteurii. Enzyme Microb. Technol. 28, 404–409. https://doi.org/10.1016/S0141-0229(00)00348-3

Barabesi, C., Rossi, M., Galizzi, A., Tamburini, E., Perito, B., Mastromei, G., 2006. Bacillus subtilis Gene Cluster Involved in Calcium Carbonate Biomineralization. J. Bacteriol. 189, 228–235. https://doi.org/10.1128/jb.01450-06

Beniash, E., 2012. Biominerals- hierarchical nanocomposites : the example of bone 1–41. WIREs Nanomedicine and Nanobiotechnology. 3, 47-69. https://doi.org/10.1002/wnan.105.Biominerals-

Butler, M.F., Glaser, N., Weaver, A.C., Kirkland, M., Heppenstall-Butler, M., 2006. Calcium Carbonate Crystallization in the Presence of Biopolymers. Cryst. Growth Des. 6, 781–794. https://doi.org/10.1021/cg050436w

Chang, I., Im, J., Cho, G.C., 2016. Introduction of microbial biopolymers in soil treatment for

future environmentally-friendly and sustainable geotechnical engineering. Sustainability. 8, 251-274. https://doi.org/10.3390/su8030251

Cheng, L., Cord-Ruwisch, R., Shahin, M.A., 2013. Cementation of sand soil by microbially induced calcite precipitation at various degrees of saturation. Can. Geotech. J. 50, 81–90. https://doi.org/10.1139/cgj-2012-0023

Chou, C.W., Seagren, E.A., Aydilek, A.H., Lai, M., 2011. Biocalcification of Sand through Ureolysis. J. Geotech. Geoenvironmental Eng. 137, 1179–1189. https://doi.org/10.1061/(asce)gt.1943-5606.0000532

Danjo, T., Kawasaki, S., 2016. Microbially Induced Sand Cementation Method Using *Pararhodobacter* sp. Strain SO1, Inspired by Beachrock Formation Mechanism. Mater. Trans. 57, 428–437. https://doi.org/10.2320/matertrans.m-m2015842

DeJong, J.T., Fritzges, M.B., Nüsslein, K., 2006. Microbially Induced Cementation to Control Sand Response to Undrained Shear. J. Geotech. Geoenvironmental Eng. 132, 1381–1392. https://doi.org/10.1061/(asce)1090-0241(2006)132:11(1381)

Dejong, J.T., Martinez, B.C., Ginn, T.R., Hunt, C., Major, D., Tanyu, B., 2014. Development of a scaled repeated five-spot treatment model for examining microbial induced calcite precipitation feasibility in field applications. Geotech. Test. J. 37, 424-235. https://doi.org/10.1520/GTJ20130089

DeJong, J.T., Mortensen, B.M., Martinez, B.C., Nelson, D.C., 2010. Bio-mediated soil improvement. Ecol. Eng. 36, 197–210. https://doi.org/10.1016/j.ecoleng.2008.12.029

Dixon, N.E., Gazzola, C., Blakeley, R.L., Zerner, B., 1975. Jack Bean Urease (EC 3.5.1.5). A Metalloenzyme. A Simple Biological Role for Nickel? J. Am. Chem. Soc. 97, 4131–4133. https://doi.org/10.1021/ja00847a045

Estroff, L.A., Addadi, L., Weiner, S., Hamilton, A.D., Whiteside, G.M., Science, M., Investigator, W.Y., 2008. Introduction : Biomineralization 108, 10–12.

Ferris, F.G., Phoenix, V., Fujita, Y., Smith, R.W., 2004. Kinetics of calcite precipitation induced by ureolytic bacteria at 10 to 20°C in artificial groundwater. Geochim. Cosmochim. Acta. 68, 1701–1710. https://doi.org/10.1016/S0016-7037(03)00503-9

Ferris, F.G., Stehmeier, L.G., Kantzas, A., Mourits, F.M., 1996. Bacteriogenic mineral plugging. J. Can. Pet. Technol. 35, 56–61. https://doi.org/10.2118/96-08-06

Fujita, M., Nakashima, K., Achal, V., Kawasaki, S., 2017. Whole-cell evaluation of urease activity of Pararhodobacter sp. isolated from peripheral beachrock. Biochem. Eng. J. 124, 1–5. https://doi.org/10.1016/j.bej.2017.04.004

Fujita, Y., JL, T., TLT, G., Delwiche, M., Colwell, F., Mcling, T., Petzke, L., Smith, R., 2008. Stimulation Of Microbial Urea Hydrolysis In Groundwater To Enhance Calcite Precipitation. Environ. Sci. Technol. 2008, 42, 3025–3032.

Gomez, M.G., Hunt, C.E., Major, D.W., DeVlaming, L.A., DeJong, J.T., Dworatzek, S.M., Martinez, B.C., 2014. Field-scale bio-cementation tests to improve sands. Proc. Inst. Civ. Eng. Gr. Improv. 168, 206–216. https://doi.org/10.1680/grim.13.00052

Gowthaman, S., Mitsuyama, S., Nakashima, K., Komatsu, M., Kawasaki, S., 2019. Biogeotechnical approach for slope soil stabilization using locally isolated bacteria and inexpensive low-grade chemicals: A feasibility study on Hokkaido expressway soil, Japan. Soils Found. 59, 484-499. https://doi.org/10.1016/j.sandf.2018.12.010

Hamdan, N., Zhao, Z., Mujica, M., Kavazanjian, E., He, X., 2016. Hydrogel-Assisted Enzyme-Induced Carbonate Mineral Precipitation. J. Mater. Civ. Eng. 28, 04016089–04016098. https://doi.org/10.1061/(ASCE)MT.1943-5533

Hansma, P.K., Weaver, J.C., Cidade, G.A.G., Morse, D.E., Fantner, G.E., Hassenkam, T., Pechenik, L., Cutroni, J.A., Birkedal, H., Kindt, J.H., Stucky, G.D., 2005. Sacrificial bonds and hidden length dissipate energy as mineralized fibrils separate during bone fracture. Nat. Mater. 4, 612–616. https://doi.org/10.1038/nmat1428

He, G., Dahl, T., Veis, A., George, A., 2003. Nucleation of apatite crystals in vitro by self-assembled dentin matrix protein 1. Nat. Mater. 2, 552–558. https://doi.org/10.1038/nmat945

Holm, L., Sander, C., 1997. An evolutionary treasure: Unification of a broad set of amidohydrolases related to urease. Proteins Struct. Funct. Genet. 28, 72–82. https://doi.org/10.1002/(SICI)1097-0134(199705)28:1<72::AID-PROT7>3.0.CO;2-L

Hughes, A.B., 2012. Amino Acids, Peptides and Proteins in Organic Chemistry.

Ivanov, V., Chu, J., 2008. Applications of microorganisms to geotechnical engineering for bioclogging and biocementation of soil in situ. Rev. Environ. Sci. Biotechnol. 7, 139–153. https://doi.org/10.1007/s11157-007-9126-3

Ivanov, V., Chu, J., Stabnikov, V., He, J., Naeimi, M., 2010. Iron-Based Bio-Grout For Soil Improvement and Land Reclamation. Second Int. Conf. Sustain. Constr. Mater. Technol. 1–3.

Jackson, A.P., Vincent, J.F.V., Turner, R.M., 1990. Comparison of nacre with other ceramic composites. J. Mater. Sci. 25, 3173–3178. https://doi.org/10.1007/BF00587670

Jimenez-Lopez, C., 2008. Nanocrystalline structures in calcium carbonate biominerals. J. Nanophotonics. 2, 021935. https://doi.org/10.1117/1.3062826

Kang, C.H., Han, S.H., Shin, Y., Oh, S.J., So, J.S., 2014. Bioremediation of Cd by microbially induced calcite precipitation. Appl. Biochem. Biotechnol. 172, 1929–1937. https://doi.org/10.1007/s12010-013-0626-z

Karimi, Z., Bullock, Z., Dashti, S., Liel, A., Porter, K., 2017. Influence of Soil and Structural Parameters on Liquefaction-Induced Settlement of Foundations Foundations. 3rd Int. Conf. Perform. Based Des.

Karol, R., 2010. Chemical Grouting And Soil Stabilization, Revised And Expanded, https://doi.org/10.1201/9780203911815

Kato, B.T., Sugawara, A., Hosoda, N., 2002. Calcium Carbonate - Organic Hybrid Materials , Advanced materials, 869–877.

Kaur, N., Reddy, M.S., Mukherjee, A., 2013. Biomineralization of calcium carbonate polymorphs by the bacterial strains isolated from calcareous sites. J. Microbiol. Biotechnol. 23, 707–714. https://doi.org/10.4014/jmb.1212.11087

Kenji Ishihara, M.Y., 1992. Evaluation of settlement in sand deposits following liquefaction during earthquakes. Soils Found. 33, 173–188.

Kim, I.W., Robertson, R.E., Zand, R., 2005. Effects of some nonionic polymeric additives on the crystallization of calcium carbonate. Cryst. Growth Des. 5, 513–522. https://doi.org/10.1021/cg049721q

Krajewska, B., Chudy, M., Drozdek, M., Brzózka, Z., 2003. Potentiometric study of urease kinetics over pH 5.36-8.21. Electroanalysis. 15, 460–466. https://doi.org/10.1002/elan.200390054

L.Addadi, S.W., 1985. Interaction between acidic proteins and crystals: Stereochemical

requirements in biomineralization. Proc. Natl. Acad. Sci. 82, 4110–4114.

Lopez, M.I., Lin, A.Y.M., Chen, P.-Y., Seki, Y., Meyers, M.A., 2010. Biological materials: A materials science approach. J. Mech. Behav. Biomed. Mater. 4, 626–657. https://doi.org/10.1016/j.jmbbm.2010.08.005

Martines, B.C., 2008. Up-Scaling of Microbial Induced Calcite Precipitation in Sands for Geotechnical Ground Improvement , PhD thesis, University of California , Davis

Masica, D.L., Schrier, S.B., Specht, E.A., Gray, J.J., 2010. De novo design of peptide-calcite biomineralization systems. J. Am. Chem. Soc. 132, 12252–12262. https://doi.org/10.1021/ja1001086

Menig, R., Meyers, M.H., Meyers, M.A., Vecchio, K.S., 2000. Quasi-static and dynamic mechanical response of Haliotis rufescens (abalone) shells. Acta Mater. 48, 2383–2398. https://doi.org/10.1016/S1359-6454(99)00443-7

Mesri, G., Shahien, M., Kane, T., 2018. Seismically induced settlement of ground experiencing undrained shaking and laterally constrained compression. Can. Geotech. J. 56, 155–172. https://doi.org/10.1139/cgj-2017-0419

Mitchell, A.C., Ferris, F.G., 2005. The coprecipitation of Sr into calcite precipitates induced by bacterial ureolysis in artificial groundwater: Temperature and kinetic dependence. Geochim. Cosmochim. Geochimica et Cosmochimica Acta. 69, 4199–4210. https://doi.org/10.1016/j.gca.2005.03.014

Montoya, B.M., DeJong, J.T., 2015. Stress-Strain Behavior of Sands Cemented by Microbially Induced Calcite Precipitation. J. Geotech. Geoenvironmental Eng. 141, 04015019–04015029. https://doi.org/10.1061/(ASCE)GT.1943-5606

Mor, S., Ravindra, K., Dahiya, R.P., Chandra, A., 2006. Leachate characterization and assessment of groundwater pollution near municipal solid waste landfill site. Environ. Monit. Assess. 118, 435–456. https://doi.org/10.1007/s10661-006-1505-7

Mortensen, B.M., Nelson, D.C., DeJong, J.T., Caslake, L.F., Haber, M.J., Mortensen, B.M., 2011. Effects of environmental factors on microbial induced calcium carbonate precipitation. J. Appl. Microbiol. 111, 5728–5733. https://doi.org/10.1111/j.1365-2672.2011.05065.x

Mujah, D., Shahin, M.A., Cheng, L., 2017. State-of-the-Art Review of Biocementation by

Microbially Induced Calcite Precipitation (MICP) for Soil Stabilization. Geomicrobiol. J. 34, 524–537. https://doi.org/10.1080/01490451.2016.1225866

Nikolov, S., Petrov, M., Lymperakis, L., Friák, M., Sachs, C., Fabritius, H.O., Raabe, D., Neugebauer, J., 2010. Revealing the design principles of high-performance biological composites using Ab initio and multiscale simulations: The example of lobster cuticle. Adv. Mater. 22, 519–526. https://doi.org/10.1002/adma.200902019

Paassen, L.A. Van, Harkes, M.P., Zwieten, G.A. Van, Zon, W.H. Van Der, Star, W.R.L. Van Der, Loosdrecht, M.C.M., 2009. Scale up of BioGrout A biological ground reinforcement method. Proceedings of the 17th International Conference on Soil Mechanics and Geotechnical Engineering. 3, 2328–2333.

Pasillas, J.N., Khodadadi, H., Martin, K., Bandini, P., Newtson, C.M., Kavazanjian, E., 2018. Viscosity-Enhanced EICP Treatment of Soil. International Foundation Congress and Equipment Expo. 145–154. https://doi.org/10.1061/9780784481592.015

Raabe, D., Sachs, C., Romano, P., 2005. The crustacean exoskeleton as an example of a structurally and mechanically graded biological nanocomposite material. Acta Mater. 53, 4281–4292. https://doi.org/10.1016/j.actamat.2005.05.027

Roy, Surendra, S.K.B., 2017. Role of Geotechnical Properties of Soil on Civil Engineering Structures. Resour. Environ. 7, 103–109. https://doi.org/10.5923/j.re.20170704.03

Sarker, D., Abedin, Z., 2015. A Review on Ground Improvement Techniques to Improve Soil Stability Against Liquefaction. Int. J. Sci. Eng. Investig. 4, 53-55.

Sirko, A., Brodzik, R., 2000. Plant ureases: Roles and regulation. Acta Biochim. Pol. 47, 1189–1195.

Smith, B.L., Schaffer, T.E., Mario, V., Thompson, J.B., Frederick, N.A., Kindt, J., Belcher, A., Stucky, G.D., Morse, D.E., Hansama, P.K., 1999. Molecular mechanistic origin of the toughness of natural adhesives, fibres and composites. Nature. 399, 761–763. https://doi.org/10.1038/21607

Stephen Mann, 2001. Biomineralization, oxford university press.

Stephen, W., Lia, A., 1997. Design strategies in mineralized biological materials. J. Mater. Chem. 7, 689–702.

Steve Weiner & Patricia M. Dove, 2003. An Overview of Biomineralization Processes and the Problem of the Vital Effect. Rev. Mineral. Geochemistry. 54, 1–29.

van Paassen, L.A., 2009. Biogrout: Ground Improvement by Microbially Induced Carbonate Precipitation. PhD thesis, Delft University of Technology, Netherland.

van Paassen, L.A., Daza, C.M., Staal, M., Sorokin, D.Y., van der Zon, W., van Loosdrecht, M.C.M., 2010. Potential soil reinforcement by biological denitrification. Ecol. Eng. 36, 168–175. https://doi.org/10.1016/j.ecoleng.2009.03.026

Vincent, J.F.V., 2002. Arthropod cuticle: A natural composite shell system. Compos. Part A Appl. Sci. Manuf. 33, 1311–1315. https://doi.org/10.1016/S1359-835X(02)00167-7

Vincent, J.F.V., Wegst, U.G.K., 2004. Design and mechanical properties of insect cuticle. Arthropod Struct. Dev. 33, 187–199. https://doi.org/10.1016/j.asd.2004.05.006

Voet, D.J., Voet, J.G., Pratt, C.W., 2011. Fundamentals of Biochemistry, 4th Edition.

Wang, X., Tao, J., 2018a. Polymer-modified microbially induced carbonate precipitation for one-shot targeted and localized soil improvement. ActaGeotechnica. 1–15.

Wang, X., Tao, J., 2018b. Polymer-modified microbially induced carbonate precipitation for one-shot targeted and localized soil improvement. Acta Geotech. 14, 657-671. https://doi.org/10.1007/s11440-018-0757-z

Wang, Z., Zhang, N., Cai, G., Jin, Y., Ding, N., Shen, D., 2017a. Review of ground improvement using microbial induced carbonate precipitation (MICP). Mar. Georesources Geotechnol. 35, 1135–1146. https://doi.org/10.1080/1064119X.2017.1297877

Wei, S., Cui, H., Liu, H., He, H., Fang, N., 2015. Biomineralization processes of calcite induced by bacteria isolated from marine sediments. Brazilian J. Microbiol. 46, 455–464. https://doi.org/10.1590/s1517-838246220140533

Whiffin, V.S., 2004. Microbial $CaCO_3$ Precipitation for the production of Biocement. PhD thesis, Murdoch University, Australia.

Whiffin, V.S., van Paassen, L.A., Harkes, M.P., 2007. Microbial carbonate precipitation as a soil improvement technique. Geomicrobiol. J. 24, 417–423. https://doi.org/10.1080/01490450701436505

Wu, J., Zeng, R.J., 2017. Biomimetic Regulation of Microbially Induced Calcium Carbonate Precipitation Involving Immobilization of Sporasarcina pasteurii by Sodium Alginate. Cryst. Growth Des. 17, 1854–1862. https://doi.org/10.1021/acs.cgd.6b01813

Xu, Z.H., Li, X., 2011. Deformation strengthening of biopolymer in nacre. Adv. Funct. Mater. 21, 3883–3888. https://doi.org/10.1002/adfm.201100167

Yasuyuki Koga, O.M., 1990. Shaking table tests of embankments resting on liquefiable sandy ground. Soils Found. 30, 162–174.

Zhao, Z., Hamdan, N., Shen, L., Nan, H., Almajed, A., Kavazanjian, E., He, X., 2016. Biomimetic hydrogel composites for soil stabilization and contaminant mitigation. Environ. Sci. Technol. 50, 12401–12410. https://doi.org/10.1021/acs.est.6b01285

CHAPTER 2. EFFECT OF THE SYNTHETIC POLY PEPTIDES ON THE $CaCO_3$ CRYSTALIZATION AND SAND DENSIFICATION USING MICP METHOD

2.1. Introduction

Polypeptides are linear polymers consisted with repeating sequence of certain amino acids which are linked by peptide bond. Amino acids are building blocks of polypeptides and 20 types of the amino acids can be found in nature and each one has a specific structure (Hughes, 2012). On the other hand, polypeptides act as building blocks to create certain types of proteins by bonding two or more polypeptides and depending on the variation of the length and the amino acid sequence of the polypeptides different shapes of proteins are created with different biological functions (Voet et al., 2011). Polypeptides are important polymers in both of the protein and polymer sciences. However, large scale industrial production of natural polypeptides is a challenge, hence scientists have moved to create synthetic polypeptides which can function similarly as natural polypeptides (Bonduelle, 2018).

Synthetic polymers have gained big attention in the field of tissue engineering and regenerative medicine due to its excellent properties compared with the natural polypeptides. Basically, synthetic polymers are compatible with wide range of solvent, hence spinning of these polymers are easy and also they have higher purity than natural polymers (Asli et al., 2012; van Aalst et al., 2008). Shortly, synthetic polypeptides can be defined as interdisciplinary macromolecules. Though these synthetic polypeptides are extensively used in biomedical field, applications in the civil and geotechnical engineering field couldn't be found. Our interest is introducing synthetic polypeptide into the geotechnical engineering field as an organic additive combine with the MICP process.

Among the number of polypeptides, poly-L-lysine and poly-glutamate were selected for our studies since effect of these polymers on the $CaCO_3$ crystallization have been studied previously by using chemical precipitation (Kato et al., 1998; Manoli et al., 2002; Njegić et al., 2010; Njegic et al., 2009; Shih et al., 2005; Wada et al., 2018; Westwood et al., 2013; Yao et al., 2009). Chemical structure of the poly-L-lysine and poly-glutamate are shown in the Fig 2-1. In the neutral pH, poly-L-lysine charged positively while poly glutamate charged negatively.

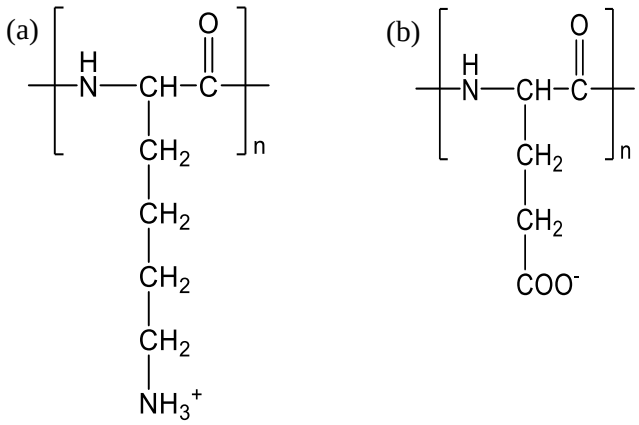

Fig. 2-1 Chemical structure of (a) Poly-L-lysine (b) Poly-glutamate

Poly-L-lysine is a bio compatible cationic polypeptide and prevalent reagent in the field of bio medical as a cell adhesion reagent to attachment of protein, DNA and cells into solid surfaces as shown in Fig. 2-2 (Mazia et al., 1975). Poly-L-lysine coating is used as an anchor for other biocompatible polymers, like poly-L-lysine-polyethyleneglycol (PEG) block copolymers and used extensively as a food preservative in Japan and Korea (Hiraki et al., 2003). Effect of the poly-L-lysine on the $CaCO_3$ crystallization has been studied previously by using gas diffusion method and found that it has positive influence on the $CaCO_3$ crystallization (Njegić et al., 2010; Njegic et al., 2009) and also morphology change of the $CaCO_3$ in the presence of the poly-L-lysine also reported (Wada et al., 2018; Yao et al., 2009). Due to the intensive cell adhesion property and $CaCO_3$ formation capacity, poly-L-lysine would be a best additive for the MICP process. Hence, in this chapter we examined the effect of this cationic polypeptide on the $CaCO_3$ precipitation and sand solidification using MICP and EICP processes.

Similarly, poly-glutamate is a linear anionic polypeptide with higher stability over wide range of pH (Bágel'ová et al., 2001). Effect of the poly-glutamate as well as poly-glutamic acid has been studies previously using chemical precipitation and found that it has a higher influence on the polymorphism and the morphology of $CaCO_3$ crystallization (Kato et al., 1998; Njegić-Džakula et al., 2010; Njegic et al., 2009). Therefore, poly-glutamate can have significant effect on the MICP process and this chapter addresses the contribution of the poly-glutamate on the $CaCO_3$ crystallization.

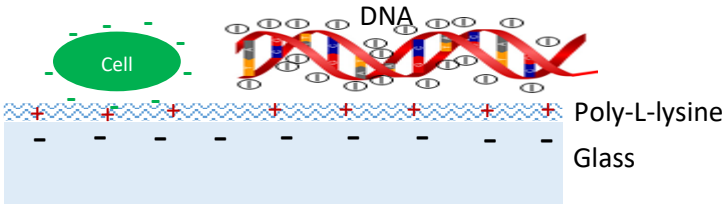

Fig. 2-2 Cell adhesion property of poly-L-lysine

2.2. Objectives

Main objective of this chapter is investigating the effect of the cationic (poly-L-lysine) and anionic (poly-glutamate) synthetic polypeptide on the $CaCO_3$ crystallization, its polymorphism and morphology by using the MICP process driven by the ureolytic bacteria *Pararhodobacter* sp. Also, effect of the synthetic polypeptide modified MICP on the sand densification was investigated.

2.3. Materials and methods

2.3.1. Preparation of bacterial cell culture

Experiments were conducted by using the ureolytic bacteria *Pararhodobacter* sp. isolated from beach sand in Sumuide, Nago, Okinawa, Japan (Danjo and Kawasaki, 2016b). Bacterial cells were pre-cultured in Zobell 2216E medium (polypeptone (Nihon Seiyaku Co., Ltd., Tokyo, Japan) 5.0 g/L, yeast extract (BD Biosciences Advanced Bioprocessing, Miami, FL, USA) 1.0 g/L, $FePO_4$ (Junsei Chemical Co., Ltd., Tokyo, Japan) 0.1 g/L in artificial sea water, pH 7.6–7.8; 5 mL) by shaking at 30 °C and 160 rpm for 24 h. The pre-culture (1 mL) was inoculated into fresh Zobell 2216E medium (100 mL). The mixture was kept in the shaking incubator under the same conditions as those used for pre-culturing for 48 h. The cells were collected by centrifugation of the bacterial culture (10 °C, 8000 rpm, 5 min) and resuspended again in sterilized distilled water to adjust the cell concentration (OD_{600} = 1). Cell concentration was determined by UV-visible spectroscopy (V-730, JASCO Corporation, Tokyo, Japan) as optical density value which is relevant to the 600 nm wave length (OD_{600}).

2.3.2. Precipitation of $CaCO_3$ by ureolytic bacteria

$CaCO_3$ precipitation experiments were conducted by hydrolysis of the urea using ureolytic bacteria, *Pararhodobacter* sp. in the presence of $CaCl_2$. The bacteria were added to a substrate solution containing urea (0.3 mol/L; Wako Pure Chemical Industries Ltd., Tokyo, Japan) and $CaCl_2$ (0.3 mol/L; Wako Pure Chemical Industries Ltd., Tokyo, Japan) in the presence or absence of poly-L-lysine/ poly-glutamate (Wako Pure Chemical Industries Ltd., Tokyo, Japan). The reaction mixture (10 mL) was shaken at 30 °C and 160 rpm for 24 h and samples were centrifuged (24 °C, 12000 rpm, 10 min) to separate the $CaCO_3$ precipitate from the supernatant. Then precipitates were dried in an oven at 100 °C for 24 h, and dry weights of the precipitates were determined.

Experiments were conducted for the different bacteria concentrations (OD_{600} = 0.01–0.2) in the presence (10 mg/L) or absence of polymer to check the effect of the bacteria concentration and the effect of the polymer on the $CaCO_3$ crystallization. Also, effect of the polymer concentration on the $CaCO_3$ crystallization was examined under the different polymer concentrations (0-50 mg/L) with a bacterial concentration of OD_{600} = 0.1. All experiments were done in triplicate.

2.3.3. Precipitation of $CaCO_3$ by urease enzyme

Same time, $CaCO_3$ precipitation experiments were conducted by using extracted jack bean urease enzyme (Wako Pure Chemical Industries Ltd., Tokyo, Japan) in the presence of $CaCl_2$ and urea. Urease solution was prepared by dissolving the urease powder in Tris-HCl buffer (0.1 M, pH -8) and diluted by using distilled water to achieve the desired activity (3 U/ml). Procedure of the precipitation test is similar to the section 2.3.2. Experiments were conducted for the different urease concentrations (0.03 U/ml–1.5 U/ml) in the presence (10 mg/L) or absence of polymer to check the effect of the urease concentration and the effect of the polymer on the $CaCO_3$ crystallization. Also, effect of the polymer concentration on the $CaCO_3$ crystallization was examined under the different polymer concentrations (0-50 mg/L) with a urease concentration of 0.3 U/ml. All experiments were done in triplicate.

2.3.4. Analysis of precipitate

(a) X-ray diffraction analysis

Polymorphism of the precipitated $CaCO_3$ was examined by conducting the X-ray diffraction (XRD; MiniFlex™, Rigaku Co., Ltd., Tokyo, Japan) analysis for the ground samples under Ni-filtered Cu 1.5406 Å radiation. The crystalline phases were identified with MATCH 3.4 software.

(b) Scanning Electron Microscopy (SEM) analysis

Morphology of the precipitated crystals were examined by using the Scanning electron microscopy (SEM; Miniscope TM3000, Hitachi, Tokyo, Japan).

(c) Fourier-transform infrared spectroscopy (FTIR) analysis

Fourier-transform infrared spectra was obtained by using FTIR spectroscopy (6200HFV Jasco, Japan). Samples were prepared by grinding the $CaCO_3$ powder with the KBr and then mixture was pressed into a transparent disk for the analysis.

2.3.5. Toxicity of the poly-L-lysine

Toxicity of the poly-L-lysine on the *Pararhodobactor* sp. was also investigated. Totally, five kind of samples were prepared by inoculated bacteria (OD_{600}-0.1) in sterilized artificial sea water with varying poly-L-lysine concentrations (0 - 50 mg/L). Artificial sea water was added into the reaction mixture to provide a favorable environment for *Pararhodobactor* sp. to grow since it is a marine bacterium. Reaction mixture (10 ml) was kept in the shaking incubator under 30 °C and 160 rpm. Samples were collected at 0, 2, 4, 8 and 24 hours and each sample was separately diluted by 10^{-1}-10^{-6} times using sterilized artificial sea water. Then samples were inoculated in the Zobell 2216E agar medium (polypeptone (Nihon Seiyaku Co., Ltd., Tokyo, Japan) 5.0 g/L, yeast extract (BD Biosciences Advanced Bioprocessing, Miami, FL, USA) 1.0 g/L, $FePO_4$ (Junsei Chemical Co., Ltd., Tokyo, Japan) 0.1 g/L, Agar (Wako Pure Chemical Industries Ltd., Tokyo, Japan) 15 g/L; in artificial sea water, pH 7.6–7.8). Finally, viable cell count was determined as colony forming unit (CFU) by using the equation 4.

$$\text{CFU} = \text{Plate colony count} * \text{Dilution factor} \quad (4)$$

2.3.6. Sand solidification in syringe

Sand solidification experiments were conducted with and without poly-L-lysine by using the method previously described by Danjo and Kawasaki (2016) to check the effect of the poly-L-lysine on the sand densification. Experiments were conducted for commercially available Mikawa and Toyoura sands. Physical properties of the both of the sands are given in the Table 2-1.

Table 2-1 Physical properties of the Mikawa and Toyoura sands

Physical Properties	Mikawa sand	Toyoura sand
Mean diameter	0.87 mm	0.2 mm
Particle density	2.66 g/cm^3	2.64 g/cm^3
Coefficient of uniformity (C_u)	1.27	1.375
Coefficient of curvature (C_c)	0.97	0.92
Sand type (USCS classification)	Poorly graded sand	Poorly graded sand

Sand samples (43 g for Mikawa sand and 48 g for Toyoura sand) were oven dried at 110 °C for 2 days and placed in a 35 mL syringe (mean diameter D_{50} = 2.5 cm and height 7 cm) in three layers. Each layer was subjected to 20 hammer blows. Then first poly-L-lysine (5 ml, 100 mg/L) was injected to the syringe and next bacterial solution (16 mL, OD_{600} = 1) was injected and kept it 10-15 min to allow fixation of the bacteria to sand particles. After that, drained out the solution from the outlet, leaving 2 mL of the solution above the surface. After that cementation solution (20 mL; 0.3 M urea, 0.3 M $CaCl_2$, 0.02 M sodium hydrogen carbonate, 0.2 M ammonium chloride, and 3 g/L nutrient broth (BD Biosciences Advanced Bioprocessing, Miami, FL, USA)) was injected into the syringe, and drained, leaving 2 mL of the solution above the surface to maintain saturation conditions. All solutions were injected through gravity. Experiments were done in triplicate in an incubator at 30 °C as shown in Fig. 2-3.

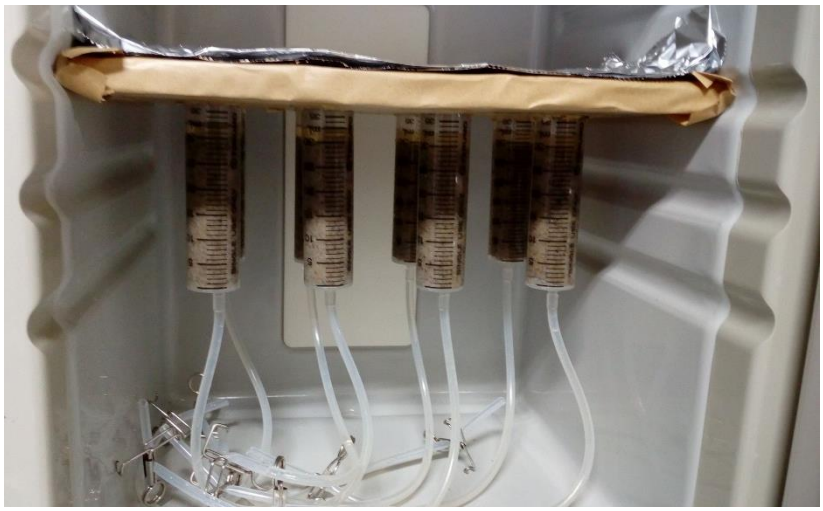

Fig. 2-3 Experiment setup of the solidification test

Every 3 days, the pH and Ca^{2+} concentration of the drainage were measured. The experiments were conducted with various bacterial injection intervals as given in the Table 2-2. In one set, bacteria were injected only once, on the first day. In another set, bacteria were injected twice, i.e., on the first day and again after 7 days. During the experiment, poly-L-lysine was injected twice, on the first day and again after 7 days.

Table 2-2 Experimental conditions for sand solidification with and without poly-L-lysine

	poly-L-lysine	bacteria injection
S1	-	once [b]
S2	100 mg/L [a]	once [b]
S3	-	twice [c]
S4	100 mg/L [a]	twice [c]

[a] Initial concentration of the poly-L-lysine solution applied to the column in solidification test.

[b] Injection of bacteria culture only at the beginning of solidification test.

[c] Injection of bacteria culture at the beginning and after 7 days of solidification test.

In addition, control experiments were conducted without adding bacteria to check the effect of the poly-L-lysine itself for the sand densification. Two kind of experiments were conducted by varying the conditions as given in the Table 2-3

Table 2-3 Experimental conditions for sand solidification without bacteria

	poly-L-lysine (100 mg/L)	cementation solution (0.3 M)
S1	1st and 7th day	Daily
S2	-	Daily

After 14 days, the unconfined compressive strength (UCS) of the samples were determined with a needle penetration device (SH70, Maruto Testing Machine Company, Tokyo, Japan) which is shown in Fig. 2-4. First, needle was injected into the sand specimen and penetration force (N) and the penetration distance (mm) were recorded. Unconfined compressive strengths (UCS) of the samples were determined by using the calibration equation given in equation 5 which was provided by the manufacture. In the instrument manual it is mentioned that this calibration equation was developed by considering 114 natural rock samples and 50 improved soils with cements.

$$\log(y) = 0.978\ \log(x) + 2.621 \qquad (5)$$

x= Penetration gradient (N/mm)

y= Unconfined Compressive Strength

Fig. 2-4 Needle Penetration Device

2.3.7. Determination of the amount of $CaCO_3$

Precipitated amount of $CaCO_3$ in the solidified sand specimen was measured by using the calcimeter (Fig. 2-5). It is a simple device which can be used to measure the amount of precipitated $CaCO_3$ approximately by using amount of gas (CO_2) released when the cemented sand sample react with HCl (3M). Experiments were conducted in a closed container under constant pressure and temperature. Approximately 1-2 g of sample was placed in a container and 10 ml of HCl was placed in plastic viral. Then container was closed and manometer was attached. After that, whole system was agitated gently until get the constant pressure value. Finally, precipitated amount of $CaCO_3$ was determined by using the calibration equation given in equation (6) which has been developed by measuring the gas pressure for the known amount of $CaCO_3$.

$$y = 125.78\,x - 0.1035 \qquad (6)$$

y- Gas Pressure (kPa)

x- Weight of $CaCO_3$ (g)

Fig. 2-5 Calcimeter

2.4. Results and Discussion

2.4.1. Effect of the synthetic polypeptides on the $CaCO_3$ Crystallization

2.4.1.1. Effect of poly-L-lysine on the $CaCO_3$ Crystallization by using bacterial urease

Variation of the measured amount of precipitated $CaCO_3$ with and without poly-L-lysine under different bacteria concentrations is given in Fig.2-6. Error bars show the standard deviation of the values in three independent experiments.

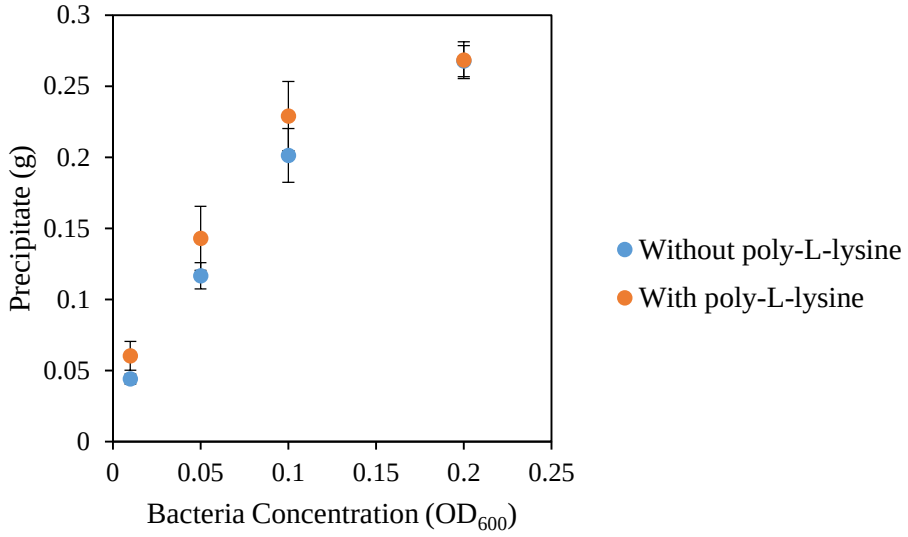

Fig. 2-6 Amounts of precipitate formed at various bacterial concentrations (OD_{600}) with or without addition of poly-L-lysine.

The amount of $CaCO_3$ increased with increasing bacteria concentration in the presence and absence of the poly-L-lysine. It is well known factor that amount of $CaCO_3$ precipitation is directly related to the urease activity of the bacteria (Al Qabany et al., 2011). Fujita et al.,(2017) have been found that urease activity of the *Pararhodobacter* sp. increases with the increasing of the cell concentration (OD_{600}). Similarly, Mortensen et al., (2011) mentioned that the rate of urea hydrolysis is mainly affect for the rate of $CaCO_3$ precipitation and ureolytic biomass should be increased to increase the rate of urea hydrolysis. Therefore, the increase in urease activity with increasing cell concentration leads to increased precipitation, and causes rapid nucleation and growth of $CaCO_3$ at high bacterial cell concentrations.

Most interesting finding is the positive effect of the poly-L-lysine on the $CaCO_3$ crystallization. Higher amount of $CaCO_3$ precipitation could be obtained by adding poly-L-lysine compared with that of without and it is very clear in lower bacteria concentrations. A significant effect of poly-L-lysine was not detected at higher bacterial concentrations; this indicates that the bacterial activity may be the dominant factor rather than the effect of poly-L-lysine at higher bacteria concentrations. Behavior of basic polypeptides on the $CaCO_3$ crystallization is little unclear and difficult to explain. However, Xie et al., (2005) have been examined the effect of the L-lysine on the $CaCO_3$ crystallization by the chemical precipitation of $CaCO_3$ from $Ca(NO_3)_2$ and Na_2CO_3. They explained that the positive charge on L-lysine strongly attracts CO_3^{2-} ions, resulting in CO_3^{2-} ion enrichment and higher super saturation of CO_3^{2-} ions in local regions which is favorable for $CaCO_3$ crystal nucleation and growth. Similar

hypothesis can be used to explain the positive effect of the poly-L-lysine on the $CaCO_3$ crystallization. Purely electrostatic interaction can be seen between the positively charged poly-L-lysine and negatively charged calcite surface.

Fig. 2-7 shows the FTIR spectrums obtained for the samples with and without poly-L-lysine. According to the Fig. 2-7(b) additional peak can be found around 1200 cm^{-1} for the samples with poly-L-lysine. According to the literature, this peak is relevant to the C-N bond. Therefore, it is look like some amount of poly-L-lysine has incorporated into the $CaCO_3$ crystals. Peaks in 713 and 876 cm^{-1} wave lengths are related to the calcite crystals (Wada et al., 2018).

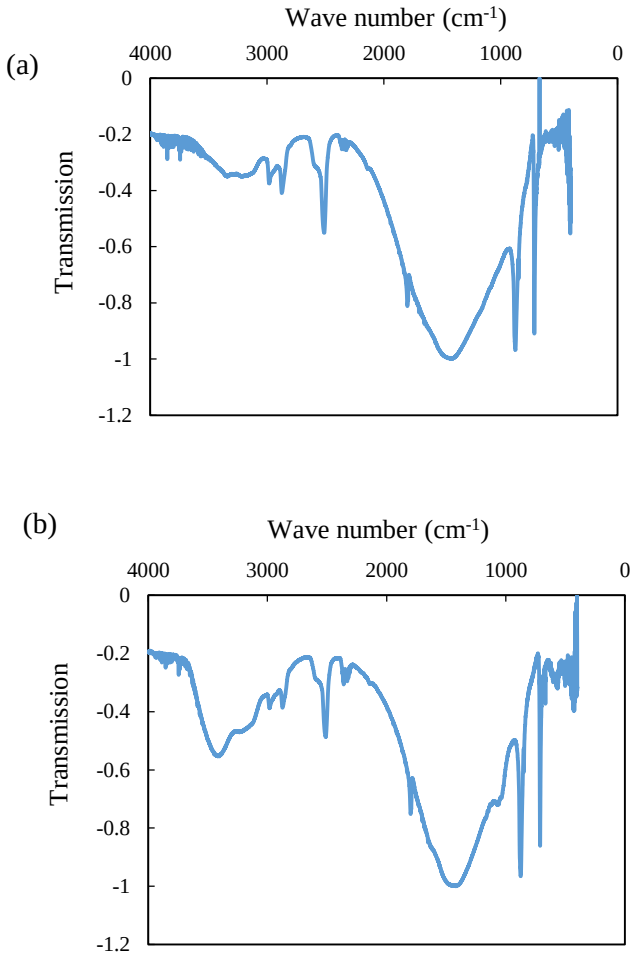

Fig. 2-7 FTIR Spectrum for $CaCO_3$ precipitation (a) Without poly-L-lysine (b) With poly-L-lysine

SEM analysis was conducted for the oven dried samples to identify the morphology of the $CaCO_3$ crystals in the presence and absence of the poly-L-lysine. Fig. 2-8 shows the crystal morphologies of the samples prepared at various bacterial concentrations without poly-L-lysine. As shown in the Fig. 2-8(a) well developed rhombohedral crystals were obtained at low bacterial concentrations while rhombohedral crystal agglomeration were obtained at higher bacterial concentrations as given in Fig. 2-8(b). Another point noticed is that the crystal size decreased with increasing bacterial concentration. Urease from *Pararhodobacter* sp. is not secreted into the extracellular medium but accumulates in or on the cell as a membrane enzyme (Fujita et al., 2017). Therefore, bacterial cells can be acted as nucleation sites for $CaCO_3$ crystals to nucleate and growth. Due to the lower amount of nucleation sites at lower bacteria cell concentrations, after the initial calcite precipitation on the nucleation sites, calcite crystals can grow continuously and produce larger crystals (Stocks-Fischer et al., 1999). However, at higher bacterial concentrations, each cell acts as a nucleation site and a large number of small crystals are produced, without growth of the individual crystals.

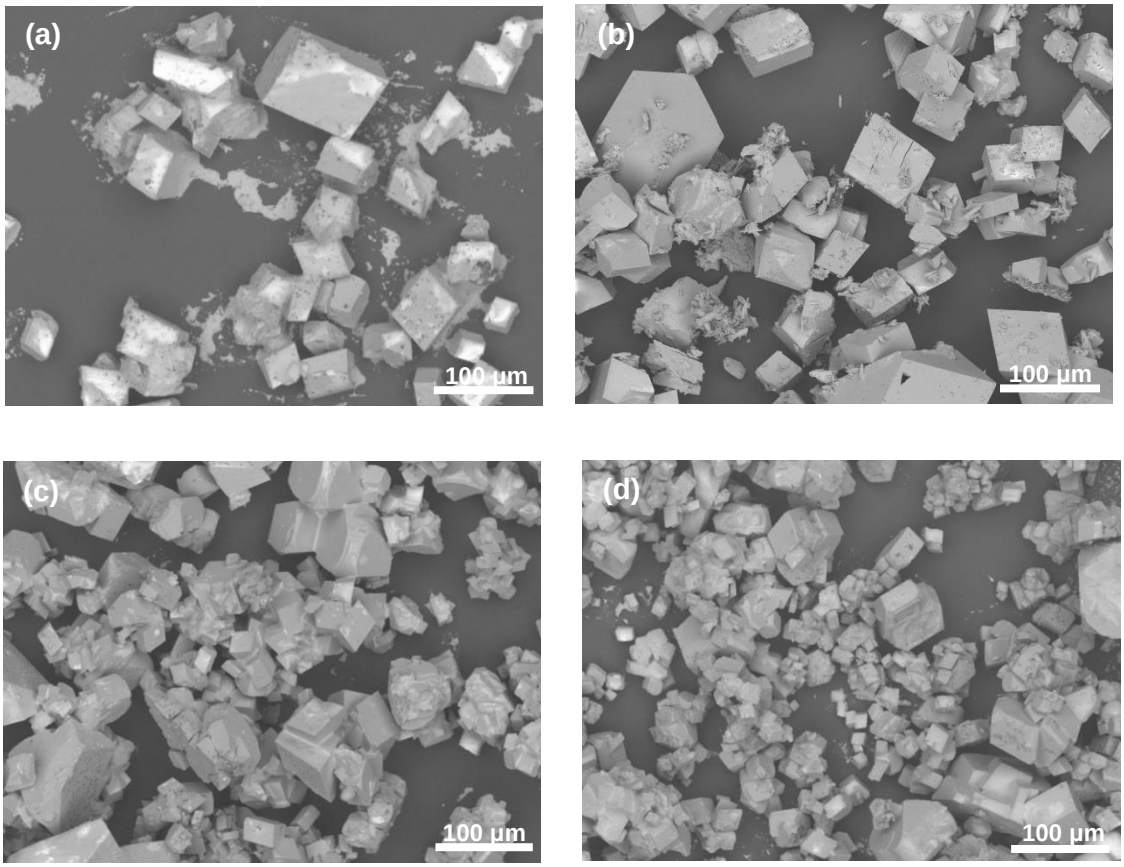

Fig. 2-8 SEM images of $CaCO_3$ precipitates at various bacterial concentrations without poly-L-lysine: (a) OD_{600} = 0.01, (b) OD_{600} = 0.05, (c) OD_{600} = 0.1, and (d) OD_{600} = 0.2.

Morphologies of the crystals at different bacteria concentrations in the presence of the poly-L-lysine are given in Fig. 2-9. In the presence of the poly-L-lysine morphology of the crystals changed into the ellipsoidal shape crystals. The effect is clearer at lower cell concentrations and at higher bacteria cell concentration combination of the ellipsoidal and rhombohedral crystals was obtained. Production of larger amount of $CaCO_3$ at higher cell concentration would be the reason for obtained both of the morphologies at higher cell concentrations. According to the XRD patterns given in Fig. 2-10 main components of the obtained crystals with and without poly-L-lysine was calcite.

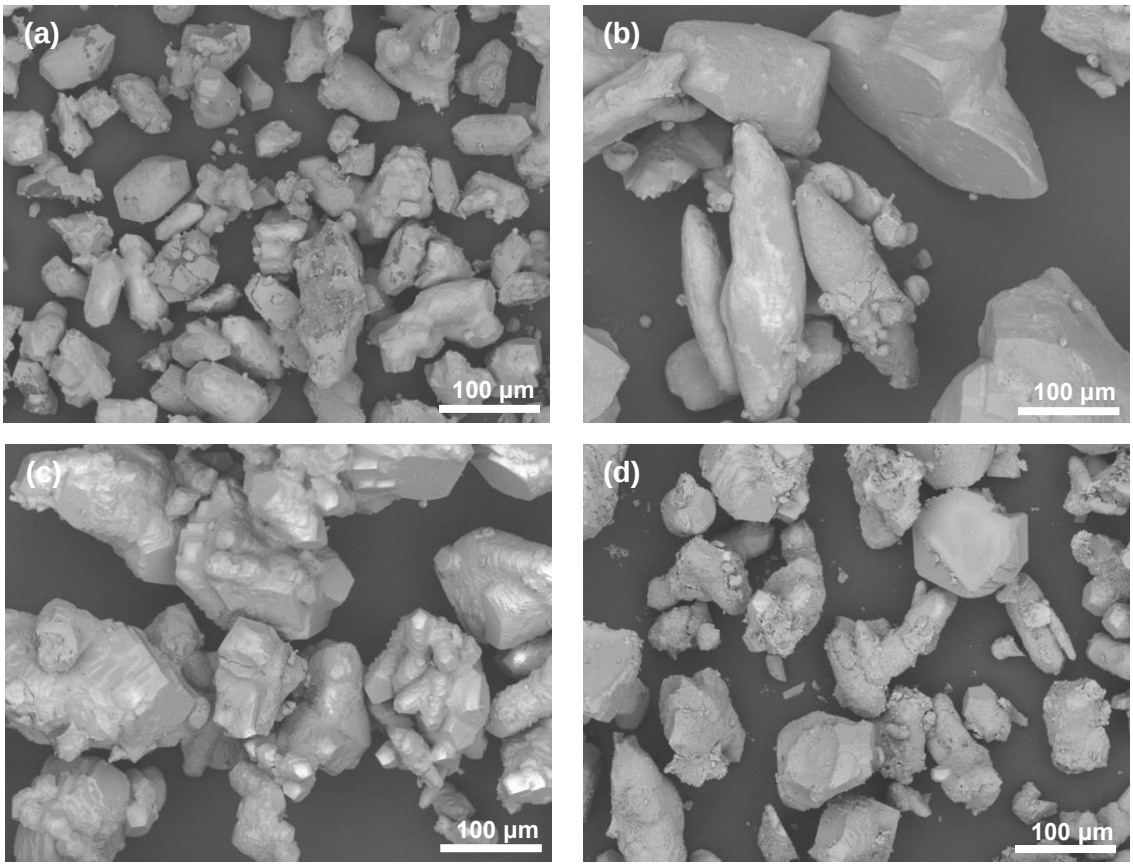

Fig. 2-9 SEM images of $CaCO_3$ precipitates at various bacterial concentrations with poly-L-lysine (10 mg/L): (a) OD_{600} = 0.01, (b) OD_{600} = 0.05, (c) OD_{600} = 0.1, and (d) OD_{600} = 0.2.

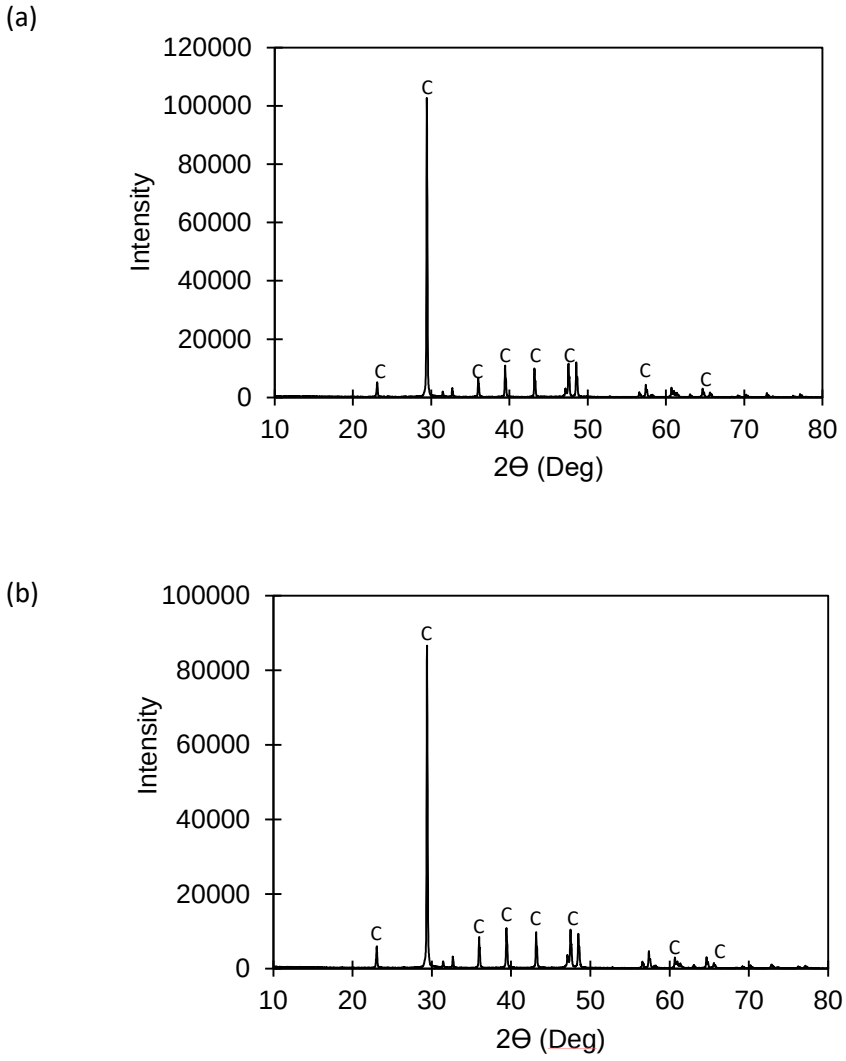

Fig. 2-10 XRD patterns of $CaCO_3$ precipitates (a) without poly-L-lysine and (b) with poly-L-lysine.

2.4.1.1.1. Effects of poly-L-lysine concentration on $CaCO_3$ crystallization

Variation of the amount of precipitate with the poly-L-lysine concentration is given in Fig. 2-11. The amount of precipitate formed at intermediate poly-L-lysine concentration was higher than those of formed at higher and lower poly-L-lysine concentrations. Hence, moderate bell-shaped relationship was detected between the amount of precipitate and the poly-L-lysine concentration. Njegic et al., (2009) have been found similar relationship by chemical precipitation of the $CaCO_3$ in the presence of poly-L-lysine. They have been reported that increased calcite growth at low concentrations of poly- L-lysine and decreased growth at higher

concentrations is typical of additives that are weakly, non-selectively bonded to the crystal surfaces.

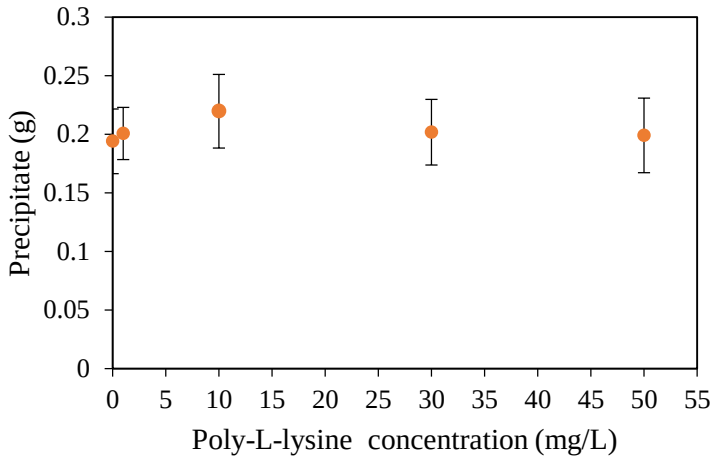

Fig. 2-11 Variation of the amount of $CaCO_3$ precipitate with the poly-L-lysine concentration

Fig. 2-12 shows the SEM images of the crystal morphology obtained for the various poly-L-lysine concentrations. At lower poly-L-lysine concentrations, effect of the poly-L-lysine on the morphology change can be neglected and polyhedron crystals were dominant as shown in Fig. 2-12(a). With increasing poly-L-lysine concentration, the morphology changed to peanut-like twin spheres, and at high poly-L-lysine concentrations, twin spheres were dominant, as shown in Fig. 2-12(b-d). This morphology Change depends on the conformation of the poly-L-lysine chain. Poly-L-lysine has a α-helix confirmation under the alkaline conditions (Shibata et al., 1992). During the urea hydrolysis, the pH of the medium increases and this weak alkaline condition is more favorable for the poly-L-lysine to change its confirmation to α-helix. As shown in Fig. 2-13, α-helix confirmation leads to tangentially oriented growth on the sphere surface and vertically oriented growth on the equatorial zone, to form peanut-like twin spheres (Yao et al., 2009). Twin spheres are probably formed because of crystal growth on both sides of the nuclear plate.

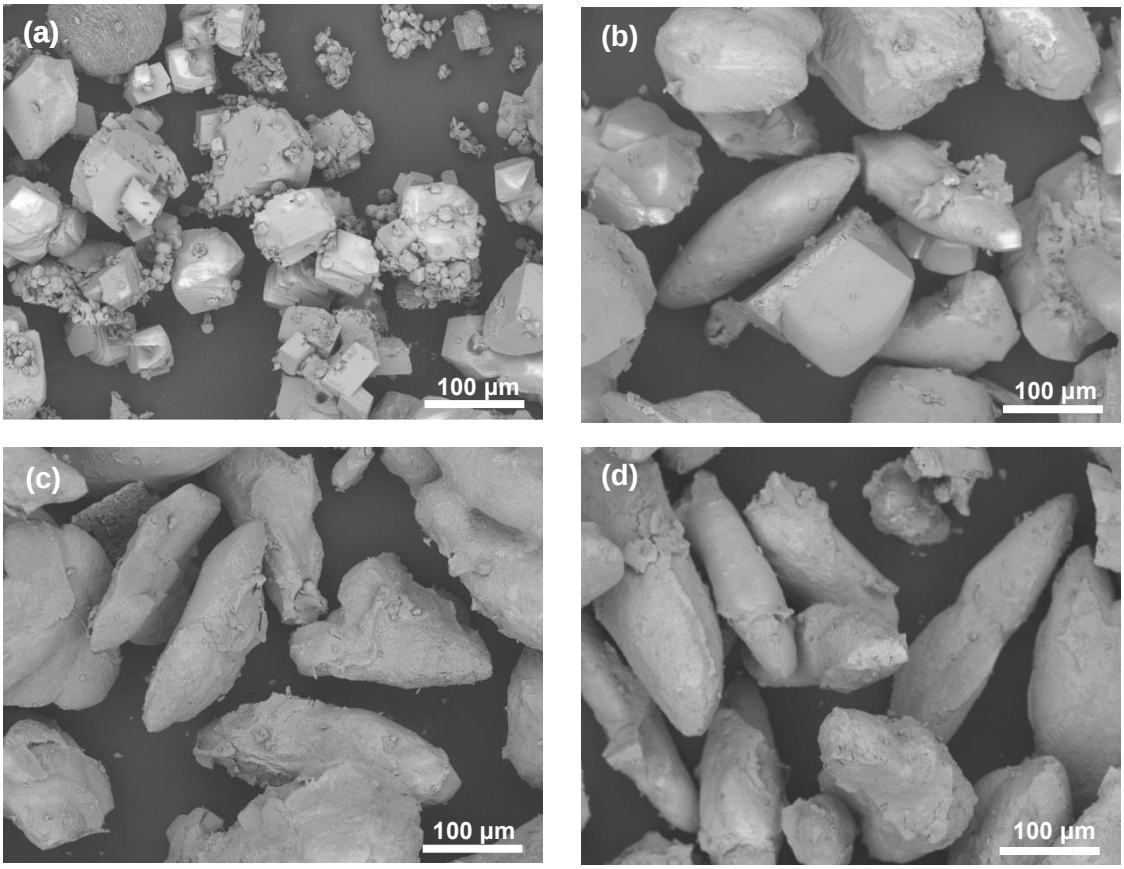

Fig. 2-12 SEM images of $CaCO_3$ precipitated by bacteria (OD_{600} = 0.1) at different poly-L-lysine concentrations: (a) 1 mg/L, (b) 10 mg/L, (c) 30 mg/L, and (d) 50 mg/L.

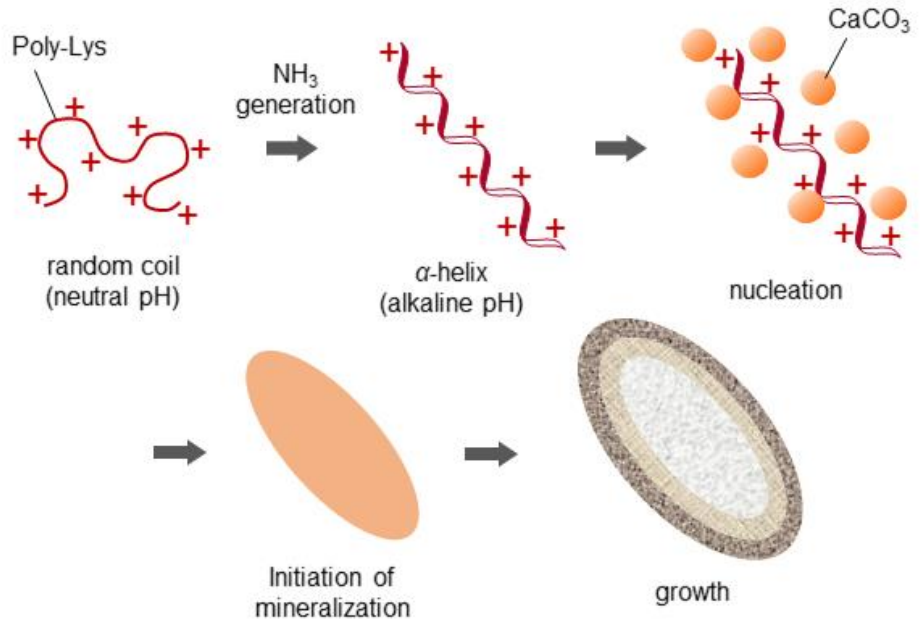

Fig. 2-13 Formation of twin-sphere crystals in presence of poly-L-lysine

2.4.1.1.2. Time course of precipitation with and without poly-L-lysine

Change of the crystal morphology with time in the presence and absence of the poly-L-lysine was observed. SEM images of the samples collected at different time intervals with and without poly-L-lysine are given in Fig. 2-14 and Fig. 2-15. In the case of without poly-L-lysine, initially more spherical vaterite crystals have been formed and it is very clear with in first 6 hours and after that calcite is the main fraction of the precipitate. After 24 hours, precipitate mainly consisted with calcite crystals. Therefore, it is look like bacteria mediated $CaCO_3$ precipitation follow osward rule, where least stable phase of polymorphism has higher solubility and transform into the more stable form with time (Kralj et al., 1994). The transformation process can be occurred following two process. Unstable phase can be transformed into the stable form by following the solid states transition or by following the solution mediated transformation. In solid state transition, internal rearrangement of the crystal lattice occurs. Solution mediated transformation includes dissolution of the unstable phase and re-precipitation as the stable phase (Davey and Cardew, 1986). Without XRD data it is difficult to explain the transformation process of the bacteria mediated precipitation. However, according to the SEM images it is mostly due to the solution mediated transformation.

In case of with poly-L-lysine, crystal morphology started to change to ellipsoidal shape from the beginning and it is difficult to find individual rhombohedral or polyhedron crystals. This provide some evidence that poly-L-lysine provide a backbone for the $CaCO_3$ crystallization and the effect is very rapid. On the other hand, crystal size increased with time and roughness of the crystal surface have been increased. Increment of the roughness is mainly due to the precipitation of polycrystalline particles due to the absorbance of the poly-L-lysine on the crystal surface (Davey and Cardew, 1986).

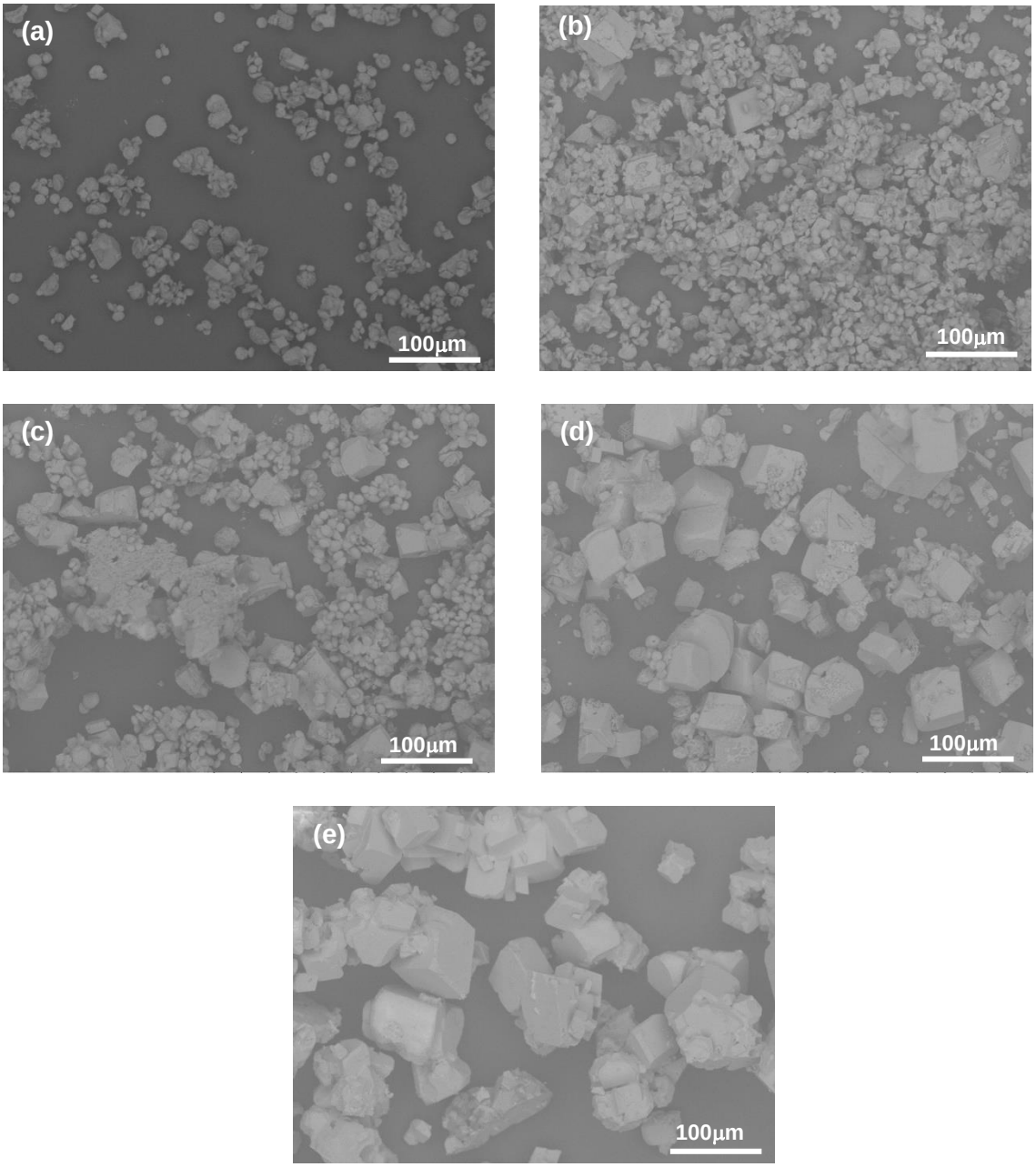

Fig. 2-14 SEM images of $CaCO_3$ precipitated by bacteria (OD_{600} = 0.1) without poly-L-lysine at different time intervals (a) 2 h (b) 4 h (c) 6 h (d) 8 h (e) 24 h

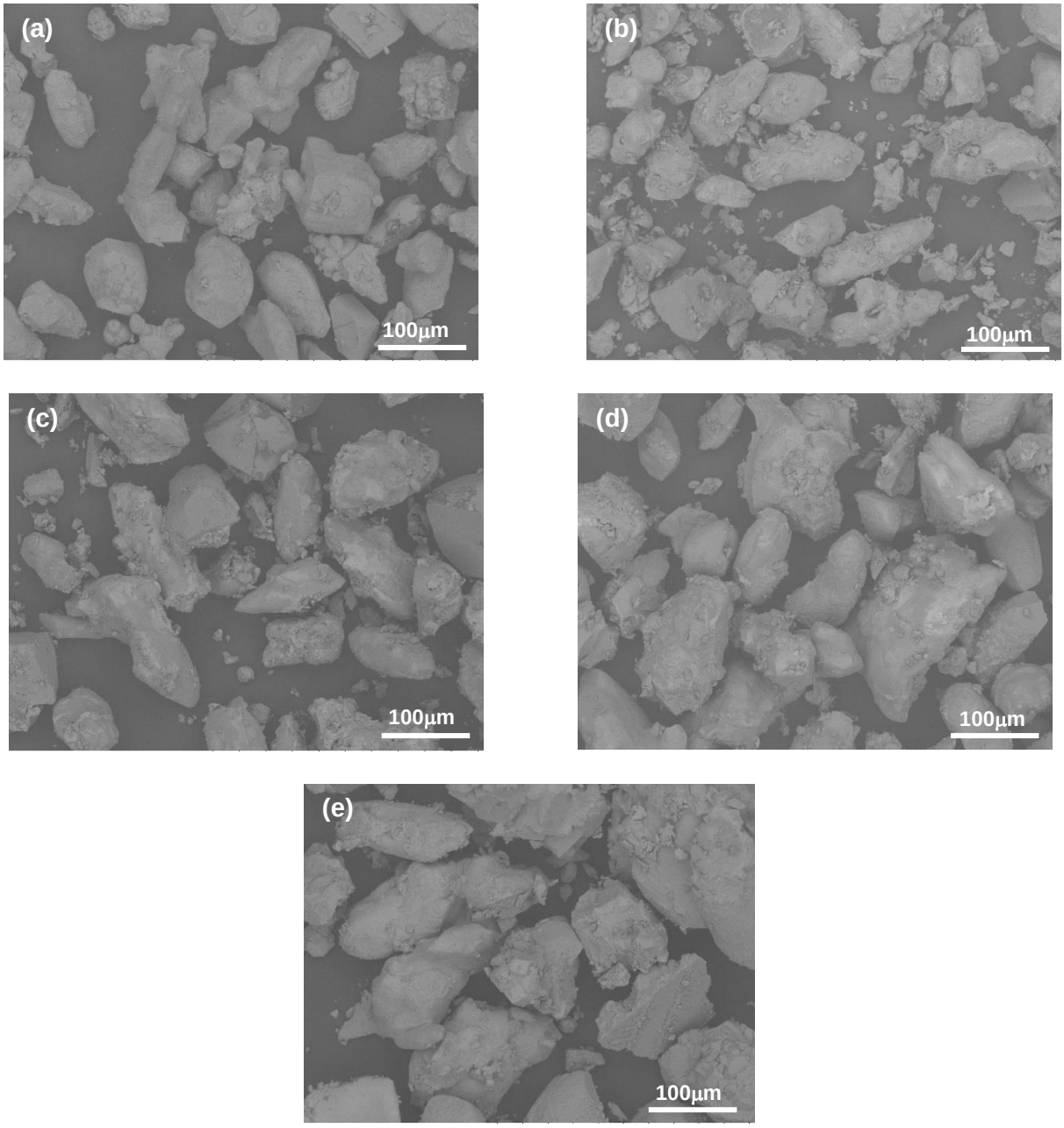

Fig. 2-15 SEM images of $CaCO_3$ precipitated by bacteria (OD_{600} = 0.1) with poly-L-lysine (10 mg/L) at different time intervals (a) 2 h (b) 4 h (c) 6 h (d) 8 h (e) 24 h

2.4.1.1.3. Cytotoxicity of poly-L-lysine on the *Pararhodobactor* sp.

Cytotoxicity of the poly-L-lysine on the *Pararhodobactor* sp. was measured by following the procedure described in the section 2.3.5. Bacteria colonies were detected very clearly after 48 h for the sample without poly-L-lysine. However, for the samples with poly-L-lysine, it took 72 h to appear colonies. For the samples with poly-L-lysine larger number of

smaller colonies were detected after 72 h as shown in Fig. 2-16 (a) compared with sample without poly-L-lysine (Fig. 2-16(b)). Colony forming unit (CFU) was calculated for the each and every case and plotted against the time as shown in Fig. 2-17 (a). Same time, relative CFU was plotted against the time for the different poly-L-lysine concentrations as shown in Fig. 2-17(b).

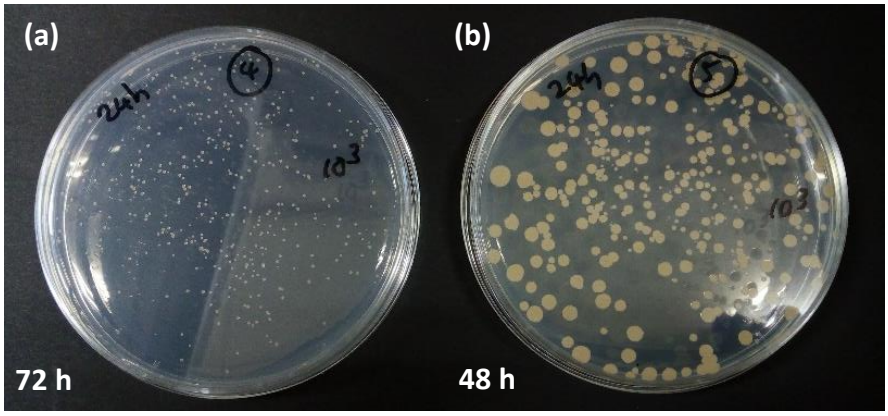

Fig. 2-16 Bacteria colonies of the sample (a) With poly-L-lysine (b) Without poly-L-lysine

According to Fig. 2-17, it can be seen that poly-L-lysine inhibits the growth rate of the bacteria. Inhibition was dominant within first 5 minutes and later maintained approximately same growth rate. However, finally it produced larger number of smaller size colonies than the normal case. May be bacteria need some time to adjust into the environment with poly-L-lysine. This antimicrobial effect of the poly-L-lysine has been reported by some previous researches (Shima et al., 2012; Ye et al., 2013).

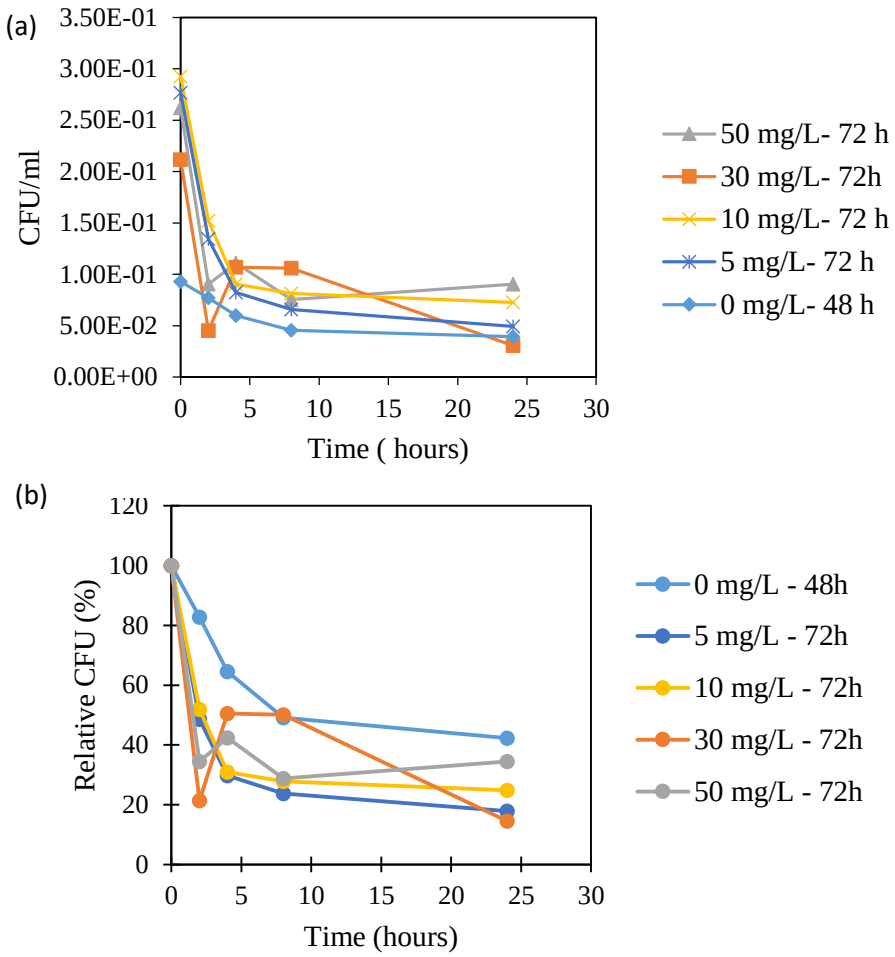

Fig. 2-17 Variation of the CFU with time under different poly-L-lysine concentrations (a) CFU (b) Relative CFU (%)

2.4.1.1.4. Effect of poly-L-lysine on the $CaCO_3$ Crystallization by using urease enzyme

Same set of experiments were conducted by using the extracted urease enzyme. Precipitation tests were conducted by varying the urease concentration in the presence and absence of the poly-L-lysine. Significant increment of the precipitate can be seen by adding poly-L-lysine than the case of without poly-L-lysine as shown in the appendix A (Figure 1). The positive effect of the poly-L-lysine on the $CaCO_3$ crystallization is clearer with urease enzyme than microbial urease. In the case of microbial urease it can contains other kind of proteins and organic matters which can interact with poly-L-lysine (Kawaguchi and Decho, 2002). Therefore, pure effect of the poly-L-lysine on the $CaCO_3$ crystallization couldn't be seen.

Morphology of the crystals changed to ellipsoidal shape aggregates in the presence of poly-L-lysine which is similar to the microbial urease. However, both of the calcite and vaterite

crystals were obtained without poly-L-lysine while only calcite crystals were obtained by microbial urease (appendix A- Figure 3). Formation of this metastable phase of $CaCO_3$ may be due to the higher local supersaturation of the environment which is induced by the urease enzyme (López et al., 2001).

2.4.1.2. Effect of poly-glutamate on the $CaCO_3$ Crystallization by using bacterial urease

Variation of the amount of precipitate with bacteria concentrations in the presence and absence of the poly-glutamate is shown in Fig.2-18

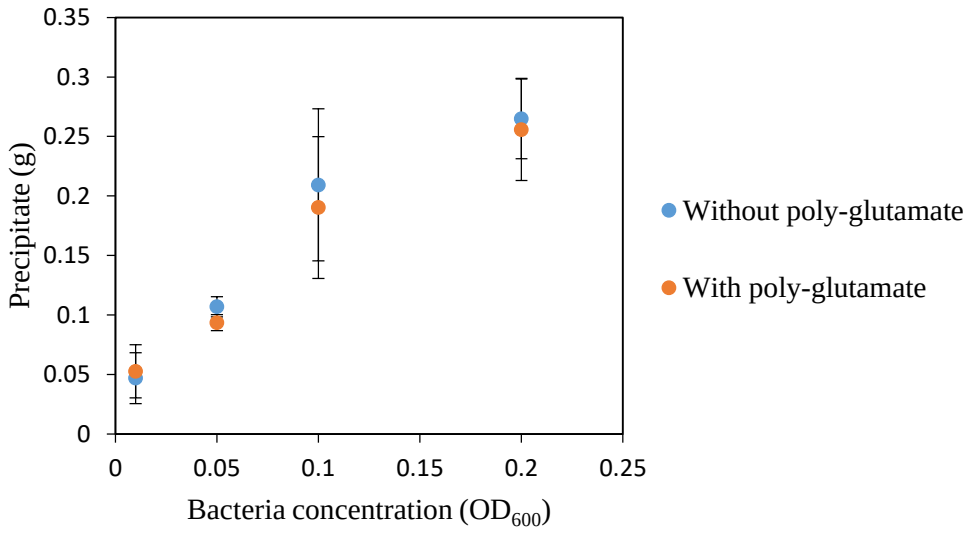

Fig. 2-18 Amounts of precipitate formed at various bacterial concentrations (OD_{600}) with or without addition of poly-glutamate.

Similar to the case with poly-L-lysine, in both of the cases amount of precipitate increased with the increasing bacteria concentration. However, in contrast to the behavior of the poly-L-lysine, significant influence from the poly-glutamate on the $CaCO_3$ crystallization couldn't be seen. It seems to be poly-glutamate inhibited the $CaCO_3$ crystal growth and nucleation. Most of the acidic polypeptides and polyelectrolytes have been inhibited the $CaCO_3$ crystallization (Manoli et al., 2002; Njegić-Džakula et al., 2010; Njegić Džakula et al., 2018; Tong et al., 2003).

In the neutral pH, carboxyl group of the poly-glutamate charged negatively, and it can bind to the positively charged Ca^{2+} ions very effectively. Therefore, it reduces the interaction with the CO_3^{2-} ions in the reaction mixture and reduces the nucleation and growth of the crystals (Tong et al., 2003). And on the other hand, interaction between the carboxylate group of the

acidic polypeptides and the Ca^{2+} ions is coordinative and negatively charged poly anions can bind to the positively charged faces of the crystals and inhibit the growth of the crystals (Njegić-Džakula et al., 2010). Njegić Džakula et al.,(2018) mentioned that retardation of the crystal growth in the presence of acidic polypeptides is related to their adsorption to the specific crystal surface. Further, mentioned that growth of the crystals stops at certain supersaturation, when the distance between the adsorbed molecules smaller than the diameter of the nucleus. In addition, Polowczyk et al., (2016) have been reported the growth inhibition of the $CaCO_3$ in the presence of ovalbumin. Ovalbumin is negatively charged in the neutral pH and it binds strongly in to the Ca^{2+} ions and forms a barrier which preventing the growth of the crystals.

According to the SEM images given in Fig. 2-19, in the presence of poly-glutamate rhombohedral as well as spherical crystals can be seen in the intermediate concentration of the bacteria. However, at higher bacteria concentrations majority is polyhedron type crystals. As mentioned in the section 2.4.1.1, reduction of the crystal size with the increasing of the bacteria concentration can be seen. According to the XRD pattern given in Fig. 2-20, both of the calcite and vaterite peaks can be seen. Hence, spherical crystals in the precipitate can be classified as vaterite. Vaterite is the least stable phase of polymorphism and easily transform into the stable phase of calcite by following the solution mediated-transformation (Kralj et al., 1994). In contrast to the poly-L-lysine, poly-glutamate has capability to stabilize the meta stable phase of $CaCO_3$ and the effect is clearer in higher poly-glutamate concentrations as shown in Fig. 2-21.

Formation of vaterite depends on the several factors such as supersaturation of the solution, reaction rate, reaction temperature, presence of organic/inorganic additives etc. (Jiménez-López et al., 2002). Among them supersaturation is the main governing factor for the formation of vaterite crystals and at higher supersaturation most soluble and least stable form of polymorphism form first (Jiménez-López et al., 2002; Trushina et al., 2015). Negatively charged carboxyl group in the poly-glutamate can be bound to the Ca^{2+} in the solution easily and formed a large-scale local supersaturation in the vicinity which led to formation of the meta stable form of polymorphism. The effect is clearer for higher poly-glutamate concentrations due to higher concentration of negatively charged carboxyl groups which led to form higher fraction of the unstable vaterite than the calcite phase.

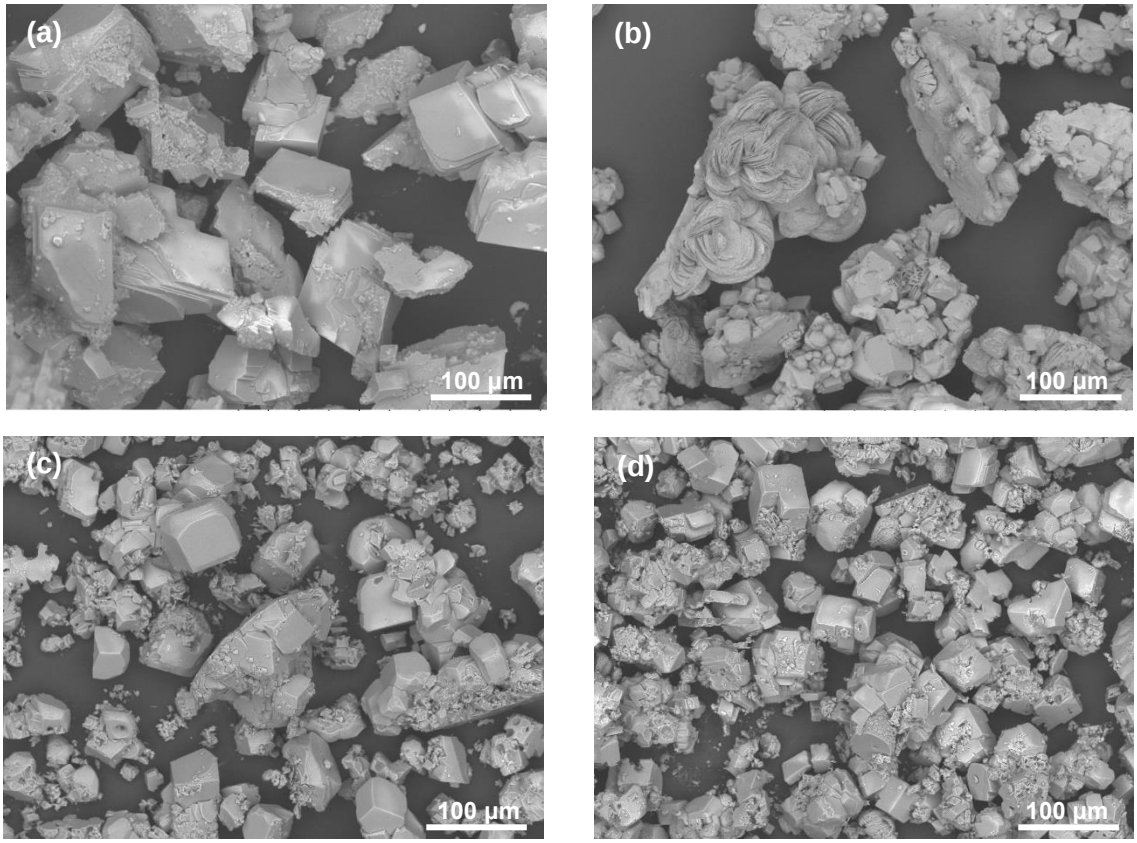

Fig. 2-19 SEM images of $CaCO_3$ precipitates at various bacterial concentrations with poly-glutamate (10 mg/L): (a) OD_{600} = 0.01, (b) OD_{600} = 0.05, (c) OD_{600} = 0.1, and (d) OD_{600} = 0.2.

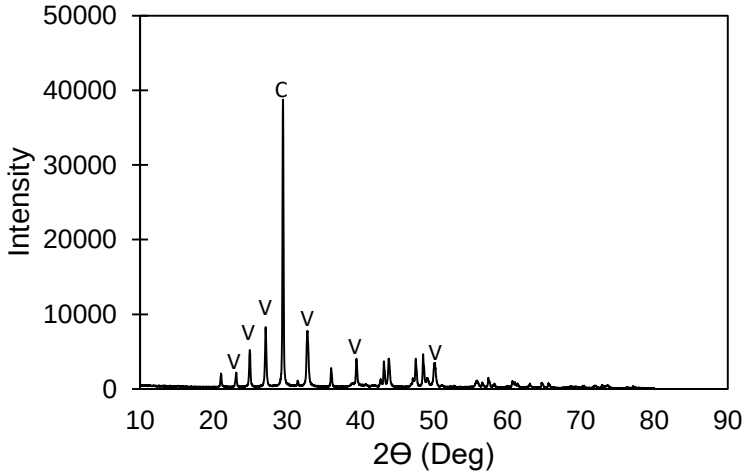

Fig. 2-20 XRD patterns of $CaCO_3$ precipitates with poly-glutamate

Although, supersaturation affects to the formation of vaterite crystals it can be transformed to the calcite by following the solution mediated transformation. However, organic materials have capability to stabilize vaterite crystals without transforming into the calcite (Trushina et al., 2015). Njegić-Džakula et al., (2010) mentioned that solution mediated transformation of precipitate can be retarded as a result of crystal growth and/or dissolution inhibition of the stable and metastable phases and nucleation of the stable phase can be completely inhibited in higher concentration of additives. Fig. 2-22 illustrate the inhibition of the solution mediated transformation in the presence of organic additives.

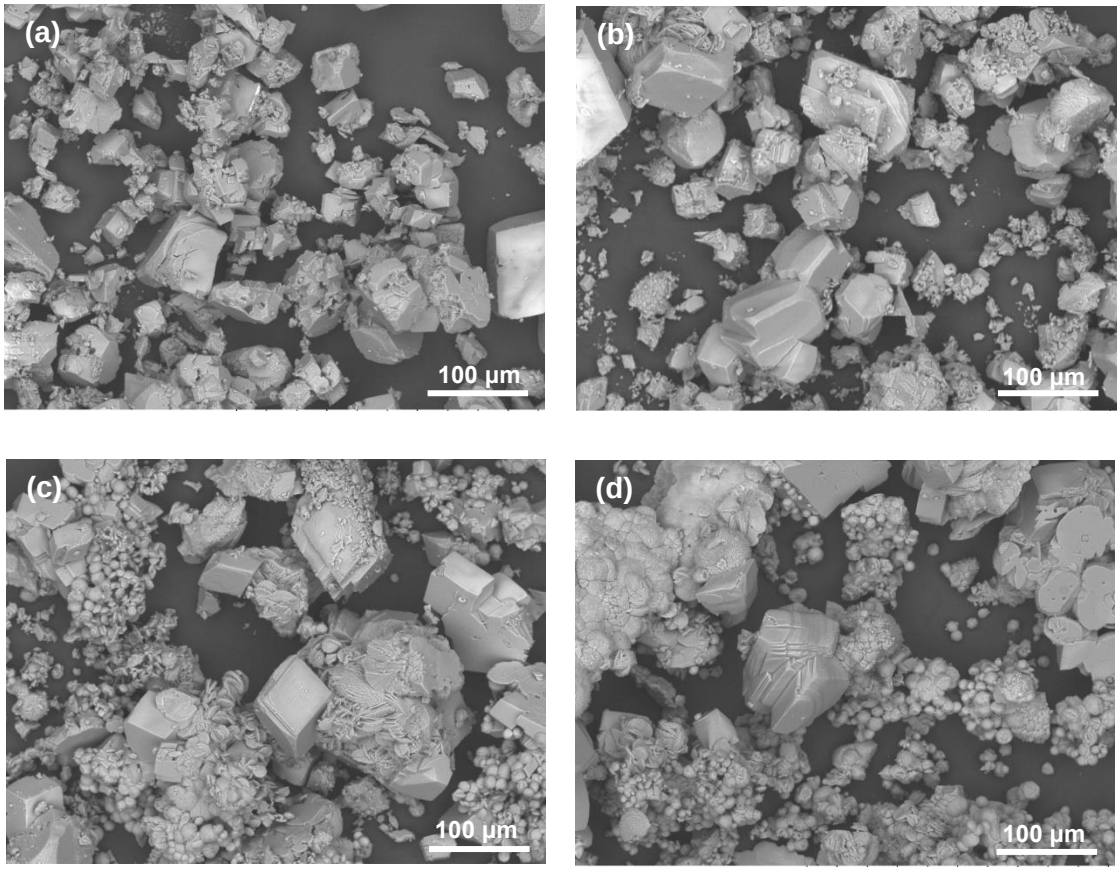

Fig. 2-21 SEM images of $CaCO_3$ precipitated by bacteria (OD_{600} = 0.1) at different poly-glutamate concentrations: (a) 1 mg/L, (b) 10 mg/L, (c) 30 mg/L, and (d) 50 mg/L.

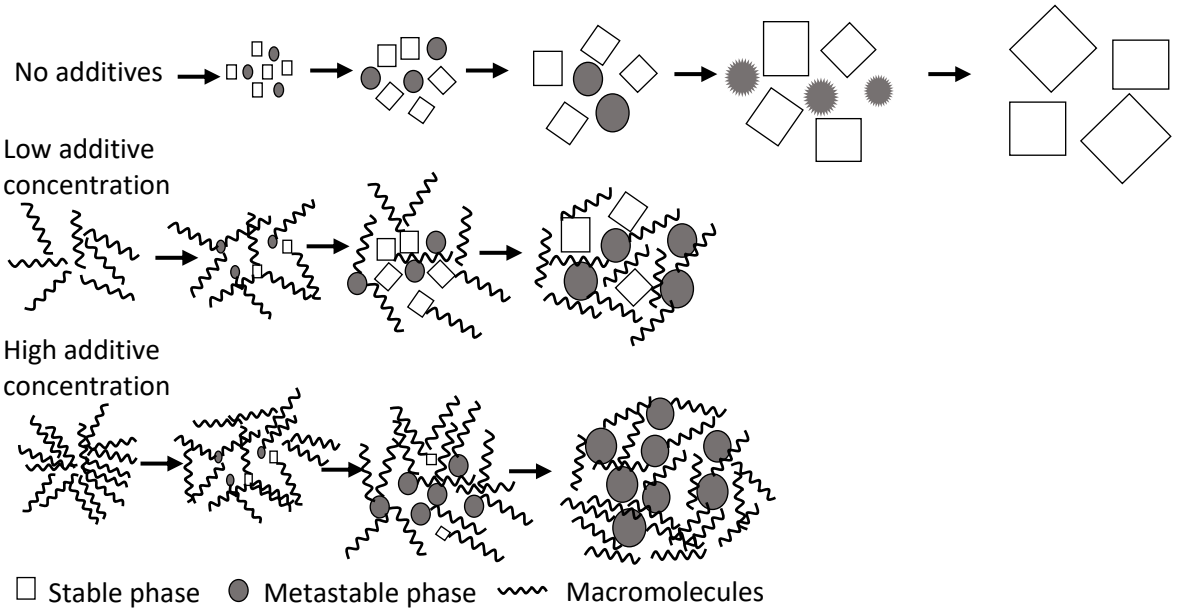

Fig. 2-22 Stabilization of the metastable phase of $CaCO_3$ in the presence of organic additives (Regenerated by using original figure generated by Dzakula et al.,2010)

2.4.1.2.1. Effect of poly-glutamate on the $CaCO_3$ Crystallization by using urease enzyme

Similar to the poly-L-lysine, effect of the poly-glutamate on the $CaCO_3$ crystallization was investigated by using the purified urease enzyme (Jack bean urease). Results are much similar to the results obtained by using the microbial urease. Results are attached in the Appendix B. Significant difference cannot be seen between the cases with and without poly-glutamate and it is look like poly-glutamate acts as an inhibitor to $CaCO_3$ crystals to nucleate and growth. Reason behind the inhibitory effect explained previously. According to the SEM images, without poly-glutamate both of the rhombohedral shape calcite crystals and spherical shape vaterite crystals were obtained. With poly-glutamate, precipitate mostly contained spherical shape vaterite crystals and it is seemed to be vaterite fraction decreased with the increasing urease concentration. Poly-glutamate actually functioned as an inhibitor for $CaCO_3$ crystallization and have an ability to stabilize the metastable phase of polymorphism by inhibiting solution mediated transformation.

2.4.2. Effect of the synthetic polypeptides on the sand densification

Since poly-glutamate has a negative effect on the $CaCO_3$ crystallization, sand solidification experiments were conducted only for the poly-L-lysine to check the effects of the

cationic polypeptides on the loose sand densification. Experiments were conducted for different types of sands.

2.4.2.1. Sand solidification for Mikawa sand

Mikawa sand classified as poorly graded silica sand with the particle diameter of 0.87 mm. Experiments were conducted for different bacteria injection intervals and every three days Ca^{2+} ion concentration and the pH of the effluent were measured. Variation of the effluent pH and the Ca^{2+} ion concentration with time for different samples are given in Fig. 2-23. During the first few days negligible amount of $Ca^{2+}$was detected in the effluent in all the samples. After 7 days Ca^{2+} ion concentration gradually increased for the samples without reinjecting of the bacteria (S1 and S2). However, samples with the reinjection of the bacteria could be maintained the low effluent Ca^{2+} ion concentration up to 12 days. Lower Ca^{2+} ion concentration in the effluent (S3 and S4) reflects that more Ca^{2+} was deposited as $CaCO_3$ in the sand column. In contrast, higher Ca^{2+} ion concentration in the effluent in the system without reinjecting of bacteria indicating insufficient consumption of Ca^{2+} ions and low precipitation of $CaCO_3$.

Similarly, pH of the effluent for the samples without reinjecting of the bacteria (S1 and S2) decreased after 7 days. However, samples with the reinjection of the bacteria could be maintained the approximately constant pH value up to 12 days and after that started to decline. During the urea hydrolysis by urease, the pH of the solution increases because of ammonia formation. Hence, when the urease activity is high, pH of the effluent also exhibited a higher value. However, urease activity of the bacteria decreased with time due to the deactivation of the bacteria. During the microbially induced carbonate precipitation, bacteria cells themselves act as nucleation sites for $CaCO_3$ deposition and leading to gradual reduction of the bacteria urease activity (DeJong et al., 2010). Reinjection of the bacteria helped to maintain the active cell density and therefore higher pH value could be maintained. On the other hand, pH influences the urease activity of the bacteria drastically. For *Pararhodobactor* sp., a significant loss of activity is seen under acidic ($pH < 5$) and alkaline ($pH > 10$) conditions, and the activity is maximum at around pH 8 (Fujita et al., 2017). Hence, for efficient precipitation of $CaCO_3$, it is important to maintain the pH around 7-8. By reinjecting of the bacteria, urease activity could be recovered, and efficient precipitation could be achieved. Fig.2-24 shows the solidified sand specimens before and after the UCS measurements.

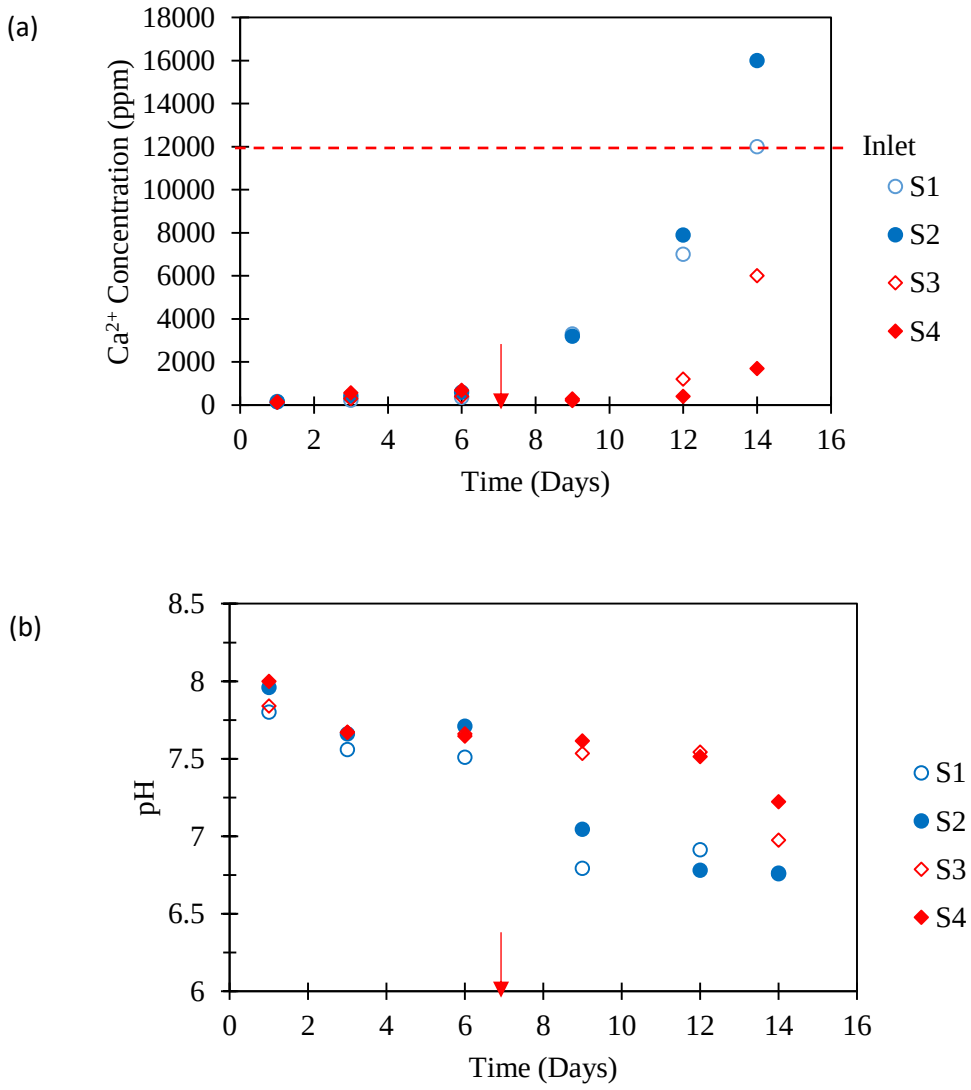

Fig. 2-23 Time courses of (a) Ca^{2+} concentration and (b) pH of effluent in sand solidification tests. (Arrows indicate the time of bacteria reinjection to the sand specimens.)

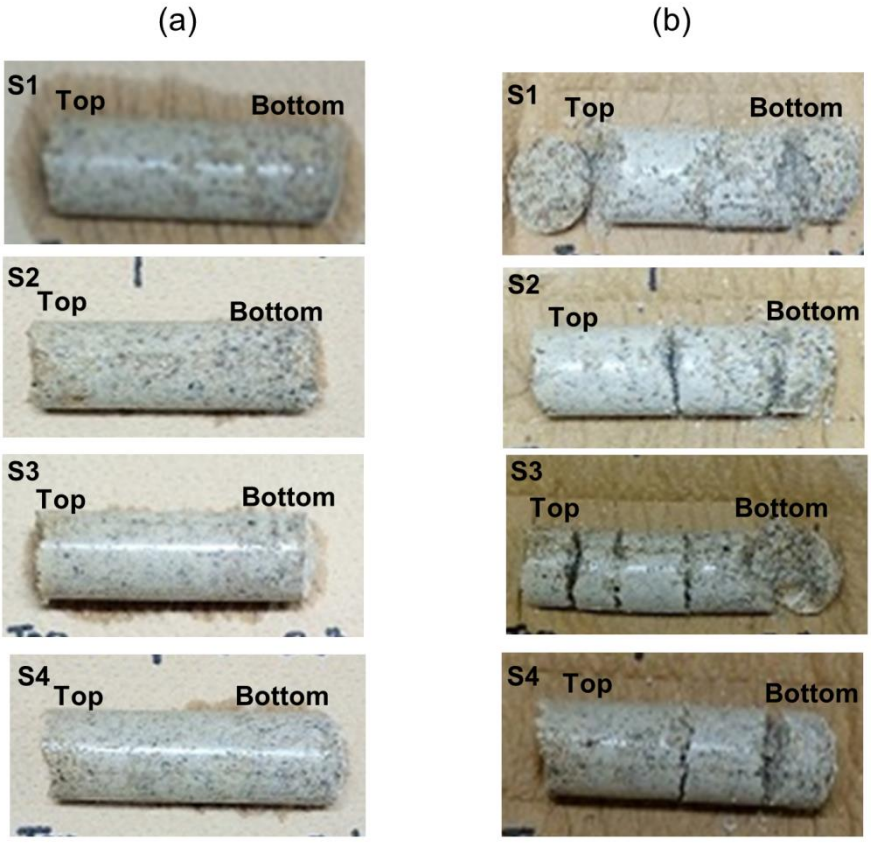

Fig. 2-24 Solidified sand specimens after 14 days (a) before UCS measurements and (b) after UCS measurements.

Estimated UCS values for the solidified sand specimens after 14 days curing are given in Fig. 2-25. According to the classification system proposed by Shafii and Clough, all the sand specimens can be classified as strongly cemented (Rab and Clough, 1982). In this classification system, the cemented soils with UCS value between 1−3 MPa are classified as strongly cemented soil and a UCS value greater than 3 MPa are classified as soft rocks.

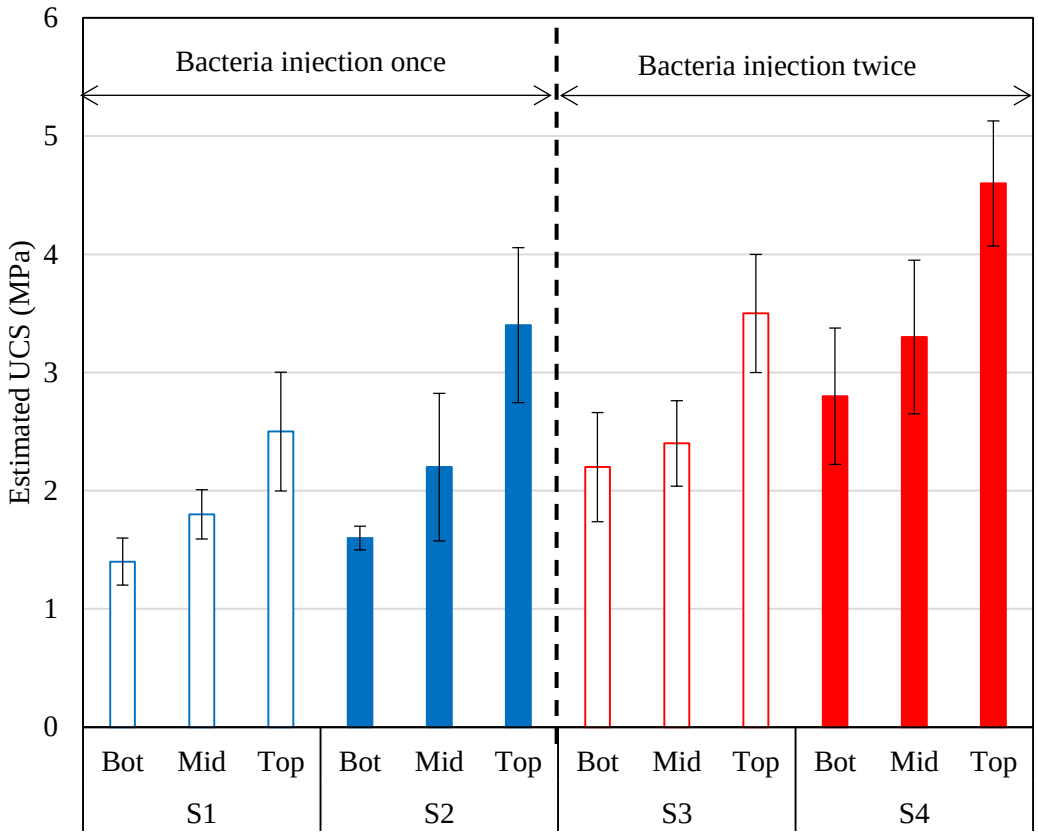

Fig. 2-25 Estimated UCS values of solidified sand specimens (Mikawa Sand).

For all cases, it can be seen that the strength of the sand column decreased from top to bottom. This may be due to the higher urease activity near the inlet, caused by accumulation of the bacteria near the injection point. Oxygen concentration in the vicinity play a significant role in the activity of the *Pararhodobacter* sp. since it is an aerobic bacterium. Therefore, strength of the sand column decreased from top to bottom due to the lower bacterial activity caused by the lack of the oxygen in the bottom of sand column (Khan et al., 2015).

Even distribution of the bacterial activity throughout the sand column is required to obtain a homogeneous sample. To achieve a uniform distribution of the bacteria throughout the sand column, it is important to control the injection rate of the cementation fluid appropriately. At a low injection rate, immediate cementation can occur near the injection point. Increases the flow rate beyond the rate of urea consumption, and precipitation will lead to a uniform distribution of chemicals along the pathway (Mortensen et al., 2011).

Reinjection of the bacteria led to increase the strength of the sand column significantly than the case without reinjection. Reinjection of bacteria after 7 days effectively maintained a high urea hydrolysis rate, which directed to higher $CaCO_3$ precipitation and higher UCS. In

addition, number of other factors can cause a decrease in urease activity over long time periods, e.g., encapsulation of bacteria as a result of precipitation or being trapped inside pores, a reduction in chemical transport (nutrients) through pore spaces because of precipitation, and space limitations caused by saturation of pore fluids and accumulation of metabolic wastes (Al Qabany et al., 2011; van Paassen, 2009).

Behavior of the poly-L-lysine on the sand solidification is very attractive. By adding poly-L-lysine strongly cemented sand column with higher UCS value could be obtained than the conventional case. In sand solidification, to achieve a good strength pore spaces between the sand particles should be filled efficiently. Also, forming a better bridge between the sand particles also important for preventing movement of sand grains and improving strength and stiffness of the specimen (Harkes et al., 2009). Cell adhesion property of the poly-L-lysine assisted to form a better and efficient bridge between the sand particles. Generally, bacteria cells have a negatively charged cell surface and sand particles have a negative charge due to the dissociated silanol groups ($–SiO^-$). Therefore, repulsive force existing between the sand particles and the bacteria cells. Positively charged poly-L-lysine can acts as a binder and attach bacterial cells to sand particles, which would promote efficient cementation.

Several other factors also affect to the adsorption of the bacteria on the sand particles such as ionic strength of the solution and the salinity of the bacterial suspension. The collision efficiency increases with increasing ionic strength of the solution, and adsorption of bacteria can be increased by increasing the salinity of the bacterial suspension (Foppen and Schijven, 2005; Harkes et al., 2009). Poly-L-lysine helps to increase the ionic strength of the solution and improves the adsorption of the bacteria on sand particles which assisted to have a better cementation. According to the SEM images shown in Fig. 2-26, it can be seen that in the absence of the poly-L-lysine cementation mainly occurred at the contact point while in the presence of the poly-L-lysine, sand particle are fully covered with the $CaCO_3$ crystals and better bridge between the sand particles are formed. Therefore, this provides an evidence that poly-L-lysine can act as a binder and it facilitates the adsorption of the bacteria cells into the sand particles.

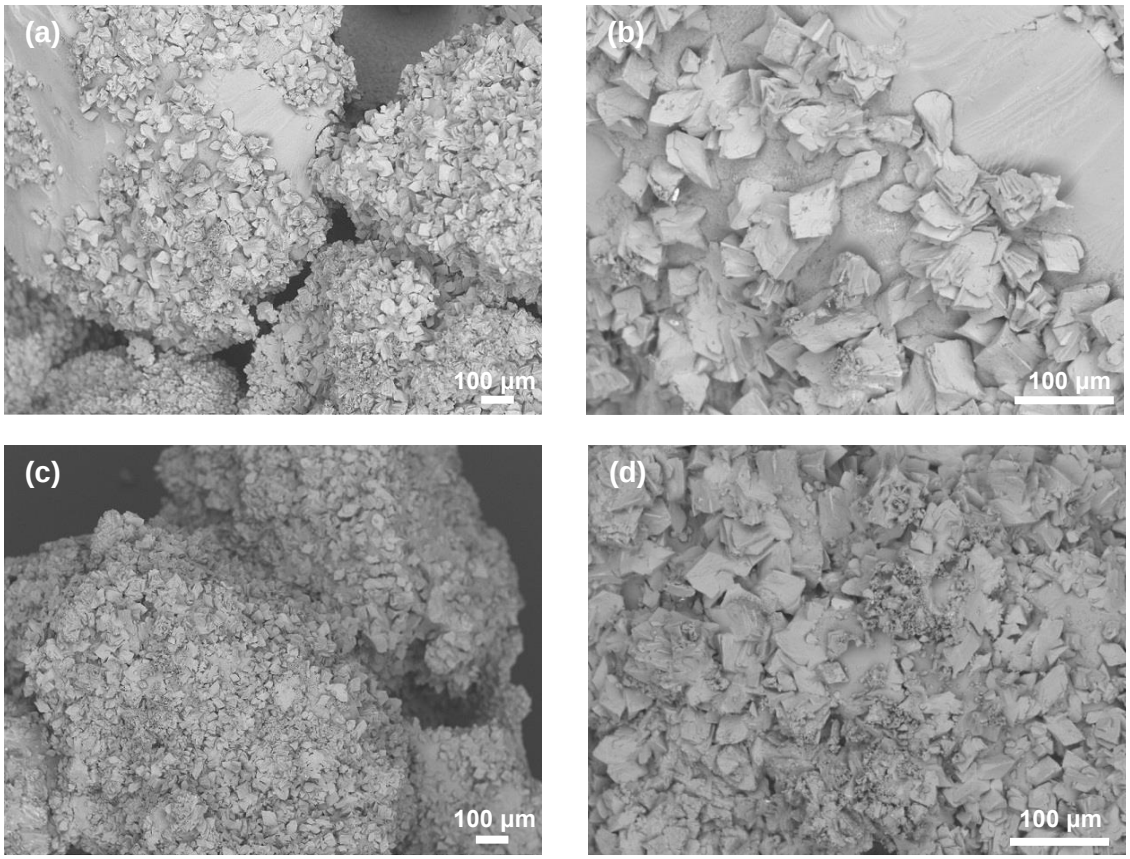

Fig. 2-26 SEM images of cemented sand samples: without poly-L-lysine (a,b) and with poly-L-lysine (c,d).

Determination of the amount of precipitated $CaCO_3$

Amount of precipitated $CaCO_3$ in solidified samples were measured by using the calcimeter. Precipitated amount of $CaCO_3$ is shown in Fig. 2-27 with the estimated UCS values.

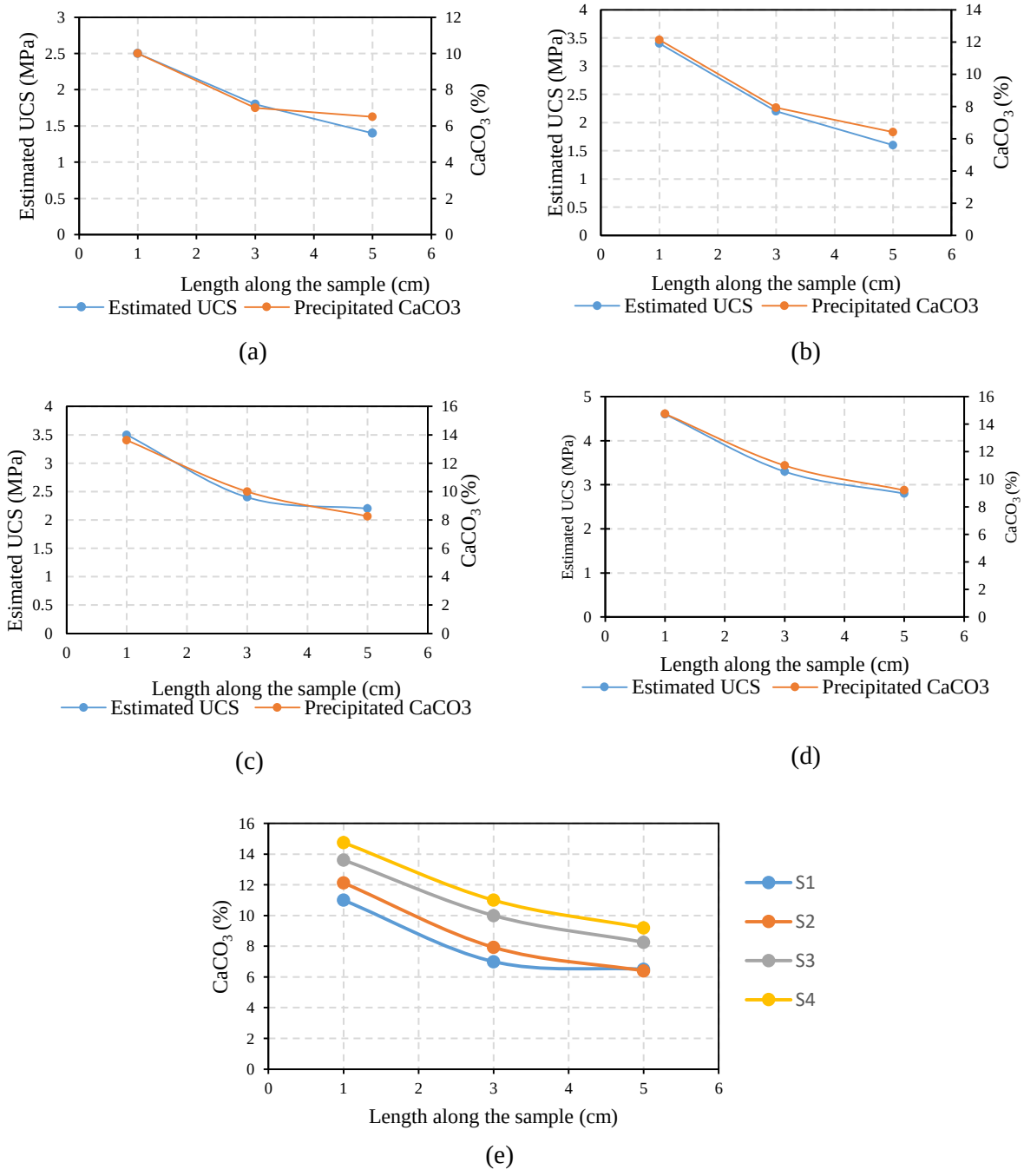

Fig. 2-27 Variation of the amount of precipitated $CaCO_3$ and UCS along the sand column (a) S1(b) S2 (c) S3 (d) S4 (e) Comparison of the precipitated $CaCO_3$ between all samples

According to the obtained results given in Fig. 2-27(a-d), in all the cases precipitated amount of $CaCO_3$ is directly related to the estimated UCS value. Similarly, in previous studies also reported the relationship between the estimated UCS value and the precipitated $CaCO_3$ (Amarakoon and Kawasaki, 2017; Danjo and Kawasaki, 2016a). The results revealed that amount of precipitated $CaCO_3$ is the main governing factor of the UCS value. Also, according to the Fig. 2-27(d) it can be seen that by adding poly-L-lysine, precipitated $CaCO_3$ have been increased. Therefore, poly-L-lysine assisted to efficient precipitation of $CaCO_3$ which led to achieve better cementation and higher strength than the conventional MICP method.

2.4.2.2. Sand solidification for Toyoura sand

Compared with the Mikawa sand, Toyoura sand is fine grained sand with the particle diameter of 0.2 mm. Fig. 2-28 shows the estimated UCS values for the Toyoura sand specimens with and without poly-L-lysine under different bacteria injection intervals. Similar to the case of Mikawa sand, strength of the solidified sand samples getting decreased along the sample length and in both of the cases, maximum strength was obtained at the top of the sample. But in contrast to the case of Mikawa sand significant effect from the reinjection of the bacteria couldn't be seen. One of the main disadvantage of the MICP process is, it is not efficient with the fine grained soils. Fragaszy et al., (2011) mentioned that MICP is more compatible with the sand with particle size of 0.3-5 mm.

If pore spaces are smaller compared with the size of the bacteria, even distribution of the bacteria suspension couldn't be expected and mostly accumulated at the top of the sand specimen and give only harder top surface. Similarly, very harder top surface could be obtained by adding poly-L-lysine than the conventional MICP method. SEM images of the solidified sand specimens with and without poly-L-lysine are given in Fig. 2-29 and poly-L-lysine have been assisted to form better bridge between the sand particles. This results again revealed that the positive effect of the poly-L-lysine on sand solidification. Also, it can be a good additive for MICP mainly for surface treatment such as for erosion prevention and other surface stabilizing projects.

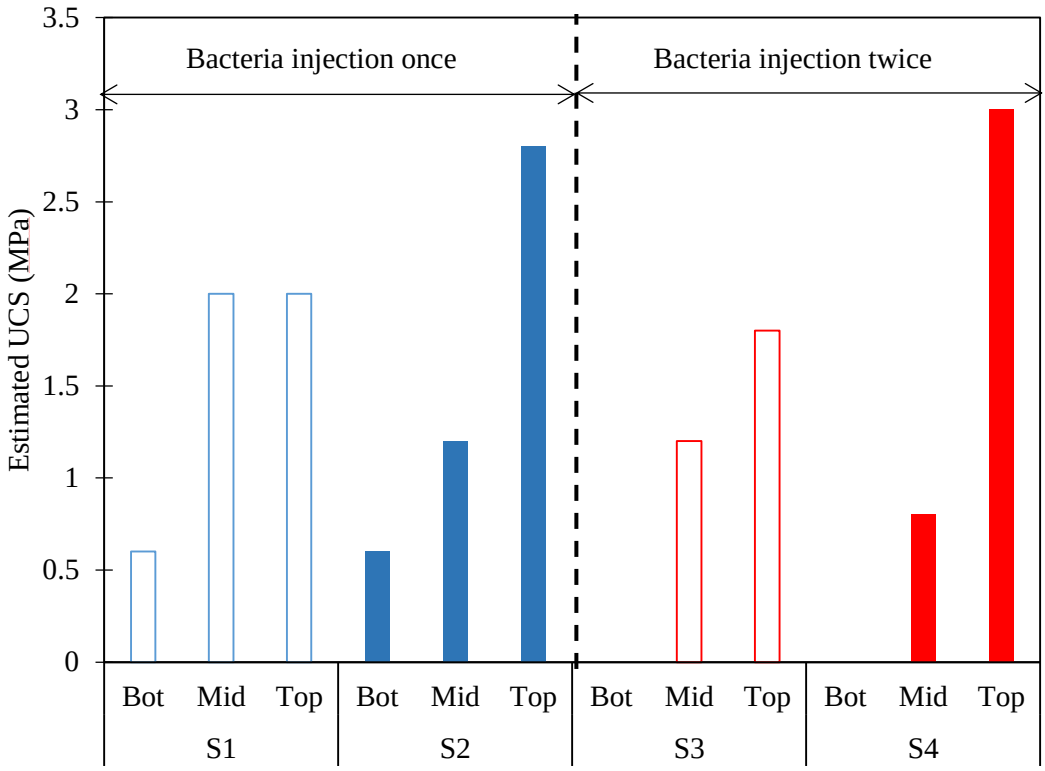

Fig. 2-28 Estimated UCS values of solidified sand specimens (Toyoura sand)

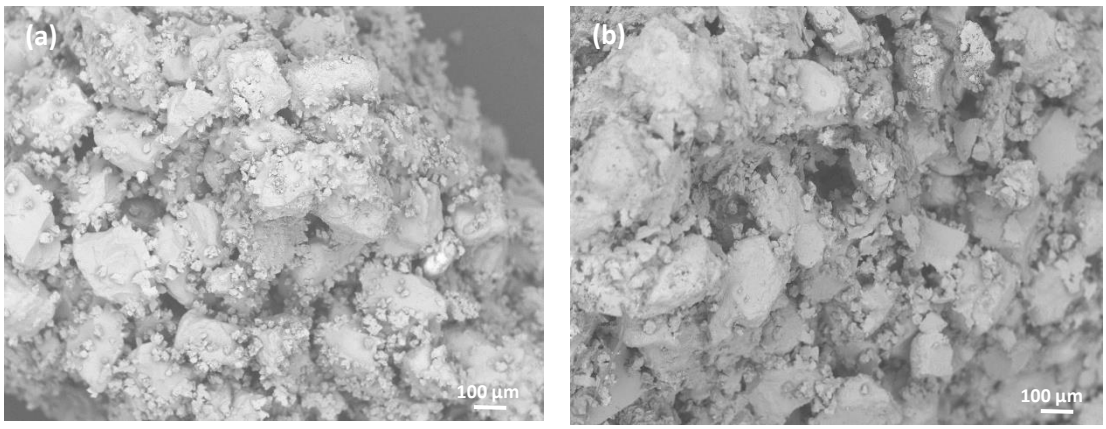

Fig. 2-29 SEM images of cemented sand samples: (a) without poly-L-lysine (b) with poly-L-lysine

2.4.2.3. Control experiments

Two control samples were analyzed without bacteria. Most interesting finding is sample with poly-L-lysine and cementation solution could be solidified even without bacteria. Significant solidification could be seen at the top of the sample as shown in Fig. 2-30 and sample without poly-L-lysine couldn't give any solidification. According to the SEM images given in Fig. 2-31, calcite like crystals have been precipitated. It is look like poly-L-lysine acts as a template to crystals to nucleate and growth. Even without bacteria, $CaCO_3$ have been deposited by chemical precipitation between the $NaHCO_3$ and $CaCl_2$.

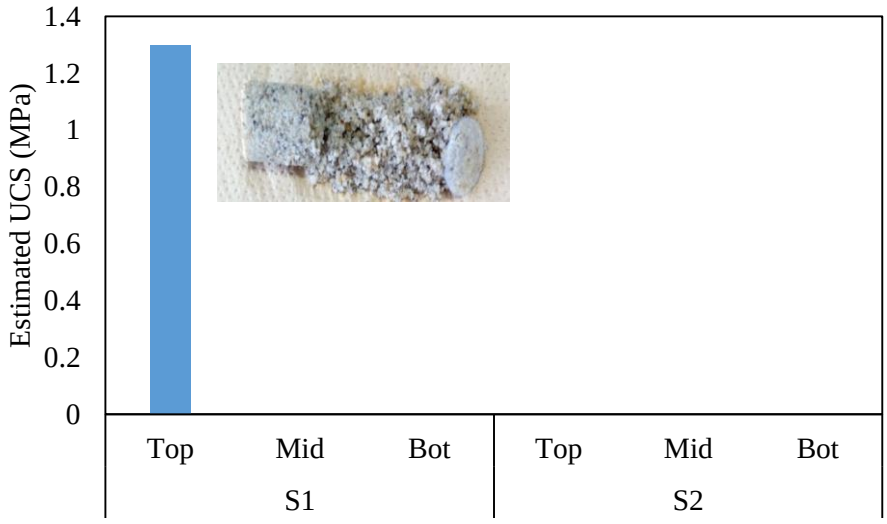

Fig. 2-30 Estimated UCS values of sand specimens without bacteria

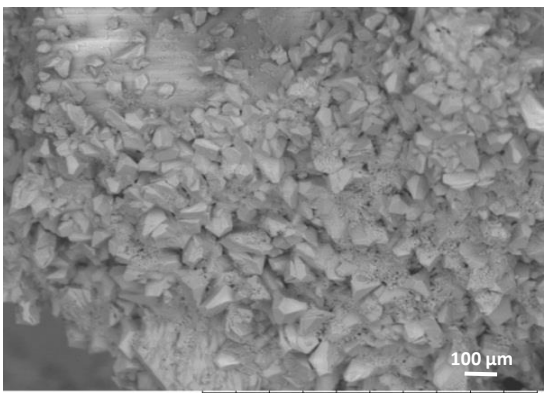

Fig. 2-31 SEM image of the solidified sand specimen with poly-L-lysine and without bacteria

2.4.2.4. Fixation of bacteria on the sand surface in the presence of poly-L-lysine

As mentioned earlier, poly-L-lysine acts as a binder to attach bacteria cells into the sand surface. To prove this hypothesis number of bacteria in the out let of the sand solidification experiment were investigated in the cases of with and without poly-L-lysine. Out let collected from the 2nd day was inoculated in the Zobell 2216E agar plates and checked the number of colonies after 3 days. According to the observations, higher number of colonies were detected for the sample without poly-L-lysine while with poly-L-lysine lower number of colonies were detected as shown in Fig. 2-32.

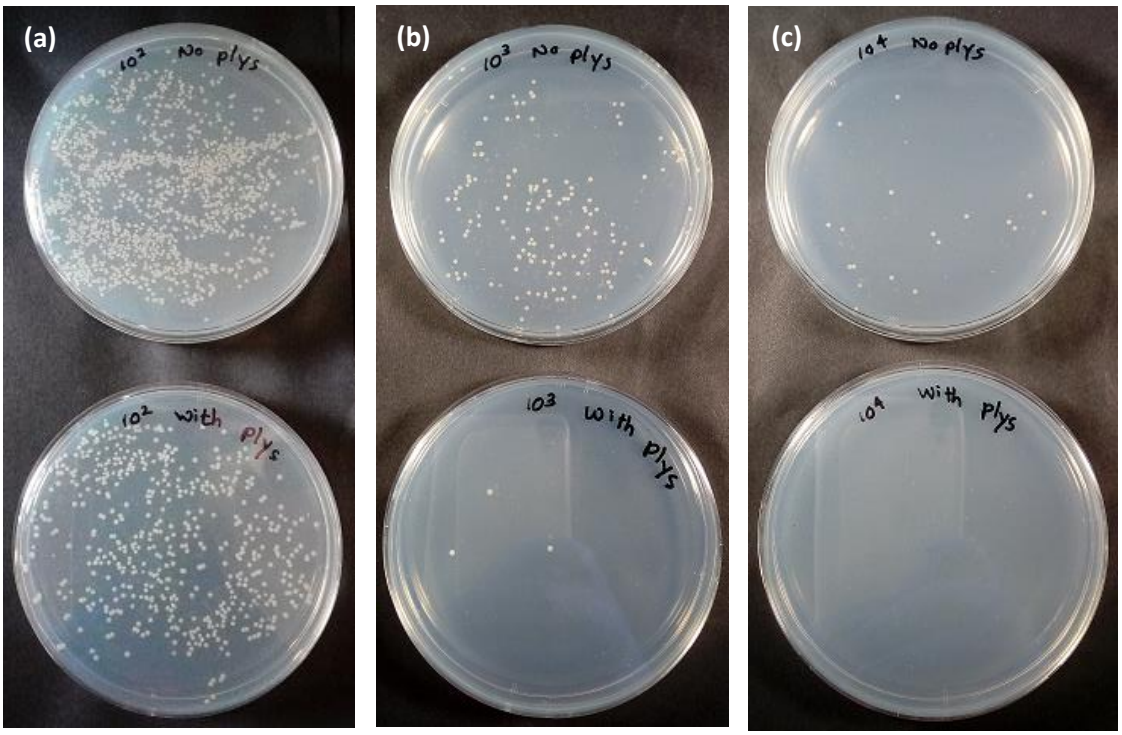

Fig. 2-32 Bacteria colonies in the outlet of the solidification experiment with and without poly-L-lysine with dilution (a) 10^2 (b) 10^3 (c) 10^4

Detection of the lower number of colonies in the presence of poly-L-lysine reflects that the higher absorbance of the bacteria cells into the sand particles. Hence, lower number of bacteria cells were washed out through the outlet.

2.5. Conclusion

Effects of the synthetic polypeptides on the $CaCO_3$ crystallization and sand densification was examined by using the MICP process. Precipitation experiments were conducted with and without polypeptides under different experimental conditions. Investigations were done separately by using a cationic polypeptide; poly-L-lysine and an anionic polypeptide; poly-glutamate.

It was found that poly-L-lysine has positive effect on the $CaCO_3$ crystallization while poly-glutamate has negative effect. Higher amount of precipitate could be obtained by adding poly-L-lysine than that of without polymer. With poly-L-lysine, morphology of the crystals changed drastically into ellipsoidal shape aggregates. Formation of the ellipsoidal shape crystals is mainly due to the conformational change of the poly-L-lysine chain under the alkaline condition.

One of the most interesting finding is the positive effect of the poly-L-lysine on sand solidification. By adding poly-L-lysine strongly cemented sand specimen with higher UCS value could be obtained than without adding poly-L-lysine. Adhesion property of the positively charged poly-L-lysine play a vital role to adsorb negatively charged bacteria cells into the negatively charged sand particles and form a better bridge between the sand particles.

Significant effect from the poly-glutamate on $CaCO_3$ crystallization couldn't be seen and poly-glutamate inhibited the nucleation and growth of $CaCO_3$ by capturing Ca^{2+} ions by negatively charged carboxylic group. Also, poly-glutamate inhibited the solution mediated transformation of the unstable phase and stabilized the metastable phase of polymorphism. Therefore, with poly-glutamate vaterite crystals were dominant.

References

Al Qabany, A., Soga, K., Santamarina, C., 2011. Factors Affecting Efficiency of Microbially Induced Calcite Precipitation. J. Geotech. Geoenvironmental Eng. 138, 992–1001. https://doi.org/10.1061/(asce)gt.1943-5606.0000666

Asli, M.M., Pourdeyhimi, B., Loboa, E.G., 2012. Release Profiles of Tricalcium Phosphate Nanoparticles from Poly(L-lactic acid) Electrospun Scaffolds with Single Component, Core-Sheath, or Porous Fiber Morphologies: Effects on hASC Viability and Osteogenic Differentiation. Macromol. Biosci. 12, 893–900. https://doi.org/10.1002/mabi.201100470

Bágel'ová, J., Gažová, Z., Valušová, E., Antalik, M., 2001. Conformational stability of ferricytochrome c near the heme in its complex with heparin in alkaline pH. Carbohydr. Polym. 45, 227–232. https://doi.org/10.1016/S0144-8617(00)00253-8

Bonduelle, C., 2018. Secondary structures of synthetic polypeptide polymers. Polym. Chem. 9, 1517–1529. https://doi.org/10.1039/c7py01725a

Danjo, T., 2016. a Study of the Formation Mechanism of Beachrock in Okinawa, Japan: Toward Making Artificial Rock. Int. J. Geomate 5, 634–639. https://doi.org/10.21660/2013.9.3157

Danjo, T., Kawasaki, S., 2016. Microbially Induced Sand Cementation Method Using *Pararhodobacter* sp. Strain SO1, Inspired by Beachrock Formation Mechanism. Mater. Trans. 57, 428–437. https://doi.org/10.2320/matertrans.m-m2015842

Davey, R.J., Cardew, P.T., 1986. Rate controlling processes in solvent-mediated phase transformations. J. crysta. 79, 648–653.

DeJong, J.T., Mortensen, B.M., Martinez, B.C., Nelson, D.C., 2010. Bio-mediated soil improvement. Ecol. Eng. 36, 197–210. https://doi.org/10.1016/j.ecoleng.2008.12.029

Foppen, J.W.A., Schijven, J.F., 2005. Transport of *E. coli* in columns of geochemically heterogeneous sediment. Water Res. 39, 3082–3088. https://doi.org/10.1016/j.watres.2005.05.023

Fragaszy, R.J., Santamarina, J.C., Amekudzi, A., Assimaki, D., Bachus, R., Burns, S.E., Cha, M., Cho, G.C., Cortes, D.D., Dai, S., Espinoza, D.N., Garrow, L., Huang, H., Jang, J., Jung, J.W., Kim, S., Kurtis, K., Lee, C., Pasten, C., Phadnis, H., Rix, G., Shin, H.S., Torres, M.C., Tsouris, C., 2011. Sustainable development and energy geotechnology - Potential roles for geotechnical engineering. KSCE J. Civ. Eng. 15, 611–621. https://doi.org/10.1007/s12205-011-0102-7

Fujita, M., Nakashima, K., Achal, V., Kawasaki, S., 2017. Whole-cell evaluation of urease

activity of *Pararhodobacter* sp. isolated from peripheral beachrock. Biochem. Eng. J. 124, 1–5. https://doi.org/10.1016/j.bej.2017.04.004

Harkes, M.P., van Loosdrecht, M.C.M., Booster, J.L., Whiffin, V.S., van Paassen, L.A., 2009. Fixation and distribution of bacterial activity in sand to induce carbonate precipitation for ground reinforcement. Ecol. Eng. 36, 112–117. https://doi.org/10.1016/j.ecoleng.2009.01.004

Hiraki, J., Yanagimoto, Y., Kimura, S., Hiraki, J., Seki, H., Seki, H., Uohama, K., Ichikawa, T., Ninomiya, S., Barnett, J.W., 2003. Use of ADME studies to confirm the safety of ε-polylysine as a preservative in food. Regul. Toxicol. Pharmacol. 37, 328–340. https://doi.org/10.1016/s0273-2300(03)00029-1

Hughes, A.B., 2012. Amino Acids, Peptides and Proteins in Organic Chemistry.

Jiménez-López, C., Caballero, E., Huertas, F.., Romanek, C.., 2002. Chemical, mineralogical and isotope behavior, and phase transformation during the precipitation of calcium carbonate minerals from intermediate ionic solution at 25°C. Geochim. Cosmochim. Acta 65, 3219–3231. https://doi.org/10.1016/s0016-7037(01)00672-x

Kato, T., Suzuki, T., Amamiya, T., Irie, T., Komiyama, M., Yui, H., 1998. Effects of macromolecules on the crystallization of $CaCO_3$ the Formation of Organic/Inorganic Composites. Supramol. Sci. 5, 411–415. https://doi.org/10.1016/S0968-5677(98)00041-8

Kawaguchi, T., Decho, A.W., 2002. Kawaguchi, T. & Decho, A. W. A laboratory investigation of cyanobacterial extracellular polymeric secretions (EPS) in influencing $CaCO_3$ polymorphism. J. Cryst. 240, 230–235.

Khan, M.N.H., Amarakoon, G.G.N.N., Shimazaki, S., Kawasaki, S., 2015. Coral Sand Solidification Test Based on Microbially Induced Carbonate Precipitation Using Ureolytic Bacteria. Mater. Trans. 56, 1725–1732. https://doi.org/10.2320/matertrans.m-m2015820

Kralj, D., Brečević, L., Nielsen, A.E., 1994. Vaterite growth and dissolution in aqueous solution II. Kinetics of dissolution. J. Cryst. Growth. 143, 269–276. https://doi.org/10.1016/0022-0248(94)90067-1

López, C.J., Caballero, E., Huertas, F., Romanek, C, S., 2001. Chemical, mineralogical and isotope behavior, and phase transformation during the precipitation of calcium carbonate minerals from intermediate ionic solution at 25°C. Geochim. Cosmochim. Acta. 65, 3219–3231.

Manoli, F., Kanakis, J., Malkaj, P., Dalas, E., 2002. The effect of aminoacids on the crystal growth of calcium carbonate. 236, 363–370.

Mazia, D., Schatten, G., Sale, W., 1975. Adhesion of cells to surfaces coated with polylysine. J. Cell Biol. 66, 198–200.

Mortensen, B.M., Nelson, D.C., DeJong, J.T., Caslake, L.F., Haber, M.J., Mortensen, B.M., 2011. Effects of environmental factors on microbial induced calcium carbonate precipitation. J. Appl. Microbiol. 111, 5728–5733. https://doi.org/10.1111/j.1365-2672.2011.05065.x

Njegić-Džakula, B., Falini, G., Brečević, L., Skoko, Ž., Kralj, D., 2010. Effects of initial supersaturation on spontaneous precipitation of calcium carbonate in the presence of charged poly-l-amino acids. J. Colloid Interface Sci. 343, 553–563. https://doi.org/10.1016/j.jcis.2009.12.010

Njegic, B., Brecevic, L., Falini, G., Kralj, D., 2009. Calcite crystal growth in the presence of charged sythetic polypeptides. Cryst. Growth Des.9, 2425-2434.

Njegić Džakula, B., Falini, G., Kralj, D., 2018. Crystal Growth Mechanism of Vaterite in the Systems Containing Charged Synthetic Poly(Amino Acids). Croat. Chem. Acta. 90, 689–698. https://doi.org/10.5562/cca3290

Polowczyk, I., Bastrzyk, A., Fiedot, M., 2016. Protein-mediated precipitation of calcium carbonate. Materials (Basel). 9, 1–16. https://doi.org/10.3390/ma9110944

Rab, N.S., Clough, G.W., 1982. The Influence of Cementation of the Static and Dynamic Behavior of Sands. Stanford University, California.

Shibata, A., Yamamoto, M. Y., Amashita, T., Chiou, J.S., Kamaya, H., Ueda, I., 1992. Biphasic Effects of Alcohols on the Phase Transition of Poly(L-lysine) between a-Helix and ,&Sheet Conformations. Biochemistry. 31, 5728-5733.

Shih, I., Van, Y., Shen, M., 2005. Biomedical Applications of Chemically and Microbiologically Synthesized Poly(Glutamic Acid) and Poly(Lysine). Mini-Reviews Med. Chem. 4, 179–188. https://doi.org/10.2174/1389557043487420

Shima, S., Matsuoka, Hi., Iwamoto, T., Sakai, H., 2012. Antimicrobial action of .EPSILON.-poly-L-lysine. J. Antibiot. (Tokyo). 37, 1449–1455. https://doi.org/10.7164/antibiotics.37.1449

Stocks-Fischer, S., Galinat, J.K., Bang, S.S., 1999. Microbiological precipitation of CaCO3. Soil Biol. Biochem. 31, 1563–1571. https://doi.org/10.1016/S0038-0717(99)00082-6

Tong, H., Ma, W., Wang, L., Wan, P., Hu, J., Cao, L., 2003. Control over the crystal phase, shape, size and aggregation of calcium carbonate via a l-aspartic acid inducing process. Biomaterials. 25, 3923–3929. https://doi.org/10.1016/j.biomaterials.2003.10.038

Trushina, D.B., Bukreeva, T. V., Kovalchuk, M. V., Antipina, M.N., 2015. $CaCO_3$ vaterite

microparticles for biomedical and personal care applications. Mater. Sci. Eng. C. 45, 644–658. https://doi.org/10.1016/j.msec.2014.04.050

van Aalst, J.A., Reed, C.R., Han, L., Andrady, T., Hromadka, M., Collins, J.B., Loboa, E.G., Bernacki, S., Kolappa, K., 2008. Cellular Incorporation Into Electrospun Nanofibers. Ann. Plast. Surg. 60, 577–583. https://doi.org/10.1097/sap.0b013e318168db3e

van Paassen, L.A., 2009. Biogrout: Ground Improvement by Microbially Induced Carbonate Precipitation, PhD thesis, Delft University of Technology, Netherland.

Voet, D.J., Voet, J.G., Pratt, C.W., 2011. Fundamentals of Biochemistry, 4th Edition.

Wada, N., Horiuchi, N., Nakamura, M., Nozaki, K., Nagai, A., Yamashita, K., 2018. Calcite Crystallization on Polarized Single Calcite Crystal Substrates in the Presence of Poly-Lysine. Cryst. Growth Des. 18, 872–878. https://doi.org/10.1021/acs.cgd.7b01364

Westwood, M., Noel, T.R., Parker, R., 2013. The effect of poly-l-lysine structure on the pH response of polygalacturonic acid-based multilayers. Carbohydr. Polym. 94, 137–146. https://doi.org/10.1016/j.carbpol.2012.12.065

Xie, A.J., Shen, Y.H., Zhang, C.Y., Yuan, Z.W., Zhu, X.M., Yang, Y.M., 2005. Crystal growth of calcium carbonate with various morphologies in different amino acid systems. J. Cryst. Growth 285, 436–443. https://doi.org/10.1016/j.jcrysgro.2005.08.039

Yao, Y., Dong, W., Zhu, S., Yu, X., Yan, D., 2009. Novel morphology of calcium carbonate controlled by poly(L-lysine). Langmuir 25, 13238–13243. https://doi.org/10.1021/la901913d

Ye, R., Peng, S., Xiong, Y., Wang, L., Xu, H., Zeng, Z., Xu, H., Aguilar, Z.P., Wei, H., Wan, C., 2013. Antibacterial activity and mechanism of action of ε-poly-l-lysine. Biochem. Biophys. Res. Commun. 439, 148–153. https://doi.org/10.1016/j.bbrc.2013.08.001

CHAPTER 3. EFFECT OF THE NATURAL BIOPOLYMER ON THE $CaCO_3$ CRYSTALLIZATION AND THE SAND SOLIDIFICATION BY USING MICP METHOD

3.1. Introduction

In nature, formation of biominerals are mainly associated with the organic macromolecules and these organic materials provide structural support, protection and strength for the organisms. Among the organic macromolecules, polysaccharides are mostly associated with the biomineral formation. Polysaccharides are higher molecular weight polymers of monosaccharide which are joined by glycosidic bonds (Choct, 1997). Polysaccharides can be found in most of the living systems as a structural material and as an energy storage system. Therefore, polysaccharides have been roughly classified as storage polysaccharides and structural polysaccharides (M.Partain, 2000). Among the structural polysaccharides, chitin and cellulose are the mostly abundant natural polysaccharides.

Chitin can be widely found in nature, mainly in exoskeleton of arthropods, marine diatoms, and certain types of algae (Nisticò, 2017; Yang, 2011). Also, chitin mainly associated with the formation of biogenic minerals. One of the best example is nacre of mollusca, in which $CaCO_3$ is deposited upon the organic matrix of silk- fibroin like protein and polysaccharide chitin (Munro et al., 2011; Munro and McGrath, 2012). This organic-inorganic hierarchical structure provides a better mechanical strength for the organisms (Stephen Mann, 2001).

However, chitin has limited number of field applications due to its huge insolubility and complications in processing. Therefore, number of byproducts have been developed from chitin which can be used for number of field applications. Chitosan is one of the most important derivative of chitin which is obtained by the deacetylation of the chitin by chemical hydrolysis under different alkaline conditions or by enzymatic hydrolysis (Croisier and Jérôme, 2013). Chitosan is a linear, semi-crystalline polysaccharide composed of (1→4)-2-acetamido-2-deoxy-b-D-glucan (N-acetyl D-glucosamine) and (1→4)-2-amino-2-deoxyb-D-glucan (D-glucosamine) units (Croisier and Jérôme, 2013; Kumirska et al., 2011). Chemical structures of chitin and chitosan are given in Fig. 3-1.

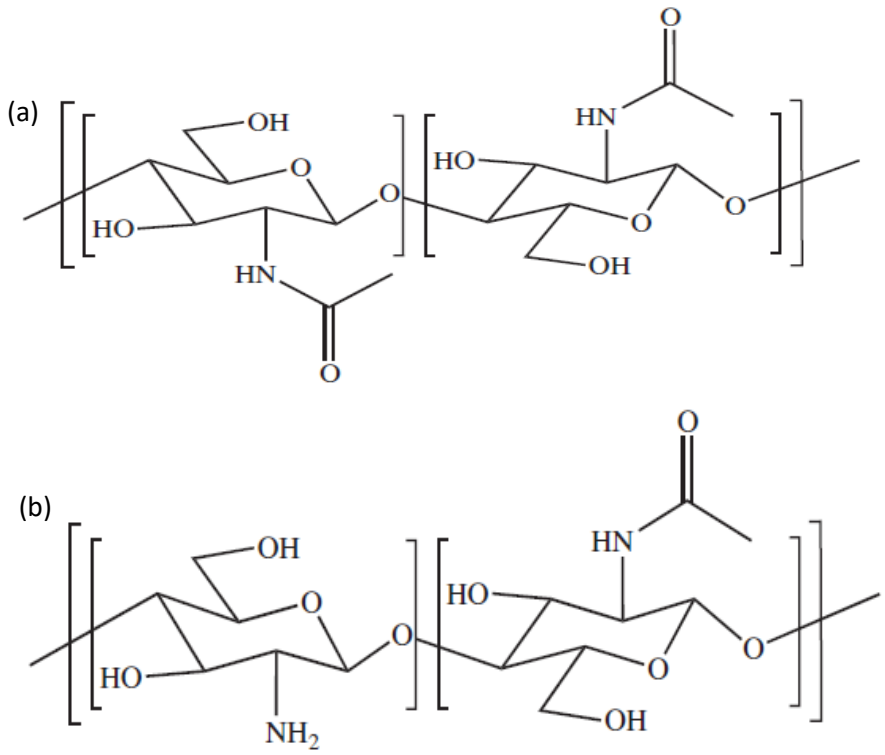

Fig. 3-1 Chemical structure of (a) Chitin (b) Chitosan

Chitosan is the only cationic natural polysaccharide which is charged positively in the diluted acidic environments (pH < 6.5) (Liu et al., 2015; Wang and Heuzey, 2016). Compared with other natural polysaccharides, chitosan has excellent biological properties such as biocompatible, biodegradable, non-toxic, antioxidant activity, mucoadhesion etc. Due to these admirable biological properties, chitosan has been used in number of industrial applications mainly, medical and pharmaceutical, agriculture and waste water engineering field (de Queiroz Antonino et al., 2017; Montembault et al., 2005; Rami et al., 2014). However, applications of the chitosan in geotechnical engineering is very rare and fewer number of research works have been carried out recently to check the applicability of the chitosan on soil stabilization.

Previously, Hataf et al.,(2018) have been investigated the stabilization of the clayey soils by using chitosan. They found that the chitosan can enhance the interparticle cohesion and therefore could be increased the mechanical properties of soils. However, in dry condition cohesive gel shrunk and converted to brittle which lead to reduce the bond strength. Kavazanjian et al., (2009) have been investigated the applicability of chitosan for wind erosion prevention and found that it has better ability to prevent wind erosion and also remained effective even under the summer temperatures. These literatures revealed that chitosan can acts

as a better stabilizer. Hence, our interest is introducing chitosan into the MICP process to mimic the organic matrix mediated biomineralization.

As described in the Chapter 2, cationic polypeptide poly-L-lysine has excellent capability to improve the efficiency of the MICP process. However, poly-L-lysine is bit expensive and it is not practical to use for large scale applications. Chitosan is a natural polymer, cheap and widely available in nature. Therefore, use of chitosan would be helped to improve the efficiency of the MICP process very effectively.

3.2. Objectives

Investigate the effect of chitosan on the $CaCO_3$ crystallization, and its polymorphism and morphology by using MICP and EICP. In addition, performance of chitosan on weak sand densification also examined.

3.3. Materials and methods

3.3.1. Preparation of bacterial cell culture

Experiments were conducted by using the ureolytic bacterium, *Pararhodobacter* sp., which is a gram-negative bacterium with high urease activity (Danjo and Kawasaki, 2016a; Khan et al., 2015), isolated from beach sand in Sumuide, Nago, Okinawa (Danjo and Kawasaki, 2016b). Bacterial cell culture was prepared by using the same method described in the section 2.3.1.

3.3.2. Preparation of chitosan solution

Chitosan with degree of deacetylation 80%, purchased from the Wako Pure Chemical Industries Ltd. (Tokyo, Japan) was used for these experiments. Solution of 1% chitosan was prepared by dissolving chitosan powder in 1% acetic acid solution. After complete dissolution, chitosan solution was neutralized at pH 6.8 by using 0.1 M NaOH solution.

3.3.3. Precipitation of $CaCO_3$

$CaCO_3$ precipitation experiment was conducted with and without chitosan under different experimental conditions. *Pararhodobacter* sp. cells were added to a substrate solution containing urea (0.3 mol/L) and $CaCl_2$ (0.3 mol/L), in the presence or absence of chitosan. The reaction mixture (10 mL) was shaken at 30 °C and 160 rpm for 24 h. $CaCO_3$ precipitate was separated from the supernatant by centrifugation (24 °C, 12000 rpm, 10 min) and oven dried at 90 °C for 24 h. Then dry weights of the precipitates were measured. Experiments were conducted at various bacterial concentrations (OD_{600} = 0.01– 0.1) in the presence (0.03%) or absence of chitosan. Effect of the chitosan concentration on the $CaCO_3$ precipitate was also measured. All experiments were done in triplicate and mean value was plotted. In addition, to check the interaction of the chitosan with the urea and $CaCl_2$ control precipitation experiment was conducted by varying chitosan concentration (0-0.15%) without adding bacteria.

3.3.4. Precipitation of $CaCO_3$ by urease enzyme

Similar to the synthetic polypeptides, precipitation experiments were conducted by using the extracted urease enzyme (jack bean urease) in the presence of urea and $CaCl_2$. Experiments were conducted for different urease concentrations (0 – 2.1%) in the presence (0.03%) or absence of chitosan to check the actual behavior of the chitosan on urease enzyme since bacterial urease contains lot of other organic matters which can influence the behavior of the chitosan. Effect of the chitosan concentration (0 – 0.15%) on the $CaCO_3$ crystallization was also examined (urease concentration-0.3 U/ml). All experiments were done in triplicate.

3.3.5. X-ray diffraction and scanning electron microscopy analyses

Polymorphism and the morphology of the precipitated $CaCO_3$ crystals were analyzed by using X-ray diffraction (XRD; MiniFlex™, Rigaku Co., Ltd., Tokyo, Japan) analysis and scanning electron microscopy (SEM; Miniscope TM3000, Hitachi, Tokyo, Japan).

3.3.6. Sand solidification in syringe

Sand solidification experiments were conducted in 35 mL syringes with and without chitosan by using the method previously described (Danjo and Kawasaki, 2016a). Laboratory scaled sand solidification experiments were conducted for oven dried Mikawa sand. Sand was placed into the syringe as three layers and each layer was subjected to 20 hammer blows. Firstly,

bacteria suspension (16 mL) was injected into the syringe and kept 10-15 min to allow the fixation of bacteria into the sand particles. Subsequently, the cementation solution (20 mL; 0.3 M urea, 0.3 M $CaCl_2$, 0.02 M sodium hydrogen carbonate, 0.2 M ammonium chloride, and 3 g/L nutrient broth) was injected into the syringe and the solution drained out from the outlet, leaving 2 mL of the solution above the surface to maintain the sand in saturated condition.

Experiments were conducted under different concentration of the chitosan and the various bacteria injection intervals as given in the Table 3-1. In one set, bacteria were injected only once on the first day and chitosan was injected on the 8th day. In another set, the bacteria were injected twice, i.e., on the first day and again after 7 days, and the chitosan was injected on the 11th day. After 14 days, UCS values of the cemented samples were determined by using the needle penetration device following the same procedure described in the section 2.3.6.

Amount of precipitated $CaCO_3$ also determined by using the calcimeter using the procedure described in the section 2.3.7.

Table 3-1 Experimental conditions for the sand solidification test with and without chitosan

	Chitosan	Bacterial injection
S1	-	once [b]
S2	0.15 % [a]	once [b]
S3	0.3 % [a]	once [b]
S4	-	twice [c]
S5	0.15 % [a]	twice [c]
S6	0.3 % [a]	twice [c]

[a] Initial concentration of the chitosan solution applied to the column in the solidification test.

[b] Injection of bacterial culture only at the beginning of the solidification test.

[c] Injection of bacterial culture at the beginning and after 7 days of the solidification test.

3.4. Results and Discussion

3.4.1. Effect of chitosan on the $CaCO_3$ Crystallization

3.4.1.1. Effect of chitosan on the $CaCO_3$ Crystallization by using bacterial urease

Fig. 3-2 shows the variation of the amount of $CaCO_3$ precipitate with and without chitosan under different bacteria concentrations.

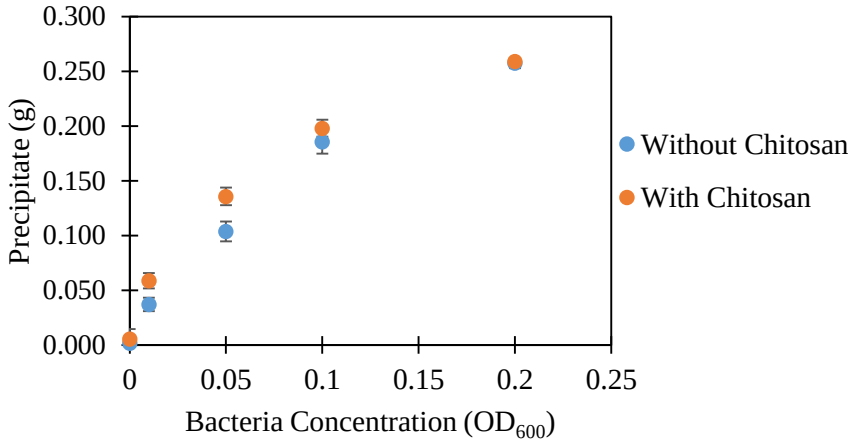

Fig. 3-2 Amounts of precipitate formed at various bacterial concentrations (OD_{600}) with or without addition of chitosan

Results are bit similar to the behavior of poly-L-lysine. Amount of precipitate increased with the bacterial concentration in both of the cases. Increase in urease activity of the *Pararhodobacter* sp. with the increasing cell concentration led to rapid nucleation and growth of the crystals and produced larger amount of $CaCO_3$ (Fujita et al., 2017; Nawarathna et al., 2018). Similar to the poly-L-lysine, higher amount of precipitate could be obtained for the system with chitosan than that of without chitosan and effect is clearer with lower bacteria concentrations.

Precipitate with chitosan consisted two main components, precipitated $CaCO_3$ and precipitated chitosan hydrogel. Chitosan can form its hydrogel under weak alkaline conditions since its pKa value is approximately 6.5 (Inshu et al., 2006; Kumirska et al., 2011; Liu et al., 2015). When pH of the solution is lower than the pKa value of the amino groups in the chitosan, amino groups are protonated and offer a positive charge for the chitosan (Jóźwiak et al., 2016; Liu et al., 2015). Similarly, when increasing the pH above the 6.5, amino groups in the chitosan

chains are deprotonated and formed its hydrogel (Kumirska et al., 2011; Nilsen-Nygaard et al., 2015) as shown in Fig. 3-3.

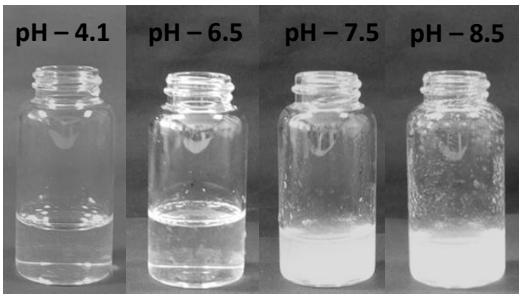

Fig. 3-3 Formation of the chitosan hydrogel under different pH conditions

During the hydrolysis of urea, ammonia was formed and it led to increase the pH of the reaction mixture. However, after some time pH started to decrease due to the $CaCO_3$ precipitation as shown in Fig. 3-4 and pH of the reaction mixture after the 24 hours approximately 7.1. This weak alkaline condition is more favorable for chitosan to precipitate as its hydrogel by the hydrogen bonds and hydrophobic interaction between molecules (Nilsen-Nygaard et al., 2015; Rami et al., 2014).

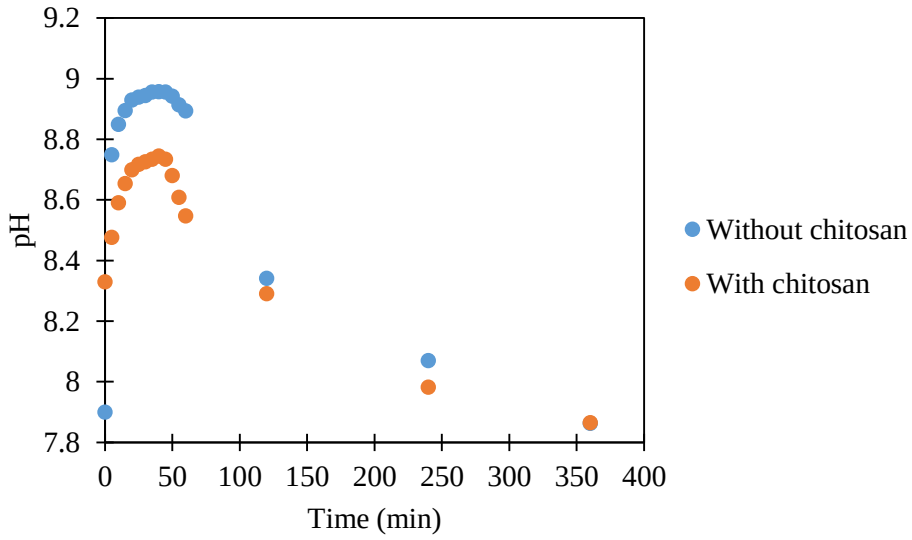

Fig. 3-4 Variation of the pH of the reaction mixture with time in the presence and absence of the chitosan

As mentioned in the Chapter 2, most of the acidic poly-peptides inhibit the $CaCO_3$ nucleation and growth while basic poly-peptides promote the $CaCO_3$ crystallization. Chitosan also didn't interfere with the $CaCO_3$ crystallization and assisted to its nucleation and growth. Interaction between the chitosan and $CaCO_3$ crystals is bit difficult to explain and further investigations are needed. However, it is not electrostatic interaction because chitosan is electroneutral under weak alkaline condition.

Morphologies of the crystals in the presence of the chitosan under different bacteria concentrations are given in Fig. 3-5. As shown in the Fig. 3-5(a) at lower bacteria concentrations, good rhombohedral crystals with chitosan hydrogel was precipitated. With the increase of the bacteria cell concentration, crystal shape deformed gradually. Finally, at higher cell concentrations, distorted-shaped larger crystals with poly crystalline particles were formed as shown in Fig. 3-5(c-1). In addition, spherical crystals can be seen at higher cell concentrations.

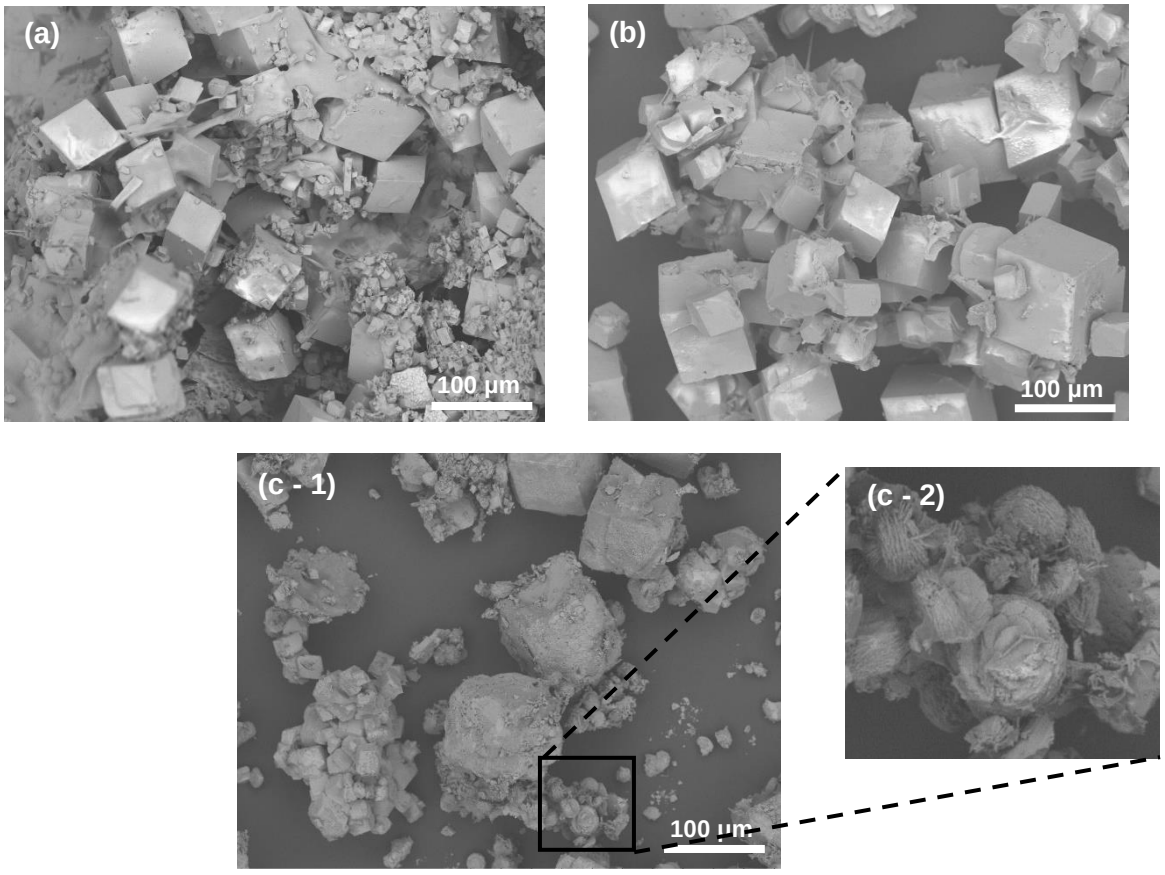

Fig. 3-5 SEM images of $CaCO_3$ precipitates at various bacterial concentrations with chitosan (0.03 %) (a) OD_{600} = 0.01, (b) OD_{600} = 0.05, (c-1) OD_{600} = 0.1 and (c-2) spherical vaterite crystals

It is a well-known factor, that chitosan has ability to make complexes with certain metal ions. The amino groups and the hydroxyl groups presence in the chitosan are contributed to the metal adsorption through chelation and sorption (Benavente, 2008; Nie et al., 2016). Ca^{2+} ions can absorb into the chitosan hydrogel by hard acid-hard base reaction. According to the Lewis acid-base classification, Ca^{2+} is classified as a hard acid and R-NH_2 groups classified as hard base (Pearson, 1968). Ca^{2+} ions are embedded into the chitosan hydrogel due to this acid-base interaction and provide nucleation sites for $CaCO_3$ crystals to nucleate and grow (Greer et al., 2017).

At lower bacteria concentrations, lower amount of precipitation was formed due to lower urease activity. Hence, both of the individual chitosan hydrogel and good rhombohedral calcite crystals can be seen at lower cell concentrations. Similarly, at higher bacteria cell concentrations, higher amount of precipitate was formed due to the associated higher urease activity (Nawarathna et al., 2018) and distorted shape crystal agglomerations and spherical crystals are dominant. In addition, polycrystalline particles can be seen on the surface of the crystals and this may be due to the binding of the -OH and -NH_2 functional groups of the chitosan on to the surface of the crystals. Adsorption of the functional groups on to the crystal surface repressed the growth of the individual crystals and accumulated to form polycrystalline particles (Greer et al., 2017). According to the XRD pattern given in Fig. 3-6, spherical crystals can be classified as vaterite.

As mentioned in the Chapter 2, vaterite is the least stable phase of $CaCO_3$ and easily transformed into the stable form (Jiménez-López et al., 2002). Formation of vaterite crystals is mainly associated with the supersaturation of the reaction mixture and higher supersaturation is more favorable for the formation of meta stable form of crystals (Jiménez-López et al., 2002; Trushina et al., 2015). Generally, supersaturation of the reaction mixture is related to its viscosity and at higher viscosity, supersaturation of the reaction mixture is relatively high due to the enrichment of local ion concentration (Svenskaya et al., 2018). In the presence of chitosan, viscosity of the reaction mixture is relatively higher and it led to increase the supersaturation of the reaction mixture and formation of the vaterite crystals.

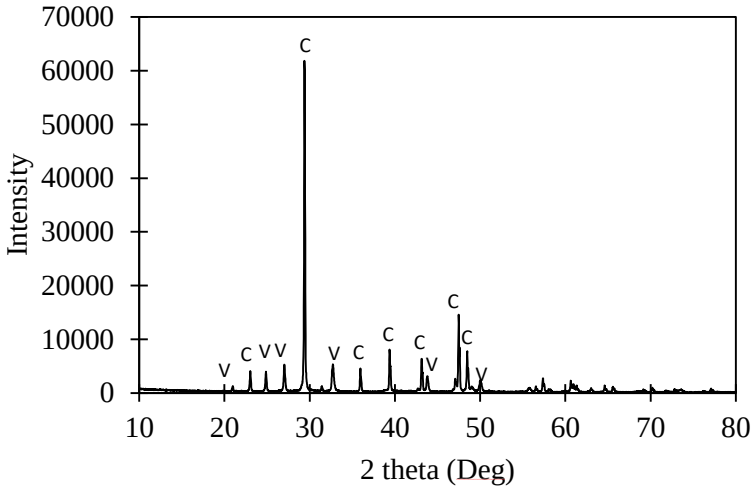

Fig. 3-6 XRD pattern of $CaCO_3$ precipitates with chitosan

With time vaterite crystals convert into its stable form by following the solution mediated transformation. However, organic materials have a capability to stabilize the vaterite crystals by inhibiting the solution mediated transformation (Falini et al., 1998; Ouhenia et al., 2008). Generally, organic materials have several functional groups and can easily interact with the calcium and the carbonate ions in the solution and reduce the free ions in the solutions. This led to reduces the nucleation rate and promote the formation of vaterite crystals (Trushina et al., 2015). Similar phenomena can be applied for the chitosan also. In the presence of chitosan, Ca^{2+} ions are embedded into the chitosan hydrogel by hard acid hard base reaction (Pearson, 1968) and reduced the available free ions in the solution which encourage the formation of meta stable crystals.

3.4.1.1.1. Rate of precipitation

Fig. 3-7 shows the rate of precipitation with and without chitosan. By adding chitosan, precipitation rate has been accelerated and it is dominant within first 2 days. After that, same precipitation rate has been maintained in both of the cases. In the case of with chitosan, higher amount of precipitate was obtained in the initial stage. It reflects the rapid formation of chitosan hydrogel under the alkaline conditions. However, pH of the reaction mixture getting decreased with time due to the precipitation of the $CaCO_3$. Therefore, hydrogel is formed at the initial stage of the reaction. Morphology changes of the precipitate with chitosan at different time intervals are given in Fig. 3-8.

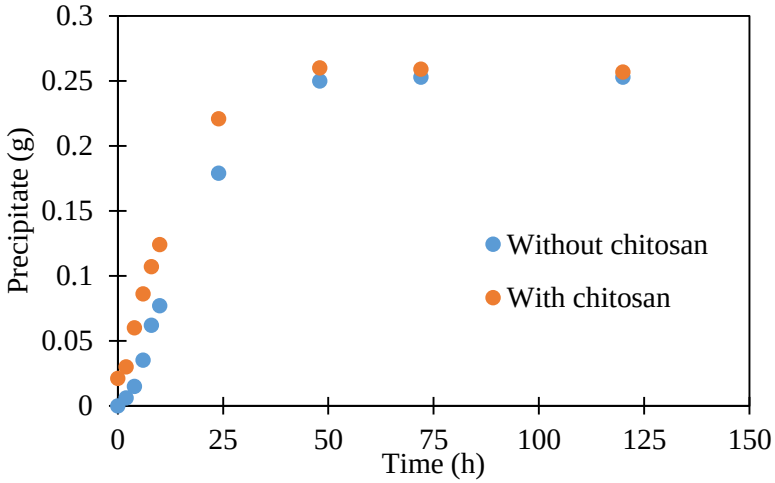

Fig. 3-7 Rate of precipitation with and without chitosan

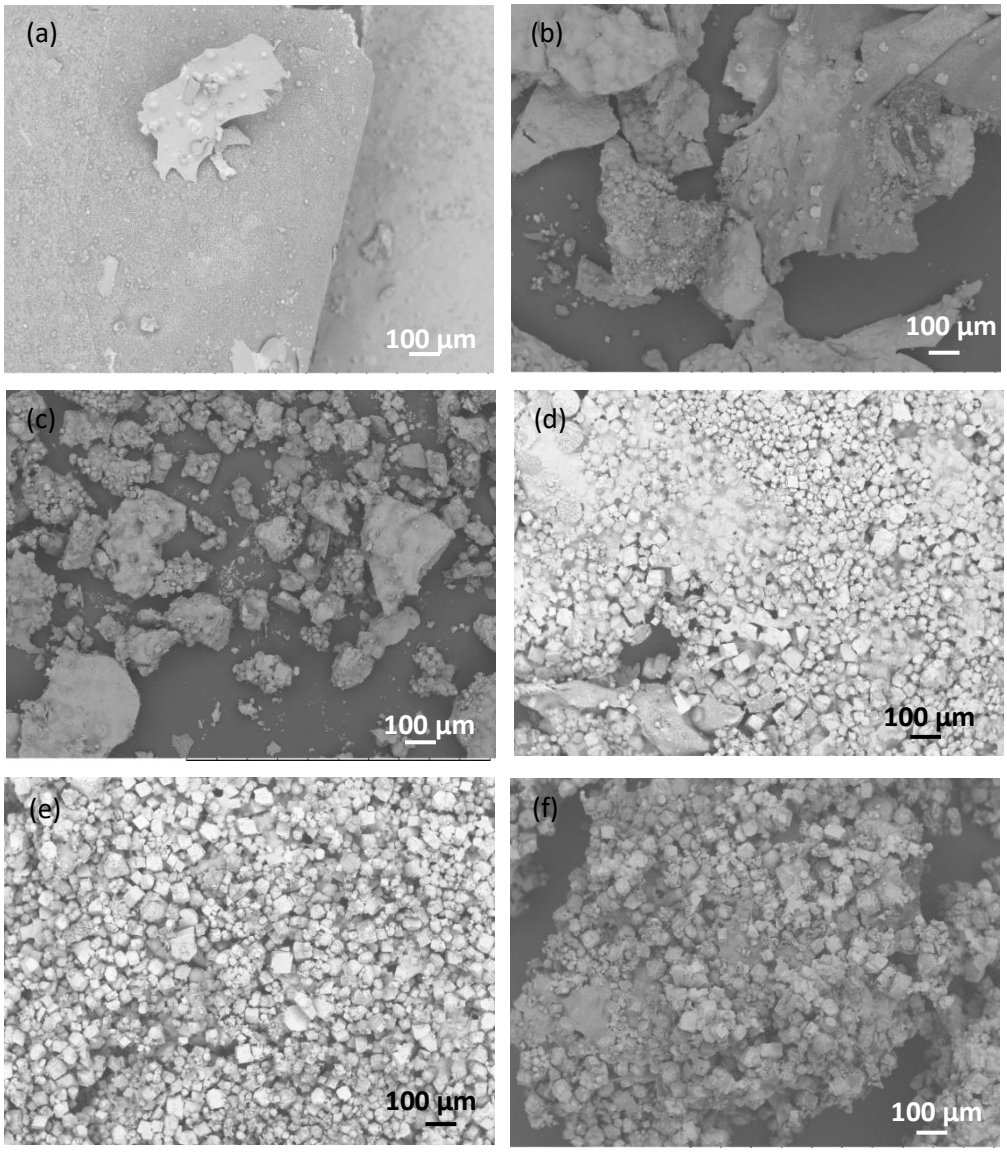

Fig. 3-8 SEM images of the precipitate with chitosan at different time intervals (a) 0 h (b) 2 h (c) 4 h (d) 6 h (e)8 h (f) 10 h

3.4.1.1.2. Effect of the chitosan concentration

Effect of the chitosan concentration on the $CaCO_3$ crystallization was investigated by varying the chitosan concentration under constant cell concentration (OD_{600} - 0.1). As shown in Fig. 3-9, amount precipitate increased slightly with the chitosan concentration.

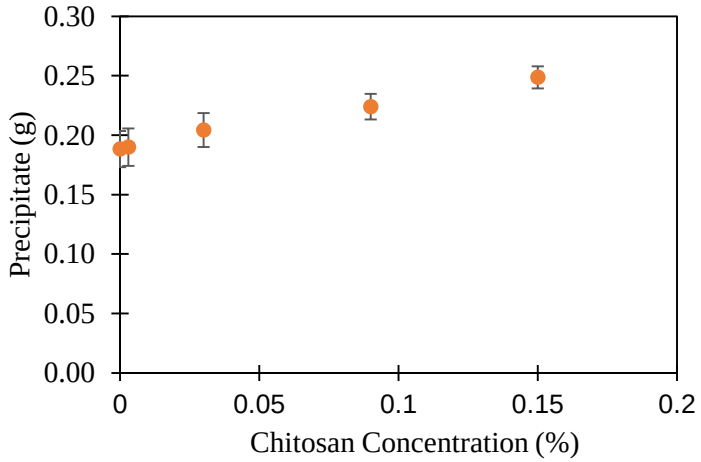

Fig. 3-9 Variation of the amount of precipitate with the chitosan concentration

Increment of the precipitate with the chitosan concentration is mainly due to the increment of the chitosan hydrogel rather than the $CaCO_3$. When increase the chitosan concentration, distance between the chitosan chains decrease due to the presence of excess amount of chitosan chains. This facilitate the easy interaction between the chains and formed higher amount of precipitate through inter molecular hydrogen bonds (Liu and Li, 2018). Fig. 3-10 shows the variation of the crystal morphology with the chitosan concentration.

At lower chitosan concentrations, both of the spherical and polyhedron type crystals have been formed and at higher chitosan concentrations, larger polyhedron crystals were formed with the individual chitosan hydrogel. Interestingly, at the intermediate concentrations, distorted shaped spherical and polyhedron crystals can be seen. Presence of the spherical crystals at lower chitosan concentration and disappear at higher chitosan concentrations implies that crystals have been subjected to the solution mediate transformation. Distorted shaped of crystals present in Fig. 3-10(b) provide evidence for the solution mediate transformation of the meta stable phase of crystals.

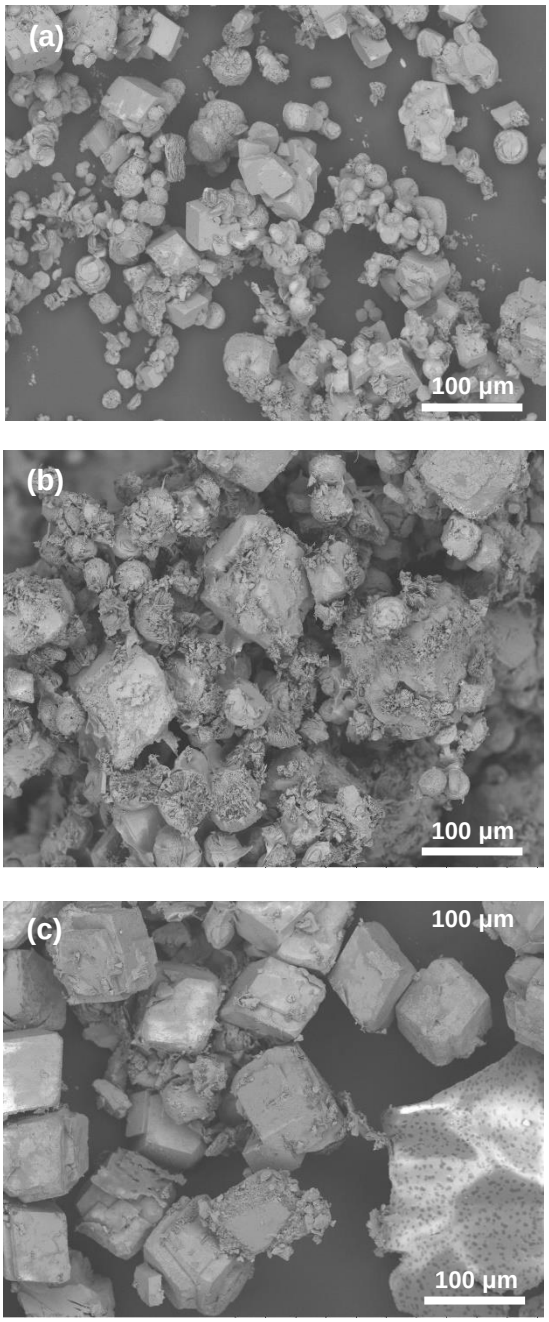

Fig. 3-10 SEM images of precipitated by bacteria (OD_{600} = 0.1) at different chitosan concentrations: (a) 0.003%, (b) 0.03% and (c) 0.15%.

Due to the high solid content and the limited diffusivity, initially both of the vaterite and calcite crystals were formed (Kosanović et al., 2011). Then vaterite crystals started to dissolve and re-precipitated on the calcite crystals. When supersaturation of the reaction mixture drops below the solubility of the vaterite crystals, dissolution of the vaterite crystals start (Kralj et al., 1994). It looks like higher chitosan concentrations, accelerate the conversion of the metastable phase into the stable phase. Formation of larger size distorted shaped crystals

may be due to the adsorption of the functional groups of the chitosan onto the crystal surface (Greer et al., 2017).

3.4.1.1.3. Control experiment without bacteria

Control experiment was conducted only with urea, chitosan and $CaCl_2$ without bacteria for different chitosan concentrations. Amount of precipitate increased with the chitosan concentration as shown in the Fig. 3-11. Increase of the precipitate with the chitosan concentration mainly due to the increase of the chitosan hydrogel. As explained earlier at higher chitosan concentrations, more chitosan chains are present. Hence, distance between the two chains reduced which helped to form chitosan hydrogel easily through hydrophobic interaction (Liu and Li, 2018). One of the interesting point noted is, in addition to the chitosan hydrogel some kind of crystals have been precipitated as shown in the SEM images in Fig. 3-12. Mostly this precipitate can be $Ca(OH)_2$ or $CaCO_3$. $Ca(OH)_2$ can be formed due to interaction of the Ca^{2+} with OH^- group. Then due to the interaction of the $Ca(OH)_2$ with the CO_2, there is a possibility to form $CaCO_3$ (Nie et al., 2016).

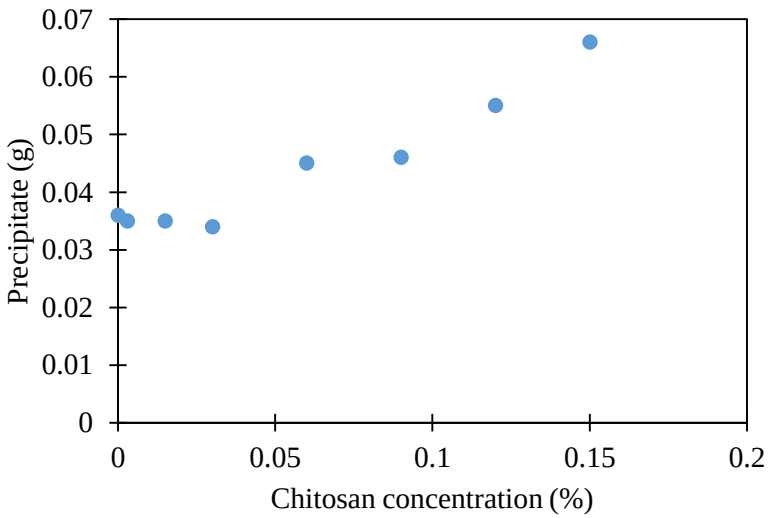

Fig. 3-11 Variation of the amount of precipitate with the chitosan concentration without bacteria

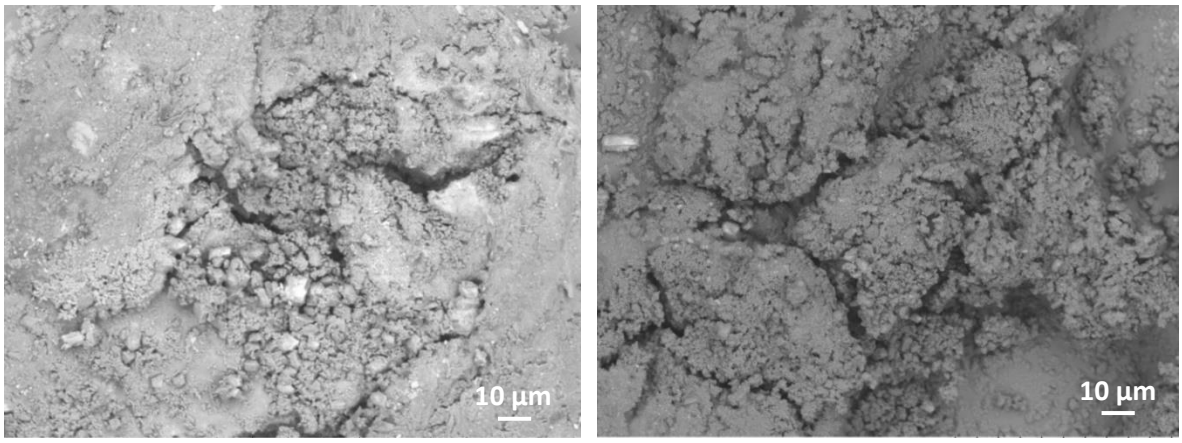

Fig. 3-12 SEM images of the precipitate with chitosan without bacteria

3.4.1.2. Effect of chitosan on the $CaCO_3$ Crystallization by using extracted urease enzyme

To understand the behavior of the chitosan on the $CaCO_3$ crystallization, $CaCO_3$ precipitation experiments were conducted by using the extracted urease enzyme (jack bean urease) with and without chitosan. In contrast to the microbial cell urease, the positive effect of the chitosan on the $CaCO_3$ crystallization is clearer with the extracted urease enzyme. Results are attached into the appendix C. Also, significant increment of the precipitate with the chitosan concentration can be seen.

According to the SEM and XRD results, without chitosan both of the polyhedron calcite crystals and spherical vaterite crystals were formed. In the case of with chitosan, similar to the microbial cell urease at lower urease concentration good rhombohedral crystals were precipitated with the chitosan hydrogel. As explained in the section 3.4.1.1, chitosan forms its hydrogel under alkaline condition and during the urea hydrolysis reaction mixture can maintain weak alkaline condition as shown in the Fig. 3-13. At higher urease concentrations, distorted shape larger crystals were formed with the polycrystalline particle. The polycrystalline particle appeared on the surface of the crystals are mainly due to the adsorption of the functional groups of the chitosan onto the crystal surface. Similar to the microbial cell urease, with chitosan both of the vaterite and calcite crystals were formed.

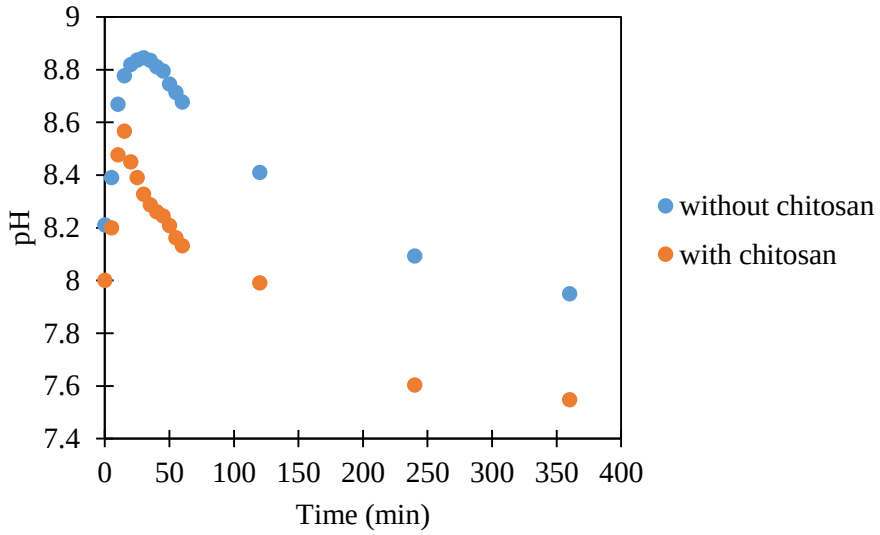

Fig. 3-13 Variation of the pH in the reaction mixture with and without chitosan under extracted urease enzyme

3.4.2. Effect of chitosan on sand solidification

Laboratory scaled sand solidification experiments were conducted in syringe with and without chitosan under different chitosan concentrations and the different bacteria injection intervals as given in the Table 3-1. In contrast to the poly-L-lysine, chitosan is bit toxic to the bacteria (Goy et al., 2009). Also, initial formation of hydrogel may be blocked the penetration of the cementation solution. Hence, considering above facts, different time schedules were suggested to inject chitosan into the samples.

Fig. 3-14 shows the estimated UCS values for the solidified samples and according to the classification system proposed by Rab and Clough (1982) all the specimens can be classified as strongly cemented samples since strength values are in the range of 1-3 MPa. As similar to the poly-L-lysine, strength of the samples decreases from top to bottom. This is mainly due to the accumulation of the bacteria at the top of the sand specimen and decrease it along the length of the sample. Higher amount of bacteria near the inlet course to higher urease activity and produced higher amount of $CaCO_3$. The main reason behind this is lack of oxygen at the bottom of the samples. Since *Pararhodobactor* sp. is an aerobic bacteria, bacterial activity decrease with the depth due to lack of oxygen (Khan et al., 2015).

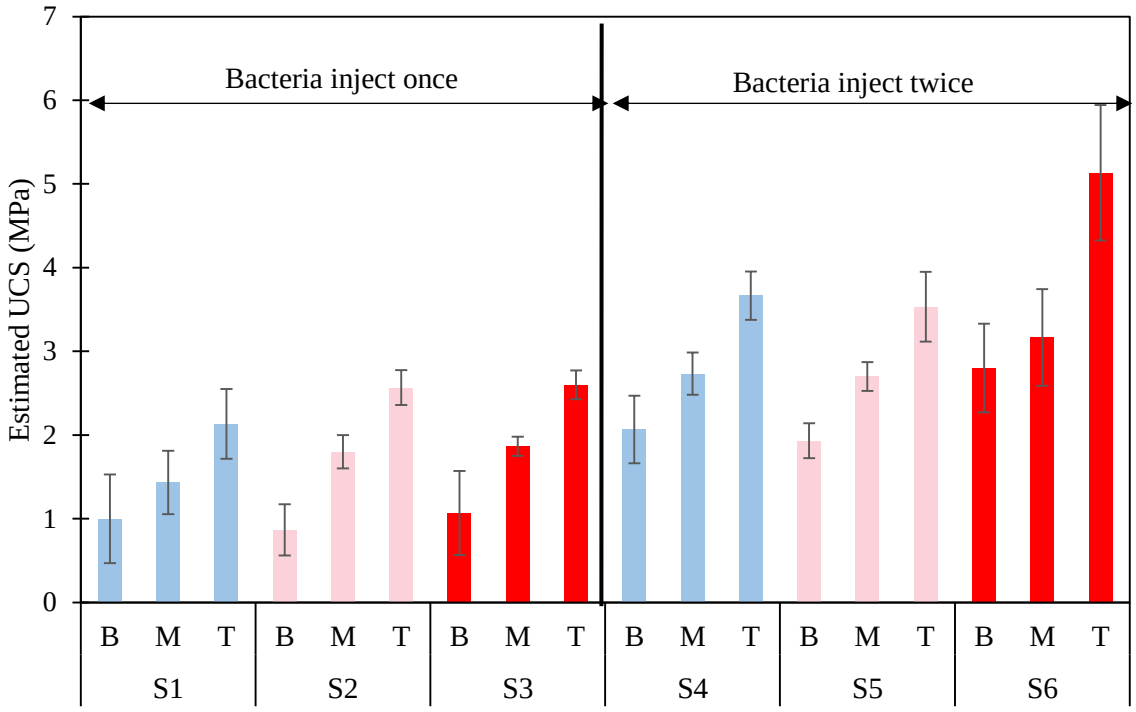

Fig. 3-14 Estimated UCS values of solidified sand specimens with and without chitosan.

As described in the section 2.4.2.1, by reinjection of the bacteria, higher strength could be achieved than that of without reinjecting. Approximately, 96% of strength increment was achieved for the top of the sample by adding chitosan and without chitosan strength increment was around 76%. By reinjecting of the bacteria, higher urea hydrolysis rate can be maintained throughout the experimental period. It assisted to higher $CaCO_3$ precipitation and better cementation between the sand particles (Nawarathna et al., 2018).

By adding chitosan, strongly cemented sand specimen could be obtained than that of without chitosan. Compared with the case of without chitosan, UCS of the top of the sample has been increased by 38%. In sand solidification, to achieve a better cementation pore spaces between the sand particles should be filled effectively and better bridge should be formed between the sand particles (Harkes et al., 2009). Hydrogel formed by chitosan under the alkaline condition assisted to form better bridge between the sand particles. Thicker hydrogel was formed under the higher chitosan concentrations, which led to form better bridge. Therefore, better cementation and strength could be achieved. As mentioned earlier, selection of the suitable time to introduce chitosan also important. Initially, experiments were conducted by introducing the chitosan at the beginning. However, it didn't give good results due to the early formation of chitosan hydrogel and blocked the penetration of the cementation solution.

It led to form lower $CaCO_3$ precipitation. Therefore, in the experiment with bacteria injection twice, the injection of the chitosan on the 11^{th} day was successful and the injection of the chitosan during the 8^{th} day was efficient for the specimens with single dose of bacterial injection.

Fig. 3-15 shows the amount of precipitated $CaCO_3$ and the estimated UCS values in the solidified samples. For all the cases, UCS values are directly related to the precipitated amount of $CaCO_3$. Similar kind of relationships between the UCS and precipitated $CaCO_3$ have been found by previous researchers (Amarakoon and Kawasaki, 2017; Whiffin et al., 2007). According to the Fig. 3-15(e), with the increase of the chitosan concentration amount of precipitated $CaCO_3$ also increased. It provides an evidence that chitosan assisted for efficient precipitation of $CaCO_3$ between the sand particles.

Without addition of the chitosan, cementation mainly occurred at the contact point of sand particles as shown in Fig. 3-16(a) and it is mainly due to the lower adsorption of bacteria onto the sand surface. In contrast, entire sand surface was covered with $CaCO_3$ in the case of with chitosan as shown in Fig. 3-16 (b-1). Formation of the chitosan hydrogel has provided an extra support to make a better bridge between the sand particles as shown in Fig. 3-16 (b-2). Also, chitosan acts as a template for $CaCO_3$ crystals to nucleate. It assisted to proper distribution of the $CaCO_3$ throughout the sand surface and achieve better cementation than the conventional method.

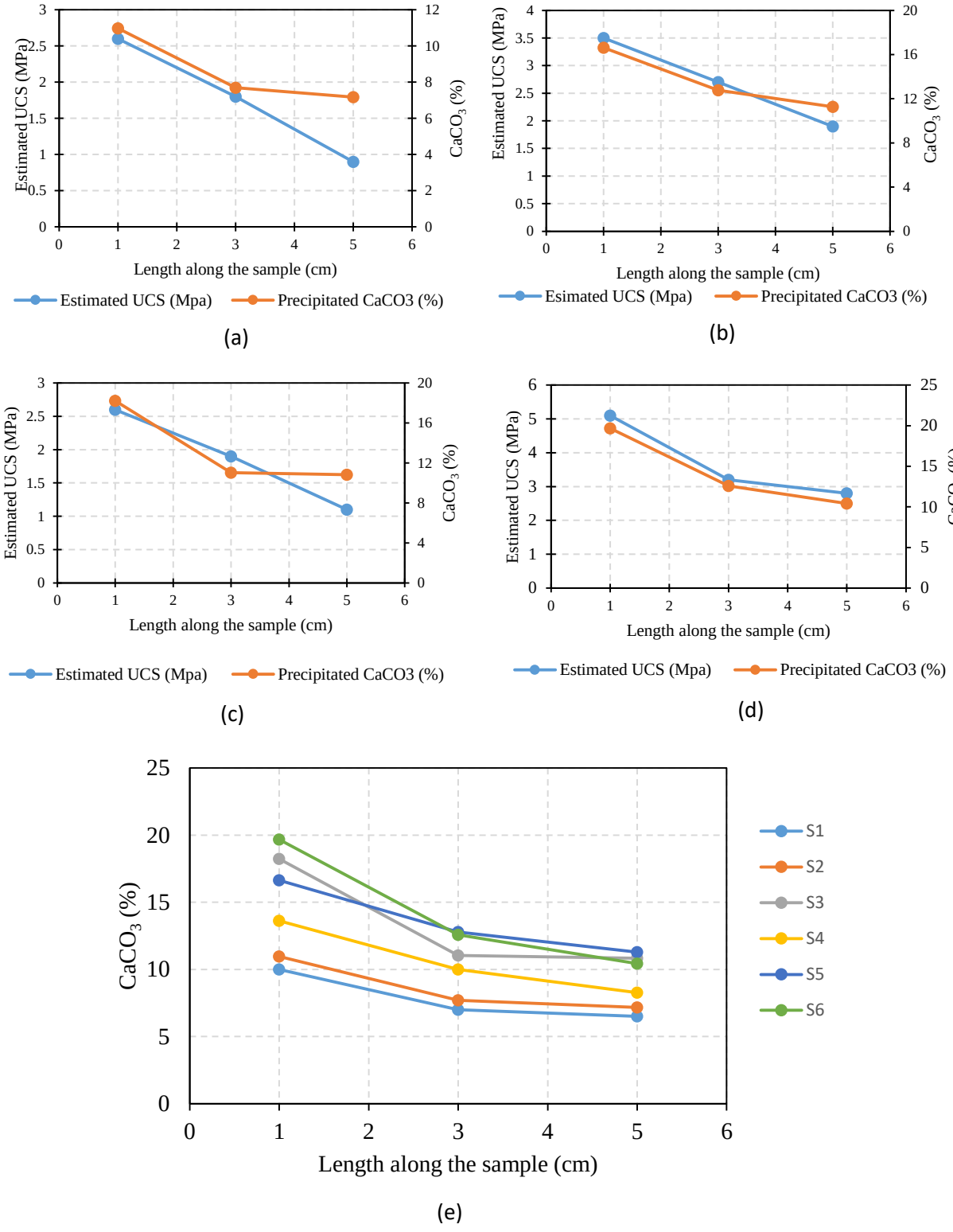

Fig. 3-15 Amount of precipitated $CaCO_3$ with the UCS value along the length of the sample (a) S2 (b) S5 (c) S3 (d) S6 (e) Comparison between all the samples

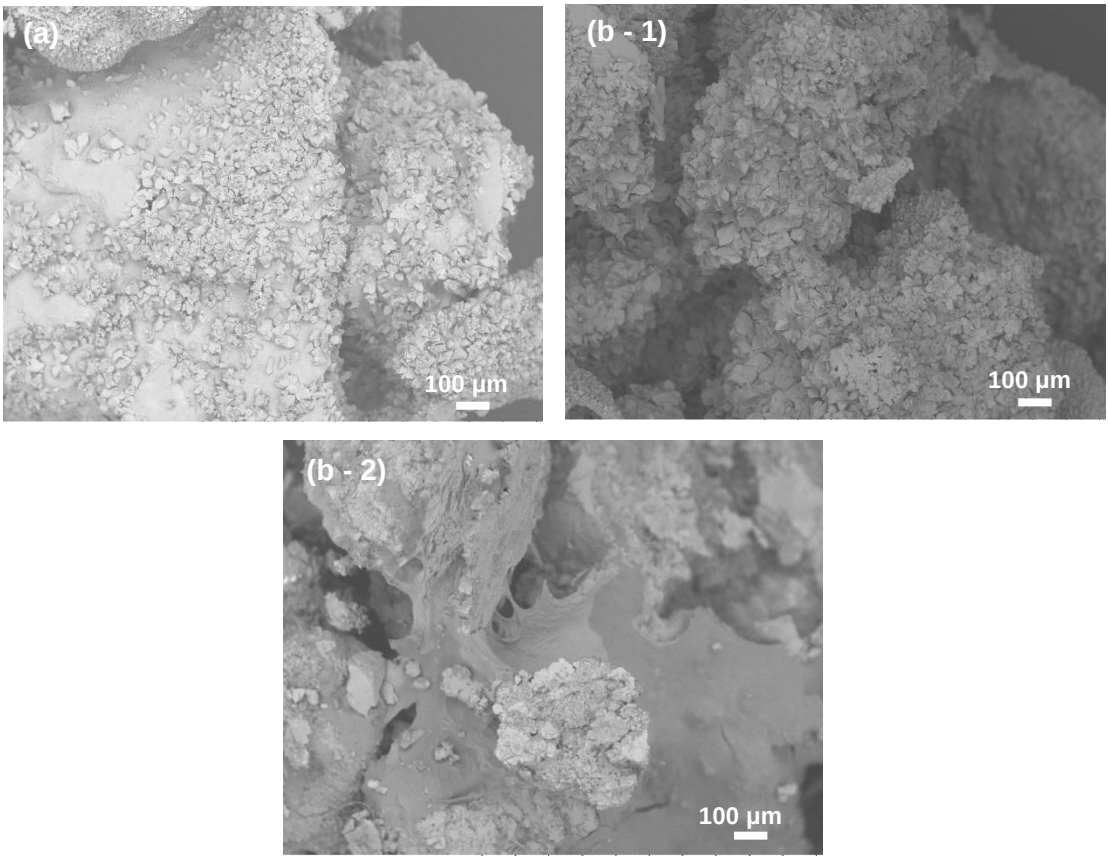

Fig. 3-16 SEM images of the cemented sand specimens: (a) without chitosan (b) with chitosan (0.3%).

3.5. Conclusion

Effect of the natural polysaccharides (chitosan) on the $CaCO_3$ crystallization and its morphology and polymorphism was studied by using the MICP and EICP methods. According to the results obtained from both of the MICP and EICP, chitosan has an ability to upgrade the $CaCO_3$ formation efficiency. By adding chitosan, higher amount of precipitate could be obtained. However, precipitate consisted both of precipitated $CaCO_3$ and precipitated chitosan hydrogel. At lower bacteria cell concentrations, good rhombohedral crystals with individual chitosan hydrogel was obtained while at higher cell concentrations distorted shaped larger crystals were obtained. Chitosan acts as a template for the $CaCO_3$ crystals to nucleate due to adsorption of the Ca^{2+} ions into the chitosan hydrogel.

XRD results confirmed that with chitosan, precipitate contained both of the calcite and vaterite crystals while without chitosan only calcite crystals were obtained. Formations of the vaterite crystals are related to the supersaturation of the reaction mixture and increase of

the supersaturation of the reaction mixture by adding chitosan led to the formation of vaterite crystals. In addition, chitosan hydrogel helped to achieve better cementation during the sand solidification by efficient bridge formation between the sand particles. Therefore, higher UCS value could be achieved by adding chitosan and it is dominant with higher chitosan concentrations.

References

Amarakoon, G.G.N.N., Kawasaki, S., 2017. Factors Affecting Sand Solidification Using MICP with *Pararhodobacter* sp. Mater. Trans. 59, 72–81. https://doi.org/10.2320/matertrans.m-m2017849

Benavente, M., 2008. Adsorption of metalic ions onto chitosan: equilibrium and kinetic studies.

Choct, M., 1997. Feed Non-Starch Polysaccharides: Chemical Structures and Nutritional Significance. Feed milling Int. 13–26.

Croisier, F., Jérôme, C., 2013. Chitosan-based biomaterials for tissue engineering. Eur. Polym. J. 49, 780–792. https://doi.org/10.1016/j.eurpolymj.2012.12.009

Danjo, T., Kawasaki, S., 2016a. Microbially Induced Sand Cementation Method Using *Pararhodobacter* sp. Strain SO1, Inspired by Beachrock Formation Mechanism. Mater. Trans. 57, 428–437. https://doi.org/10.2320/matertrans.m-m2015842

Danjo, T., Kawasaki, S., 2016b. a Study of the Formation Mechanism of Beachrock in Okinawa, Japan: Toward Making Artificial Rock. Int. J. Geomate. 5, 634–639. https://doi.org/10.21660/2013.9.3157

de Queiroz Antonino, R., Lia Fook, B., de Oliveira Lima, V., de Farias Rached, R., Lima, E., da Silva Lima, R., Peniche Covas, C., Lia Fook, M., 2017. Preparation and Characterization of Chitosan Obtained from Shells of Shrimp (Litopenaeus vannamei Boone). Mar. Drugs 15, 141. https://doi.org/10.3390/md15050141

Falini, G., Fermani, S., Gazzano, M., Ripamonti, A., 1998. Oriented crystallization of vaterite in collagenous matrices. Chem. - A Eur. J. 4, 1048–1052. https://doi.org/10.1002/(SICI)1521-3765(19980615)4:6<1048::AID-CHEM1048>3.0.CO;2-U

Fujita, M., Nakashima, K., Achal, V., Kawasaki, S., 2017. Whole-cell evaluation of urease activity of *Pararhodobacter* sp. isolated from peripheral beachrock. Biochem. Eng. J. 124, 1–5. https://doi.org/10.1016/j.bej.2017.04.004

Goy, R.C., Britto, D. De, Assis, O.B.G., 2009. A Review of the Antimicrobial Activity of Chitosan. Polímeros: Ciência e Tecnologia. 19, 241-247.

Greer, H., Zhou, W., Guo, L., 2017. Reversed Crystal Growth of Calcite in Naturally Occurring

Travertine Crust. Crystals. 7, 36. https://doi.org/10.3390/cryst7020036

Harkes, M.P., van Loosdrecht, M.C.M., Booster, J.L., Whiffin, V.S., van Paassen, L.A., 2009. Fixation and distribution of bacterial activity in sand to induce carbonate precipitation for ground reinforcement. Ecol. Eng. 36, 112–117. https://doi.org/10.1016/j.ecoleng.2009.01.004

Hataf, N., Ghadir, P., Ranjbar, N., 2018. Investigation of soil stabilization using chitosan biopolymer. J. Clean. Prod. 170, 1493–1500. https://doi.org/10.1016/j.jclepro.2017.09.256

Inshu, M., Swapna, K., Hai-Feng, J., Michael, J.M., 2006. Study of the Near-Neutral pH-Sensitivity of Chitosan/Gelatin Hydrogels by Turbidimetry and Microcantilever Deflection. Biotechnol. Bioeng. 95, 333–341. https://doi.org/10.1002/bit

Jiménez-López, C., Caballero, E., Huertas, F.., Romanek, C.., 2002. Chemical, mineralogical and isotope behavior, and phase transformation during the precipitation of calcium carbonate minerals from intermediate ionic solution at 25°C. Geochim. Cosmochim. Acta 65, 3219–3231. https://doi.org/10.1016/s0016-7037(01)00672-x

Jóźwiak, T., Filipkowska, U., Szymczyk, P., Mielcarek, A., 2016. Sorption of nutrients (orthophosphate, nitrate III and V) in an equimolar mixture of P-PO4, N-NO2 and N-NO3 using chitosan. Arab. J. Chem. https://doi.org/10.1016/j.arabjc.2016.04.008

Kavazanjian, E., Iglesias, E., Karatas, I., 2009. Biopolymer soil stabilization for wind erosion control. Proc. 17th Int. Conf. Soil Mech. Geotech. Eng. Acad. Pract. Geotech. Eng. 1, 881–884. https://doi.org/10.3233/978-1-60750-031-5-881

Khan, M.N.H., Amarakoon, G.G.N.N., Shimazaki, S., Kawasaki, S., 2015. Coral Sand Solidification Test Based on Microbially Induced Carbonate Precipitation Using Ureolytic Bacteria. Mater. Trans. 56, 1725–1732. https://doi.org/10.2320/matertrans.m-m2015820

Kosanović, C., Falini, G., Kralj, D., 2011. Mineralization of calcium carbonates in gelling media. Cryst. Growth Des. 11, 269–277. https://doi.org/10.1021/cg1012796

Kralj, D., Brečević, L., Nielsen, A.E., 1994. Vaterite growth and dissolution in aqueous solution II. Kinetics of dissolution. J. Cryst. Growth. 143, 269–276. https://doi.org/10.1016/0022-0248(94)90067-1

Kumirska, J., Weinhold, M.X., Thöming, J., Stepnowski, P., 2011. Biomedical activity of chitin/chitosan based materials- influence of physicochemical properties apart from molecular weight and degree of N-Acetylation. Polymers (Basel). 3, 1875–1901. https://doi.org/10.3390/polym3041875

Liu, H., Ojha, B., Morris, C., Jiang, M., Wojcikiewicz, E.P., Rao, P.P.N., Du, D., 2015. Positively Charged Chitosan and N-Trimethyl Chitosan Inhibit Aβ40 Fibrillogenesis. Biomacromolecules 16, 2363–2373. https://doi.org/10.1021/acs.biomac.5b00603

Liu, S., Li, L., 2018. Unique gelation of chitosan in an alkali/urea aqueous solution. Polymer. 141, 124–131. https://doi.org/10.1016/j.polymer.2018.03.012

M.Partain, E., 2000. Industrially Important Polysaccharides. Applied Polymer Science: 21st Century. pp. 303–323. 10.1016/B978-008043417-9/50018-0

Montembault, A., Viton, C., Domard, A., 2005. Rheometric study of the gelation of chitosan in aqueous solution without cross-linking agent. Biomacromolecules. 6, 653–662. https://doi.org/10.1021/bm049593m

Munro, N.H., Green, D.W., Dangerfield, A., McGrath, K.M., 2011. Biomimetic mineralisation of polymeric scaffolds using a combined soaking and Kitano approach. Dalt. Trans. 40, 9259–9268. https://doi.org/10.1039/c1dt11056j

Munro, N.H., McGrath, K.M., 2012. Biomimetic approach to forming chitin/aragonite composites. Chem. Commun. 48, 4716–4718. https://doi.org/10.1039/c2cc00135g

Nawarathna, T.H.K., Nakashima, K., Fujita, M., Takatsu, M., Kawasaki, S., 2018. Effects of Cationic Polypeptide on CaCO 3 Crystallization and Sand Solidification by Microbial-Induced Carbonate Precipitation. ACS Sustain. Chem. Eng. 6, 10315–10322. https://doi.org/10.1021/acssuschemeng.8b01658

Nie, J., Wang, Z., Hu, Q., 2016. Chitosan Hydrogel Structure Modulated by Metal Ions. Sci. Rep. 6, 1–8. https://doi.org/10.1038/srep36005

Nilsen-Nygaard, J., Strand, S.P., Vårum, K.M., Draget, K.I., Nordgård, C.T., 2015. Chitosan: Gels and interfacial properties. Polymers (Basel). 7, 552–579. https://doi.org/10.3390/polym7030552

Nisticò, R., 2017. Aquatic-Derived Biomaterials for a Sustainable Future: A European Opportunity. Resources. 6, 65-80. https://doi.org/10.3390/resources6040065

Ouhenia, S., Chateigner, D., Belkhir, M.A., Guilmeau, E., Krauss, C., 2008. Synthesis of calcium carbonate polymorphs in the presence of polyacrylic acid. J. Cryst. Growth. 310, 2832–2841. https://doi.org/10.1016/j.jcrysgro.2008.02.006

Pearson, R.G., 1968. Hard and soft acids and bases, HSAB, part 1: Fundamental principles. J. Chem. Educ. 45, 581-588. https://doi.org/10.1021/ed045p581

Rab, N.S., Clough, G.W., 1982. The Influence of Cementation of the Static and Dynamic Behavior of Sands. Stanford University, California.

Rami, L., Malaise, S., Delmond, S., Fricain, J.C., Siadous, R., Schlaubitz, S., Laurichesse, E., Am??d??e, J., Montembault, A., David, L., Bordenave, L., 2014. Physicochemical modulation of chitosan-based hydrogels induces different biological responses: Interest for tissue engineering. J. Biomed. Mater. Res. - Part A. 102, 3666–3676. https://doi.org/10.1002/jbm.a.35035

Stephen Mann, 2001. Biomineralization, oxford university press.

Svenskaya, Y.I., Fattah, H., Inozemtseva, O.A., Ivanova, A.G., Shtykov, S.N., Gorin, D.A., Parakhonskiy, B. V., 2018. Key Parameters for Size- and Shape-Controlled Synthesis of Vaterite Particles. Cryst. Growth Des. 18, 331–337. https://doi.org/10.1021/acs.cgd.7b01328

Trushina, D.B., Bukreeva, T. V., Kovalchuk, M. V., Antipina, M.N., 2015. CaCO3 vaterite microparticles for biomedical and personal care applications. Mater. Sci. Eng. C. 45, 644–658. https://doi.org/10.1016/j.msec.2014.04.050

Wang, X.Y., Heuzey, M.C., 2016. Chitosan-Based Conventional and Pickering Emulsions with Long-Term Stability. Langmuir. 32, 929–936. https://doi.org/10.1021/acs.langmuir.5b03556

Whiffin, V.S., van Paassen, L.A., Harkes, M.P., 2007. Microbial carbonate precipitation as a soil improvement technique. Geomicrobiol. J. 24, 417–423. https://doi.org/10.1080/01490450701436505

Yang, T.L., 2011. Chitin-based materials in tissue engineering: Applications in soft tissue and epithelial organ. Int. J. Mol. Sci. 12, 1936–1963. https://doi.org/10.3390/ijms12031936

CHAPTER 4. DEVELOP A NOVEL FUSION PROTEIN TO FACILITATE ORGANIC-INORGANIC HYBRID MATERIAL FORMATION

4.1. Introduction

Biomineralization can be simply defined as a process of crystal nucleation and growth which is controlled by the organic macromolecules (Stephen Mann, 2001). Biominerals are composite materials which contain inorganic minerals and organic macromolecules such as protein, polypeptides and polysaccharides. In detail, biominerals can be defined as organic-inorganic hybrid materials which is an essential component in living organisms to support specific functions (Arakaki et al., 2015; Kumagai et al., 2012). Biominerals are formed under the mild conditions at near neutral pH and ambient temperature (Arakaki et al., 2015) and use them as hard tissues such as teeth, bones, lens and exoskeletons. Hydroxyapatite in bones and teeth of mammals (Dorozhkin and Epple, 2010), calcium carbonate in molluscan shells (Stephen and Lia, 1997), amorphous silica in diatoms (Chambers et al., 1999) and marine sponges (Shimizu et al., 2002) are some examples for the biomineral formation.

Among the biominerals, 50% of are calcium bearing minerals and calcium carbonate is the most dominant type of biomineral available in nature (DeOliveira and Laursen, 1997). Mollusk shells, exoskeleton of the crustacean, coccolith of coccolithophores and egg shells are mainly consisted with $CaCO_3$. Compared with the non-biogenic minerals, biominerals have extensive physical and optical properties mainly due to the organic-inorganic hierarchical structure (DeOliveira and Laursen, 1997; Gebauer et al., 2009). Biominerals have capability to lower the activation energy of the crystal formation (Masica et al., 2010). One of the best example available in nature for the biomineral formation is nacre of the mollusk shell in which strength is 3000 times higher than that of pure aragonite (Jackson et al., 1990).

In nacre, inorganic plate like aragonite crystals are deposited in between the pre-organized chitin sheets and formed a brick and motor structure. This brick and motor structure is the reason for the extensive mechanical strength of the nacre (Sun and Bhushan, 2012). As mentioned earlier, organic macromolecules such as proteins, polysaccharides and polypeptides are playing an important role in the biomineralization and these biomacromolecules are contributed to exhibit higher mechanical strength compared with the non-biogenic minerals. Also, these macromolecules control the formation of the minerals with nano-structural regularity, specific crystallographic phase, morphologies and orientations. Another important thing is the higher fracture resistance of the biominerals (Sudo et al., 1996). Also, higher

toughness associated with the organic-inorganic hierarchical structures make it more feasible for certain types of industrial applications than the non-biogenic minerals which are more brittle (Launey and Ritchie, 2009).

Due to these excellent physical and optical properties associated with the biominerals, scientists and researchers have moved to mimic the concept of organic matrix mediated biomineralization to synthesize organic-inorganic hybrid materials which can be benefited for number of industrial applications such as biomedical engineering and tissue engineering. To date, number of proteins have been identified from the different species which are associated with the formation of $CaCO_3$ biominerals (Inoue et al., 2001; Lakshminarayanan et al., 2002). However, applications of the organic-inorganic composite materials in the geotechnical and civil engineering are still not developed and our target is develop a novel fusion protein which can be facilitated to produce organic-inorganic hybrid material for geotechnical applications.

Concept is inspired from the nature from the cray fish. Exoskeleton of the cray fish exhibits higher mechanical strength, ductility and toughness due to the associated organic-inorganic hierarchical structure. When examine the exoskeleton of the cray fish deeply, $CaCO_3$ have been deposited upon the chitin matrix at the interface by the assistance of acidic peptide (CAP-1) as shown in the Fig. 4-1 (Kumagai et al., 2012; Sugawara et al., 2006). CAP-1 has three specific features, first, it has a “Rebers-Riddiford” consensus sequence which is assisted for binding to the chitin, second, CAP-1 has highly acidic property due to the associated seven acidic amino acids in the C terminal and it has a phosphoserine residue at the 70^{th} position which is aided to stabilize the amorphous phase (Iconomidou et al., 2001; Rebers and Riddiford, 1988; Sugawara et al., 2006).

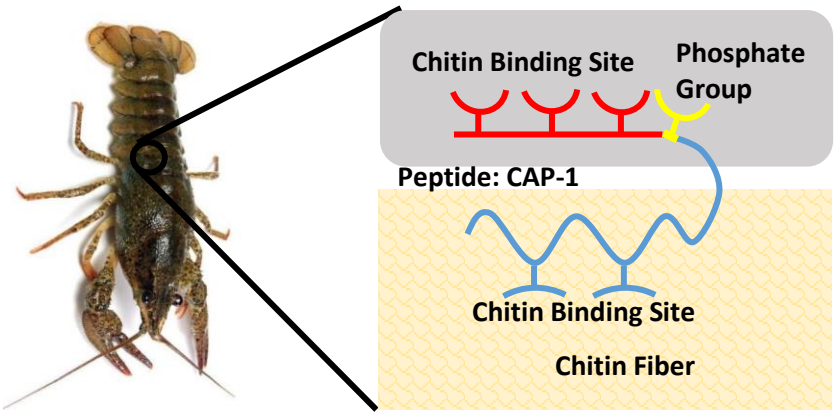

Fig. 4-1 Internal structure of the exoskeleton of the cray fish
(Regenerated by modifying the original image created by Kumagai et. al.,2012)

Also, it has been reported that CAP-1 inhibited $CaCO_3$ precipitation and has anti calcification properties due to higher acidity. However, during the post molt stage CAP-1 is expressed in the epidermal tissue where calcification take place (Inoue et al., 2001).

Our target is mimicking this concept in order to produce novel fusion protein to facilitate organic matrix mediated biomineralization. Proposed fusion protein has calcium binding site and the chitin binding site which would be assisted to efficient precipitation of the $CaCO_3$ on the chitin matrix. Chitin binding domain from the chitinase A1 from Bacillus circulans WL-12 was used as the chitin binding site and short sequence calcium binding peptide was used as calcium binding site.

4.1.1. Chitin binding domain

Chitin is a one of the most abundant, highly insoluble linear natural polysaccharide composed with the chain of β-1, 4-linked Nacetylglucosamine (GlcNAc) units (Honda et al., 2017; Lobo et al., 2013; Svitii and Kirchman, 2016). Chitin is degraded rapidly by chitinolytic enzymes such as chitinases and β-N-acetylhexosaminidases. Chitinase belong to the glycoside hydrolase families 18 and 19 and catalyzes the degradation of the chitin (Neeraja et al., 2010; Vogt et al., 2018). Chitinase can be found in number of species who produce chitin for cell wall or exoskeletons such as fungi and arthropods. Some bacteria who do not synthesize chitin also produce chitinase for the purpose of consumption of chitin as an energy and carbon source (Vogt et al., 2018). Chitinase has multi domain structures, basically consists with catalytical

domain and the chitin binding domain. Chitin binding domain is assisted to bind the enzyme into the insoluble chitin while catalytical domain is functioning as degrade the chitin (Beier and Bertilsson, 2013; Raikhel and Lee, 1993). Aalten et al., (2001) mentioned that chitin binding and catalytic modules generate a continuous substrate binding site formed by surface of aromatic residues, which direct the substrate into the enzymes active site. Chitin binding domain from the chitinase A1 from *Bacillus circulans* WL-12 was used for our experiment (Hashimoto et al., 2000; Ikegami et al., 2000). Tertiary structure of the chitin binding domain of chitinase A1 is given in the Fig. 4-2.

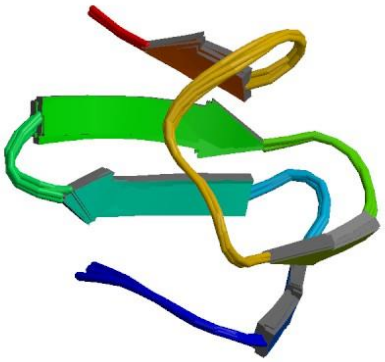

Fig. 4-2 Schematic ribbon drawing of the chitin binding domain of chitinase A1 (PDB ID (1ED7))

4.1.2. Calcium binding peptides

Recently, solid binding peptides have gained much attention as a molecular building block in nano-biotechnology. Solid binding peptides are defined as short amino acid sequences that has binding affinity for the surface of solid materials (Care et al., 2015). These solid binding peptides are mainly used in the formation of hybrid materials (Nguyen et al., 2014). In addition, used in immobilization of functional proteins (Johnson et al., 2008) and improve the compatibility of the nanomaterials (Zhang et al., 2012). Among the solid binding peptides, calcium binding peptides have been used extensively for the formation of organic-inorganic hybrid materials. Calcium binding peptides can be defined simply as short amino acid sequences which have binding affinity to calcium carbonate (Gebauer et al., 2009; Nayebi et al., 2017).

Calcium binding peptide with a higher affinity for the $CaCO_3$ which was derived from the phage-display technology was used for our experiment (Gaskin et al., 2000; Sarikaya et al., 2003). Fusion protein was constructed by introducing calcium binding peptide into the "N" terminal of the chitin binding domain while his tag was introduced in to the "C" terminal.

4.2. Objectives

Construction of a genetically modified fusion protein which can be used to produce organic-inorganic hybrid materials by efficient precipitation of the $CaCO_3$ upon the insoluble chitin matrix as given in Fig. 4-3. In addition, investigate the influence of the fusion protein (CaBP-ChBD), chitin binding domain (ChBD) and the calcium binding peptide (CaBP) on the $CaCO_3$ crystallization and the morphology of the crystals by using the enzyme induced carbonate precipitation method.

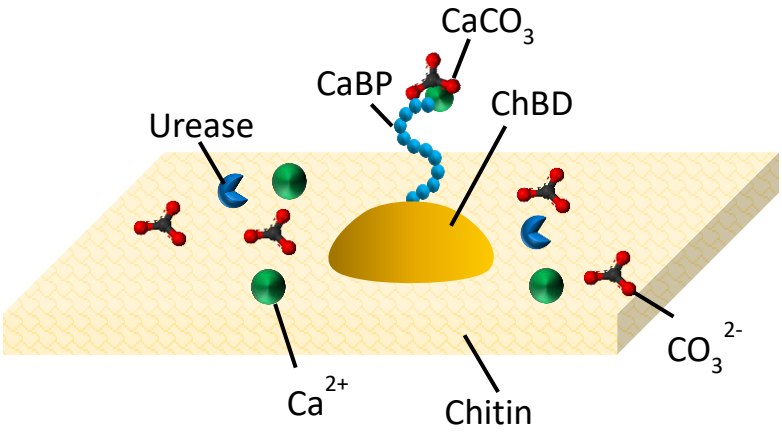

Fig. 4-3 Schematic of precipitation of $CaCO_3$ directed by CaBP-ChBD on the surface of chitin.

4.3. Materials and methods

4.3.1. Investigate the performance of Fusion protein

4.3.1.1. Construction of the target gene

Chitin binding domain (ChBD) of the chitinase A1 from *Bacillus circulans* WL-12 was used for our experiments (Hashimoto et al., 2000). Synthetic gene of the ChBD of *Bacillus circulans* was purchased from the Euro fin Genomics Co., Ltd, Tokyo. Since, gene came with a plasmid (pEX-A2J2-B.circulans-ChBD), two primers were designed to amplify the DNA region encoding ChBD using polymerase chain reaction (PCR). Peptide derived from the phage-display technology was used as the calcium binding peptide (CaBP) (Gaskin et al., 2000) and this short peptide with 12 amino acids was introduced into the forward primer. Amino acid sequences of the ChBD and the CaBP are given in the Table 4-1. pET-22b(+) vector was used as expression vector to carry target gene. Primer details are given in the Table 4-2.

Table 4-1 Amino acid sequence of the ChBD and CaBP

	Amino acid sequences	References
ChBD of *Bacillus circulans*	AWQVNTAYTAGQLVTYNGKTYKCLQPHTSL AGWEPSNVPALWQLQ	Hashimoto et al., 2000
CaBP	DVFSSFNLKHMR	Gaskin et al., 2000

Table 4-2 DNA sequence of the forward and reverse primers

Primer	Sequences (5'-3')
pET22-Cabp-Hind-bcChbD-NdeI_Fw	AAGGAGATATACATATGGATGTGTTTAGCTCGT TCAACCTGAAACATATGCGCAAGCTTGCCTGGC AAGTCAACACTGCG
pET22-bcChbD-XhoI_Rv	GGTGGTGGTGCTCGAGCTGCAGCTGCCACAACG CTG

For PCR amplification, Prime star max (Taraka bio inc., Japan) was used as DNA polymerase. Target gene (1 µl; 10 ng/ µl) contained prime star max DNA polymerase (25 µl), forward primer (1.25 µl), reverse primer (1.25 µl) and sterilized distilled water (21.5 µl) was

amplified using PCR. Amplified gene was separated by using gel electrophoresis and extracted from the agarose gel using gel/PCR extraction kit (Nippon genetics Europe, Germany). Fig. 4-4 shows the graphical representation of the target gene.

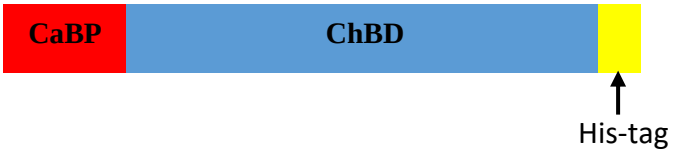

Fig. 4-4 Schematic design of the target gene

4.3.1.2. Transformation of the target gene into E.coli

pET 22b(+) vector was linearized using Xho I (New England Bio Labs, Tokyo, Japan) and Nde I (New England Bio Labs, Tokyo, Japan) restriction enzymes. Restriction sites were selected in order to incorporate the His-tag into the "C" terminal of the target gene. 10 µl of pET 22b(+) vector was mixed with 1 µl of Xho I, 1 µl of Nde I, 5 µl of cut smart (New England Bio Labs, Tokyo, Japan) and 33 µl of distilled water and incubated in 37 ºC for 10 min. linearized vector was separated using gel electrophoresis and extracted from the gel using gel/PCR extraction kit. Then target gene was inserted into the linearized pET 22b(+) vector using in-fusion enzyme (Taraka bio inc., Japan). 1.5 µl of linearized pET 22b(+) vector was mixed with 1 µl of infusion enzyme, 1 µl of target gene and 1.5 µl of sterilized distilled water and incubated 15 min at 50 ºC. Immediately after the infusion, transformation of the infused gene into the *E-coli DH5α* was carried out. Transformation was done by giving heat shock. 1 µl of the infused gene was mixed with 30 µl of the *E-coli DH5α* and kept 30 min at 4 ºC and then kept 90 sec in 42 ºC and finally incubated 5 min at 4 ºC. After transformation, bacteria cells were transferred into the LB-Amp agar plate (Tryptone (BD Biosciences Advanced Bioprocessing, Miami, FL, USA) 10 g/L, Yeast extract (BD Biosciences Advanced Bioprocessing, Miami, FL, USA) 5 g/L, Sodium Chloride (Wako Pure Chemical Industries Ltd., Tokyo, Japan) 10 g/L, Agar (Wako Pure Chemical Industries Ltd., Tokyo, Japan) 15 g/L, Ampicillin (Nacalai Tesque, Tokyo, Japan) 0.1 g/L) and kept in 37 ºC for 16-18 hours.

Obtained bacteria colonies were confirmed by using colony PCR. Sufficient amount of bacterial colony was mixed with the 12.5 µl KAPA 2G Fast Hot Start DNA polymerase (Kapa Biosystems, Wilmington, USA), 1.25 µl of T7 promotor (Eurofins Genomics, Tokyo, Japan), 1.25 µl of T7 terminator (Eurofins Genomics, Tokyo, Japan) and 10 µl of sterilized distilled water and target fragment was amplified by using PCR. Accuracy of the colony was identified

by using the gel electrophoresis. After confirmation of the accuracy of the colonies, selected colony was pre-cultured in LB-Amp medium and kept in the shaking incubator at 37 ^{o}C, 160 rpm for 16-18 h. Plasmid was extracted by using the plasmid extraction kit (Nippon genetics Europe, Germany) and confirmed the accuracy using sequence analysis.

4.3.1.3. Expression of the target protein

Extracted plasmid was transformed into the *E-Coli BL21 (DE3)* by using the same procedure described in the section 4.3.1.2 and confirmed through the colony PCR. After confirmation, selected colony was pre-cultured in LB-Amp medium and kept in the shaking incubator at 37 ^{o}C, 160 rpm for 16-18 h. Then, the pre-culture (1 mL) was inoculated into fresh LB-Amp medium (100 mL) and kept in the shaking incubator under the same conditions as those used for pre-culturing. Absorbance of the culture at 600 nm was monitored until it reaches 0.6 and protein expression was done by introducing isopropyl β-D-1thiogalactopyranoside (IPTG; Nacalai Tesque, Tokyo, Japan) at final concentration of 0.5 mM and culture temperature was changed from 37 °C to 30 °C. To check the level of protein expression, samples were collected from the culture at 0,1,3,6 and 24 h time intervals and centrifuged at 12000 rpm for 1 min and removed the supernatant and kept in the freezer.

100 µl of lysis buffer was added to the collected samples and sonicated for 2 min (Amplitude – 30 % and Pulse – 20s/20s). 10 µl of the sonicated samples were transferred into the PCR tubes and centrifuged to separate soluble and insoluble part of the cell lysate. Then, 10 µl of the supernatants were transferred into the separate tubes and both of the supernatant and pellets were treated with 10 µl of the SDS treatment buffer and incubated in 95 ^{o}C at 5 min. Expression of the protein was analyzed by using SDS-poly-acrylamide gel electrophoresis (SDS-PAGE; Atto company limited, Tokyo, Japan) which was stained with the Coomassie Brilliant Blue (CBB Stain One Super (Ready To Use), Nacalai Tesque, Inc.,Kyoto, Japan).

4.3.1.4. Purification and dialysis of the protein

Since the target protein has His tag in the “C” terminal, purification of the protein was done by using bio scale IMAC Ni-charged cartridge (Bio-rad Laboratories, Inc, Tokyo, Japan). After 24 hour culturing, cell culture was centrifuged (4 ^{o}C, 8000 g, 10 min) to separate cell

pellets and discarded the supernatant. Separated cell pellets were replaced with the lysis buffer and sonicated (5 min, 30%, 59s/59s) to disrupt the cells. After sonication cell lysate was centrifuged (4 ºC, 12000 g, 20 min) to separate soluble and insoluble fraction and supernatant was used for the purification since protein in the soluble fraction.

After introducing the sample into the cartridge, it was washed twice using wash buffers and target protein was eluted by using elution buffer with higher amount of imidazole. Eluted protein was concentrated by using the Amicon ultra filter (3 kDa) and protein was replaced into the tris-Hcl buffer (pH-9). Concentration of the protein was measured by using the Bradford protein assay kit (Taraka bio inc., Japan).

4.3.1.5. Chitin binding assay

Ability of the fusion protein for binding into the insoluble chitin was investigated. 0.01 g of insoluble chitin (Wako Pure Chemical Industries Ltd., Tokyo, Japan) was dissolved in the 1 ml of the fusion protein (CaBP-ChBD) with final concentration of 0.04 mM and kept in the shaking incubator at 25 ºC and 160 rpm. Samples were collected at different time intervals, centrifuged (13000 x g, 10 min) and protein concentration of the supernatant was measured by using Bradford protein assay kit.

4.3.1.6. Calcium binding assay

Ability of the CaBP-ChBD to bind into the $CaCO_3$ was examined. 0.01 g of $CaCO_3$ (Wako Pure Chemical Industries Ltd., Tokyo, Japan) was mixed with the 1 ml of the CaBP-ChBD with final concentration 0.04 mM and kept in the shaking incubator at 25 ºC and 160 rpm. Sample was collected at 24 hours and centrifuged (13000 x g, 10 min) and protein concentration of the supernatant was measured using Bradford protein assay kit.

4.3.2. Investigate the performance of chitin binding domain (ChBD)

4.3.2.1. Construction of the target gene

Synthetic gene of the ChBD from chitinase A1 of *Bacillus Circulans* which is purchased from the Euro fin Genomics Co., Ltd, Tokyo was used for this experiment. Experimental procedure is same as described in the section 4.3.1.1. Only forward primer was modified in order to extract ChBD. pET-22b(+) vector was used as expression vector to carry target gene. Primer detail is given in the Table 4-3. Target gene was amplified by using Prime star max as DNA polymerase. Amplified gene was separated by using gel electrophoresis and extracted from the agarose gel using gel/PCR extraction kit.

Table 4-3 Primer design for construction of ChBD

Primer	Sequences (5'-3')
pET-22b-ChbD-NdeI_Fw	AAGGAGATATACATATGGCCTGGCAAGTCAACACT

Transformation of the target gene into the *E.coli*, protein expression and purification were done by using the same procedure described in the section 4.3.1.2 – 4.3.1.3.

4.3.2.2. Chitin binding assay

Ability of the ChBD for binding into the insoluble chitin was investigated. 0.01 g of insoluble chitin (Wako Pure Chemical Industries Ltd., Tokyo, Japan) was dissolved in the 1 ml of the ChBD with final concentration of 0.04 mM and kept in the shaking incubator at 25 ^{o}C and 160 rpm. Samples were collected at different time intervals, centrifuged (13000 x g, 10 min) and protein concentration of the supernatant was measured using Bradford protein assay kit.

4.3.3. Investigate the performance of Calcium Binding Peptide (CaBP)

4.3.3.1. Preparation of the stock solution of ChBD

Synthesized CaBP was purchased from Gen Script, Tokyo, Japan and stock solution with 1mg/ml was prepared by dissolving the CaBP in tris-HCl buffer (pH-9).

4.3.4. $CaCO_3$ precipitation experiment

$CaCO_3$ precipitation experiments were conducted by hydrolysis of the urea using extracted jack bean urease enzyme (2.5 U/ml; Wako Pure Chemical Industries Ltd., Tokyo, Japan) in the presence of $CaCl_2$ and urea (0.75 mol/L; Wako Pure Chemical Industries Ltd., Tokyo, Japan). Experiments were conducted under different experimental conditions with and without chitin and fusion protein (CaBP-ChBD), ChBD and CaBP as shown in the Table 4-4. Reaction mixture was kept in the shaking incubator for 24 h at 25 ^{o}C and 160 rpm and centrifuged (24 °C, 12000 rpm, 10 min) to separate the precipitate from the supernatant. Dry weights of the precipitates were measured from the oven dried samples at 90 °C for 24 h. Morphology of the crystals were identified using SEM.

$CaCO_3$ Precipitation experiment with Bovine Serum Albumin (BSA)

$CaCO_3$ precipitation was conducted by using an inert protein BSA by following the procedure described in the section 4.3.4. Experiment was conducted under different conditions as shown in the Table 4-5.

Table 4-4 Experimental conditions for $CaCO_3$ precipitation

	Chitin (g)	CaBP-ChBD (μg/ml)	ChBD (μg/ml)	CaBP (μg/ml)
S1	-	-	-	-
S2	0.01	-	-	-
S3	-	75	-	-
S4	0.01	75	-	-
S5	-	-	75	-
S6	0.01	-	75	-
S7	-	-	-	75
S8	0.01	-	-	75
S9	-	-	75	75
S10	0.01	-	75	75

Table 4-5 Experimental conditions for $CaCO_3$ precipitation with and without BSA

	Chitin (g)	BSA (μg/ml)
S11	-	75
S12	0.01	75

4.4. Results and discussion

4.4.1. Construction of the CaBP-ChBD

Target gene could be constructed successfully, and relevant band was appeared around 171 bp as shown in Fig. 4-5. Target gene was effectively extracted from the gel/PCR extraction kit and infused with the linearized vector and transformed into the *E-coli DH5α*. Upon 18 hours incubation under 37 ºC, few numbers of colonies were obtained and confirmed the accuracy of the colonies by colony PCR as shown in Fig. 4-6. Selected colony was used to make pre-culture and after 18 h incubation at 37 ºC plasmid extraction was done by using plasmid extraction kit. Accuracy of the plasmid was confirmed through the sequence analysis.

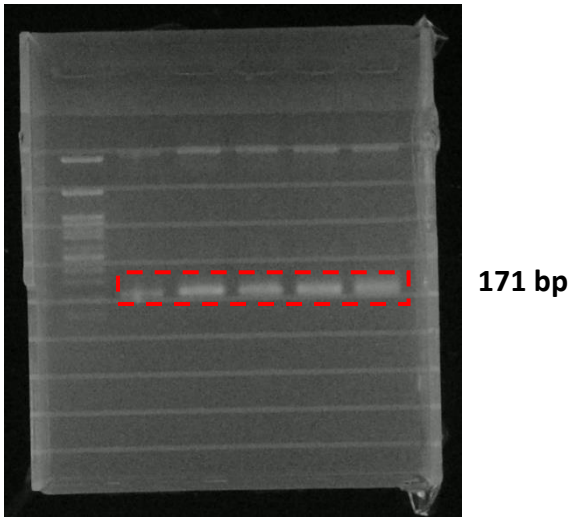

Fig. 4-5 Amplified Fragment for CaBP-ChBD

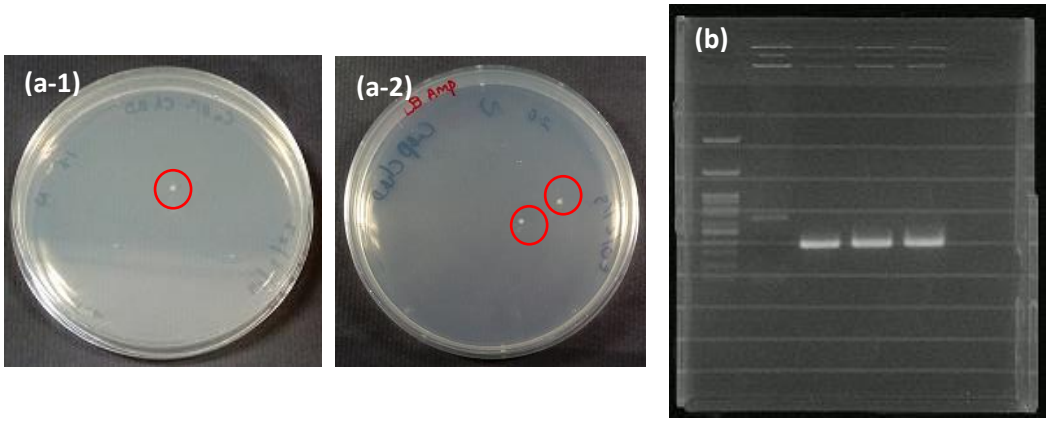

Fig. 4-6 Transformation of pET 22b(+) with target gene into *E.Coli DH5α* (a-1,2) Colonies of *E.Coli DH5α* containing target gene (b) Confirmation of *E.Coli DH5α* with pET 22b(+)-CaBP-ChBD.

4.4.1.1. Expression of the CaBP-ChBD

Plasmid was able to transformed successfully into the *E-coli BL21(DE3)* and selected colonies were confirmed through the colony PCR as shown in the Fig. 4-7.

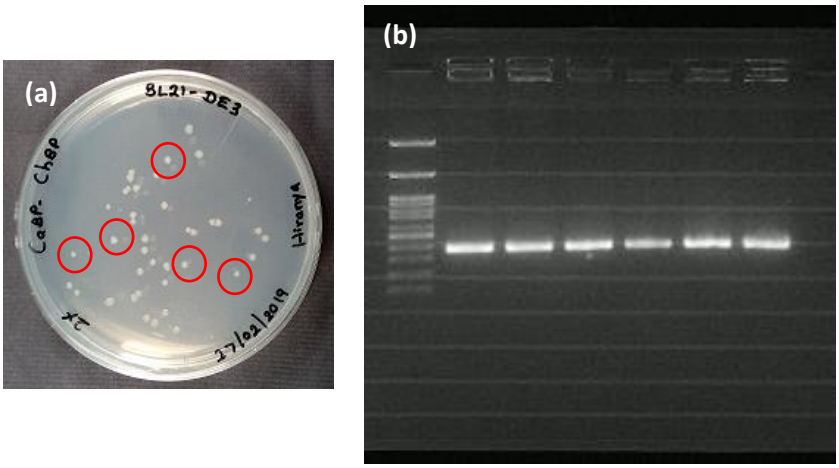

Fig. 4-7 Transformation of plasmid into *E.Coli BL21(DE3)* (a) Colonies of *E.Coli BL21(DE3)* with pET 22b(+)-CaBP-ChBD (b) Confirmation of *E.Coli BL21(DE3)* with pET 22b(+)-CaBP-ChBD.

Protein expression of the fusion protein (CaBP-ChBD) was examined for 24 hours. According to the SDS page results shown in Fig. 4-8(a), target protein has been expressed successfully as a soluble protein and protein expression has started after 3 h of incubation. Generally, genetically modified proteins have been expressed with IPTG under lower temperatures (15 ^{o}C) to prevent the over expression of other proteins. Over expression of proteins cause the misfolding of protein and the formation of the inclusion bodies which lead to lower expression of the target protein. However, we were unable to express our fusion protein under lower temperatures and protein was successfully expressed at higher temperatures (30 ^{o}C). Expression temperature mostly depends on the type of the protein and most of the time, chitin binding proteins have been expressed in higher temperatures (Ping et al., 2018; Lobo et al., 2013).

After successfully expression of the target protein, protein was purified using IMAC Ni-charged cartridge and successfully separated using elution buffer with higher concentration of imidazole as shown in Fig. 4-8(b). Since, purified protein contained higher amount of imidazole, protein was replaced into a Tris-Hcl buffer (pH-9) during the concentrate of the protein using Amicon ultra filter. Ultra-filter with molecular weight cutoff (MWCO) 3 kD was

used since molecular weight of our target protein is 6.48 kD. Previous researches reported that ChBD from chitinase A1 exhibited higher binding affinity for colloidal chitin around higher pH (8-9). Therefore, protein was replaced with Tris-Hcl buffer with pH-9 (Hashimoto et al., 2000).

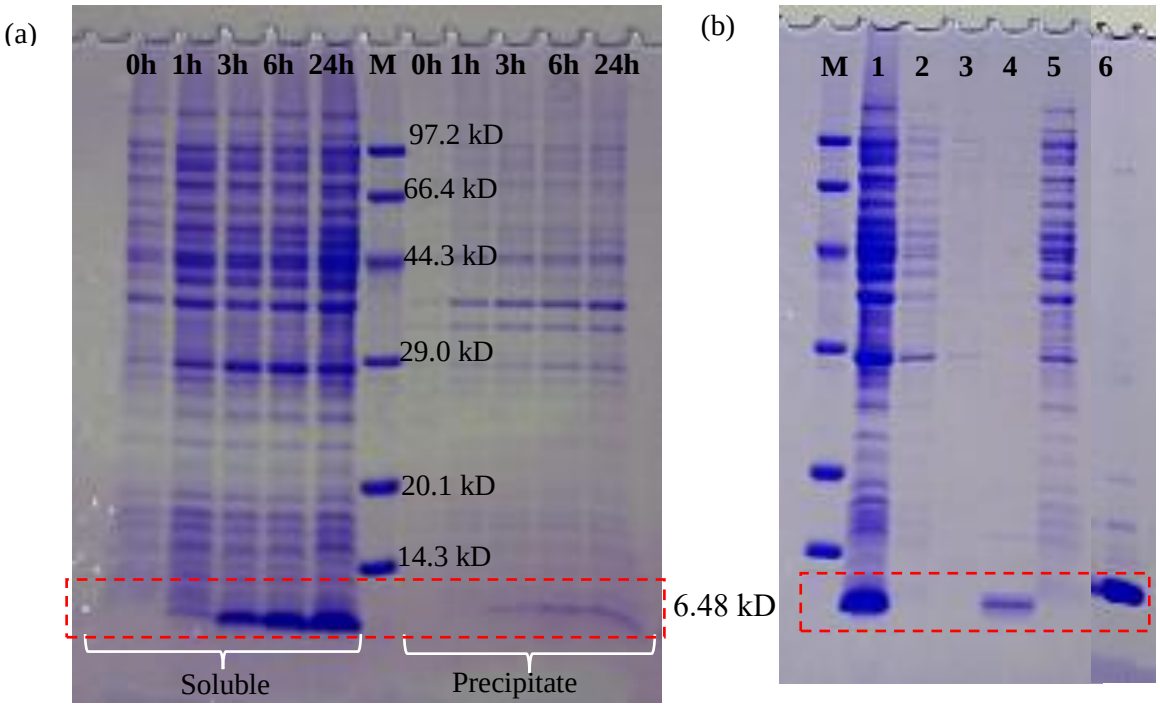

Fig. 4-8 SDS-page analysis to confirm the expression of CaBP-ChBD (a) Expression of the CaBP-ChBD with in 24 h (b) Protein purification and dialysis; M – Protein marker, 1-Sample after 24 h, 2- Wash 1, 3-Wash 2, 4- Elution, 5- Flow through, 6- After dialysis.

4.4.1.2. Chitin binding assay

Chitin binding assay was conducted according to the procedure described in the section 4.3.1.5. Protein concentration was decreased with time, other words adsorption of the CaBP-ChBD into the insoluble chitin was increased with the time as shown in the Fig. 4-9. 80% of CaBP-ChBD was bound to the insoluble chitin within the 3 hours. Results are agreed well with the previous observation made by Hashimoto et al. (2000) for the binding assay of ChBD from Chitinases A1 into the colloidal chitin. Isoelectric point (pI) of the CaBP-ChBD is around 8.9 and it is similar to the pH of the solution. Hence, interaction between the CaBP-ChBD and the insoluble chitin mostly hydrophobic (Hashimoto et al., 2000).

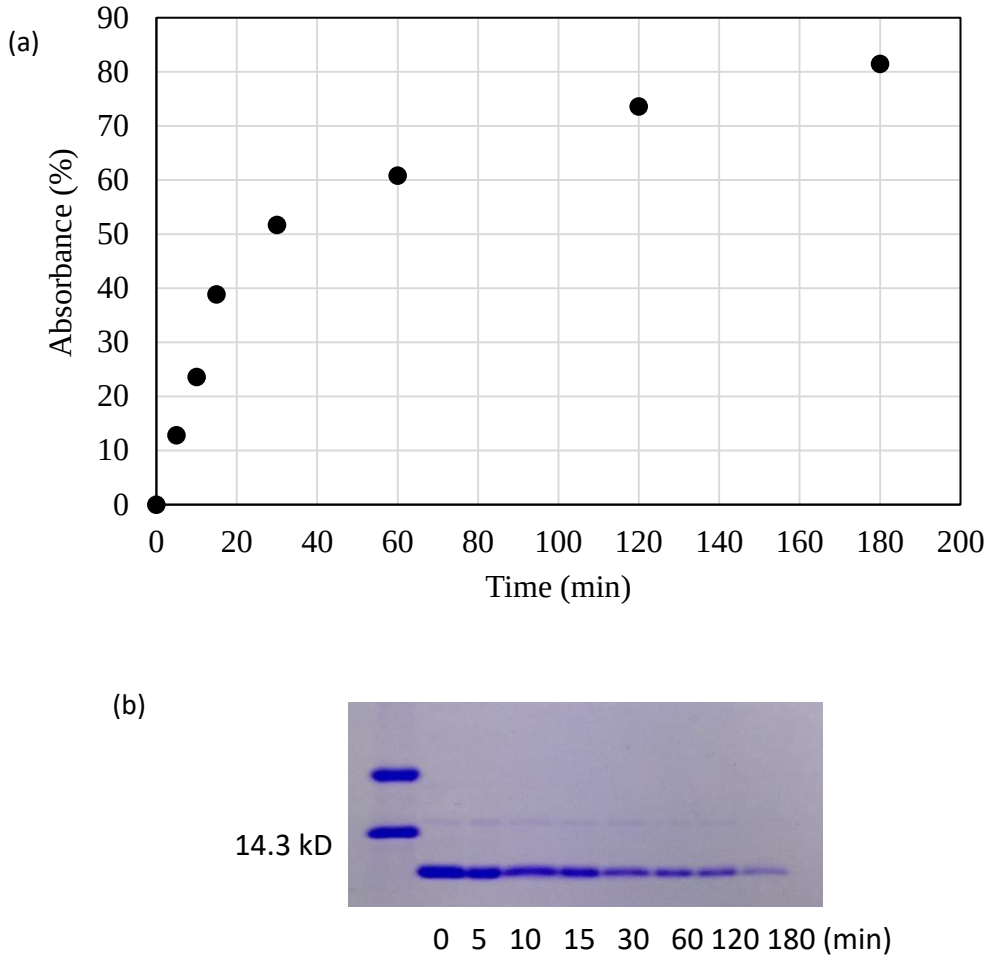

Fig. 4-9 Chitin binding assay (a) Time courses of binding of CaBP-ChBD into insoluble chitin (b) Variation of the protein concentration in the reaction mixture with time.

4.4.1.3. Calcium binding assay

Binding of the CaBP-ChBD into the $CaCO_3$ is not efficient as binding of the CaBP-ChBD into the chitin. However, Protein concentration was reduced by 30% after 24 h which reflects the 30% of the CaBP-ChBD has bound to the $CaCO_3$ within 24 hours as shown in Fig. 4-10.

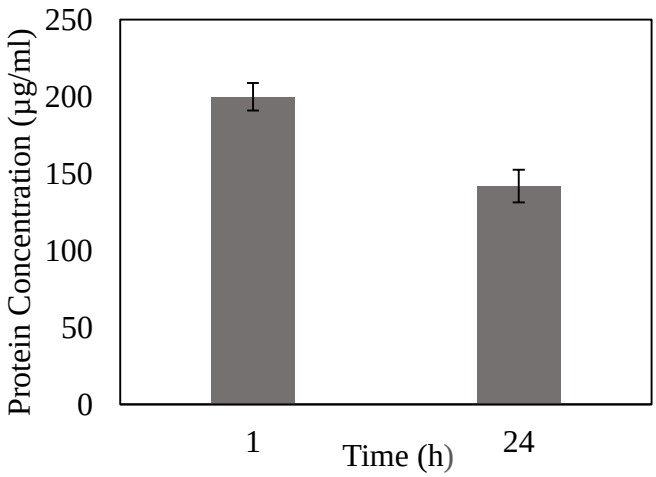

Fig. 4-10 Variation of the concentration of CaBP-ChBD with time after react with the $CaCO_3$

4.4.2. Construction of the ChBD

Target gene was constructed successfully, and band was appeared around 135 bp in agarose gel as shown in Fig. 4-11. Target gene extraction was done by using gel/PCR extraction kit and successfully fused into the linearized vector. Upon 18 h incubation of the *E.coli DH5α* containing target gene, fewer number of colonies were detected and confirmed through the colony PCR as shown in Fig. 4-12. Pre-culture was done for a selected colony and plasmid was extracted and confirmed the accuracy through sequence analysis.

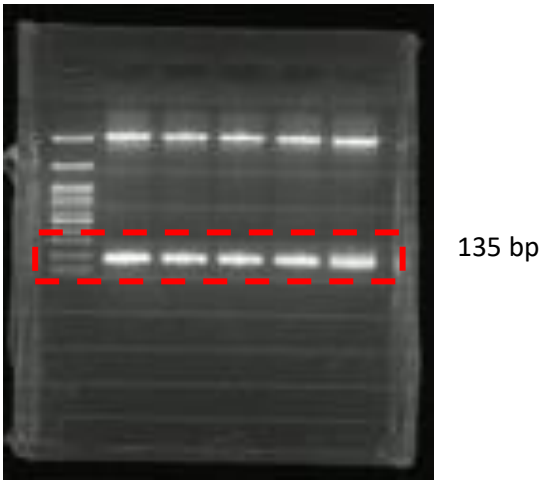

Fig. 4-11 Amplified fragment of ChBD

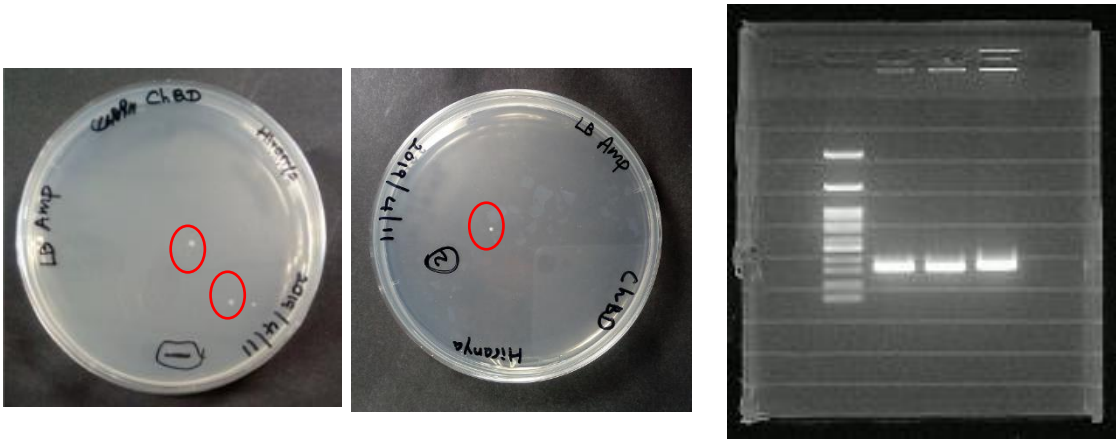

(a) (b)

Fig. 4-12 Transformation of pET 22b(+) with target gene into *E.Coli DH5α* (a) Colonies of *E.Coli DH5α* containing target gene (b) Confirmation of E.Coli DH5α with pET 22b(+)-ChBD.

4.4.2.1. Expression of the ChBD

Plasmid was transformed successfully into the *E-coliBL21(DE3)* and selected colonies were confirmed through the colony PCR as shown in Fig. 4-13.

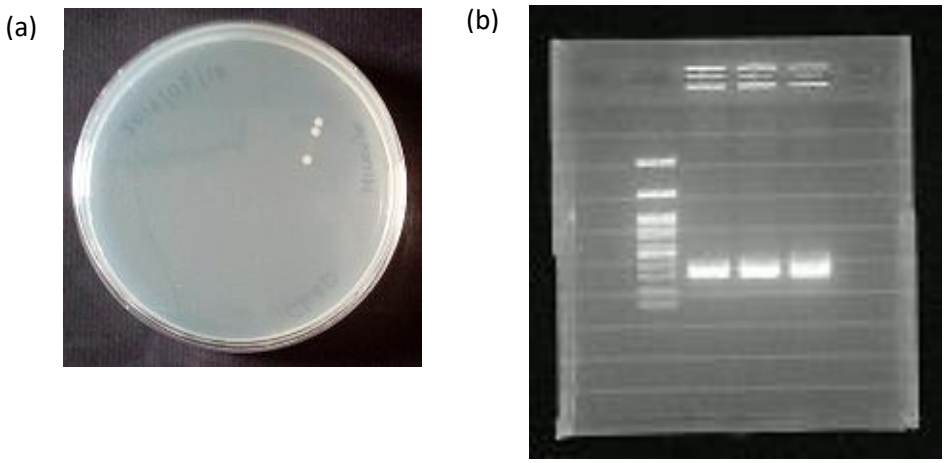

Fig. 4-13 Transformation of plasmid into *E.Coli BL21(DE3)* (a) Colonies of *E.Coli BL21(DE3)* with pET 22b(+)-ChBD (b) Confirmation of *E.Coli BL21(DE3)* with pET 22b(+)-ChBD.

Protein expression of the ChBD was examined for 24 hours. According to the SDS page results shown in Fig. 4-14(a) protein expression has been started after 3 h as a soluble protein. Protein was purified using IMAC Ni-charged cartridge and could be eluted successfully as shown in Fig. 4-14(b). Protein was concentrated using Amicon ultra filter with molecular weight cutoff (MWCO) 3 kD and replaced in to the Tris-Hcl buffer with pH-9.

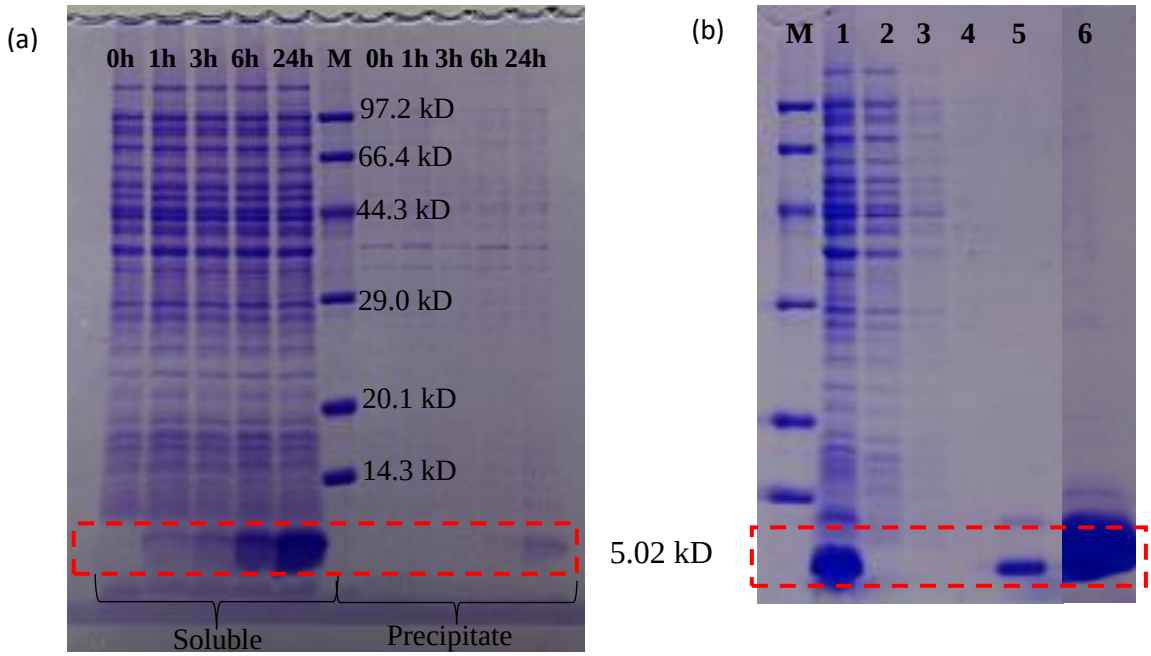

Fig. 4-14 SDS-page analysis to confirm the expression of ChBD (a) Expression of the ChBD within 24 h (b) Protein purification and dialysis; M – Protein marker, 1- Sample after 24 h, 2- Flow through , 3-Wash 1, 4- Wash 2, 5- Elution, 6- After dialysis.

4.4.2.2. Chitin binding assay

Fig. 4-15 shows the variation of the adsorption of the ChBD into the insoluble chitin with time. Approximately 80% of adsorption was achieved within 3 hours. The results are matching well with the previous observations done by Hashimoto et al., (2000) for ChBD from Chitinases A1. They have observed the adsorption of the ChBD into the colloidal chitin under different buffer conditions. As mentioned in the section 4.4.1.2 the interaction between the chitin and the ChBD can be a hydrophobic interaction since isoelectric point of the ChBD is 8.91 and the solution pH is around 9.

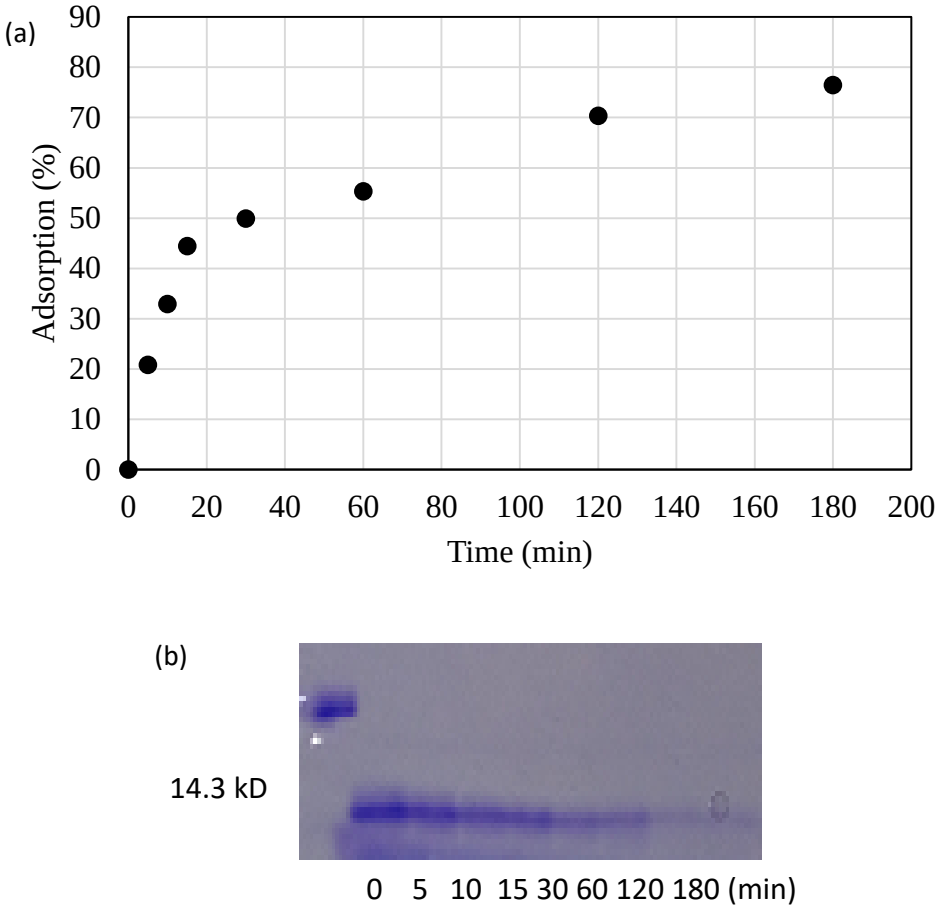

Fig. 4-15 Chitin binding assay (a) Time courses of binding of ChBD into insoluble chitin (b) Variation of the protein concentration in the reaction mixture with time.

4.4.3. $CaCO_3$ precipitation experiment

$CaCO_3$ precipitation experiment was conducted by using extracted urease enzyme under different experimental conditions as given in the Table 4-4. Fig. 4-16 shows the obtained amount of precipitate for different experimental conditions. Experimental conditions are graphically shown in Fig. 4-17. Precipitate values represents the average value of three independent experiments and standard deviation value was used to represent the error bars. By adding chitin (S2) slight increment of the precipitate could be obtained. However, by adding proteins significant increment of the precipitate could be seen. For all cases, proteins itself have an ability to upgrade the $CaCO_3$ formation efficiency even without chitin. Compared with the ChBD and CaBP, by adding fusion protein (CaBP-ChBD) extremely higher amount of precipitate could be obtained. Fig. 4-18 shows the increment of the precipitate with CaBP-

ChBD. As shown in the Fig. 4-19, by introducing CaBP-ChBD, $CaCO_3$ formation efficiency has been increased from the 55% while with ChBD and CaBP it was 25% and 18%.

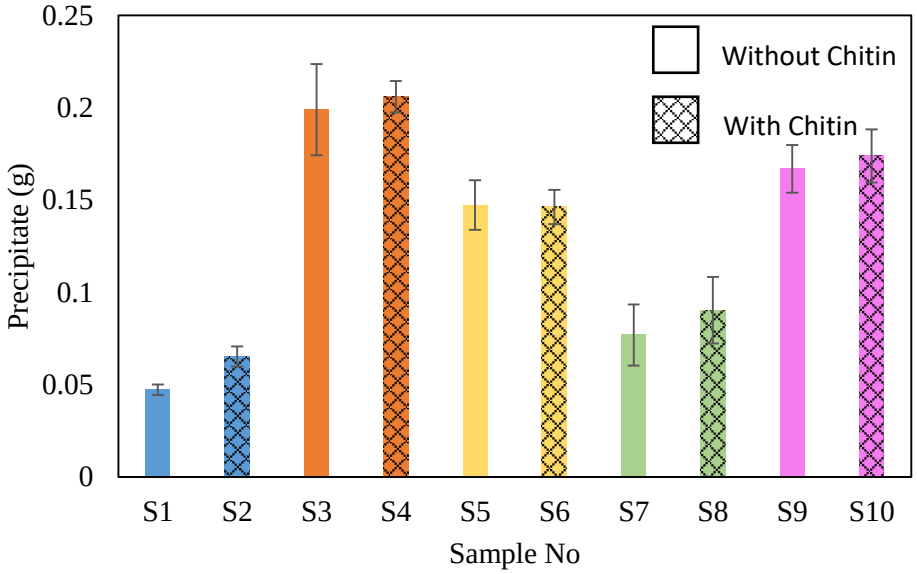

Fig. 4-16 Amount of precipitate obtained for different test cases with and without chitin

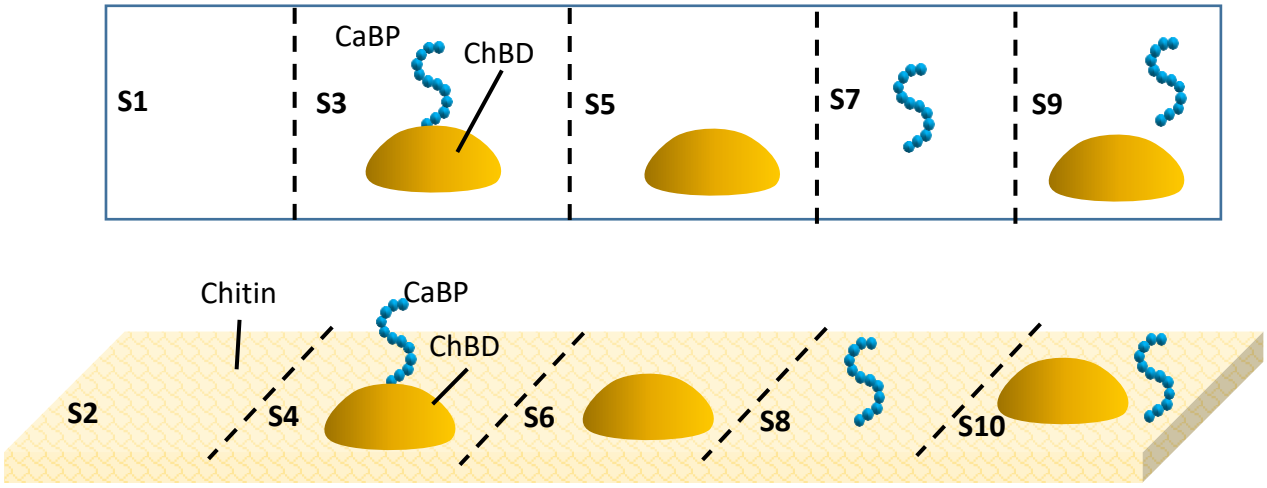

Fig. 4-17 Graphical illustration of the samples

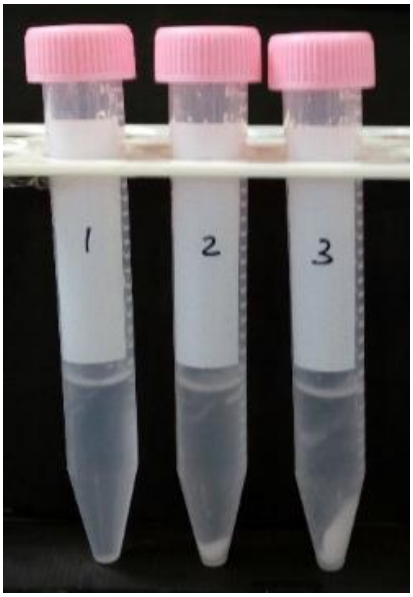

Fig. 4-18 $CaCO_3$ precipitate (1) S1 (2) S2 (3) S4

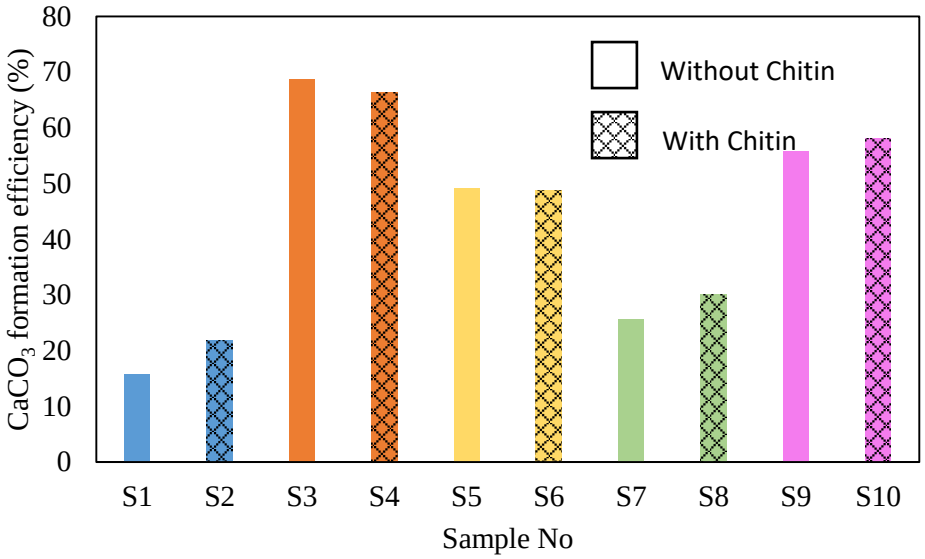

Fig. 4-19 $CaCO_3$ formation efficiency

Formation of the $CaCO_3$ in the presence of proteins mainly related to the amino acid sequence of the protein. Basically amino acids have a higher influence on the $CaCO_3$ formation and amino acids can serve as nucleation and growth promoting molecules for $CaCO_3$ formation by reducing the activation energy of nucleation and promoting the crystal growth (Briegel and Seto, 2012). CaBP used in this study has derived from the phage display analysis (Gaskin et

al., 2000) and this peptide is not rich with acidic amino acids only one aspartic acid residue is present. However, peptide is rich with basic amino acids and consisted with lysine, histidine and arginine residues. Consider about the amino acid sequence of the ChBD, it also not rich with the acidic amino acids and only one glutamic acid residue can be found and two lysine and one histidine residues are present. At pH-9, half of the amino groups in lysine, histidine and arginine residues are charged positively while carboxylic group in the glutamic acid and aspartic acid completely charged negatively. Hence, both of the acidic and basic residues have considerable influence on the $CaCO_3$ formation.

Generally, acidic amino acids are known to be associated with the proteins which are facilitated the $CaCO_3$ biomineralization (DeOliveira and Laursen, 1997; Sugawara et al., 2006). However, some researchers reported that acidic amino acids inhibit the $CaCO_3$ crystallization and promote the stabilization of the unstable phase of the $CaCO_3$ (Njegić Džakula et al., 2018; Zou et al., 2017). Also, in our previous study we have found that basic polypeptides have capability to upgrade the $CaCO_3$ formation (Nawarathna et al., 2018). Some matrix proteins which facilitate the $CaCO_3$ biomineralization are rich with more basic amino acid residues (Jain et al., 2017). Hence, the reason for the higher performance of $CaCO_3$ formation in the presence of CaBP-ChBD would be due to the presence of the basic amino acid residues. Compared with the CaBP, ChBD has more basic amino acid residues and it would be the reason for obtaining higher precipitate for ChBD compare with the CaBP.

Morphology of the crystals also changed drastically with the proteins. Without chitin or protein, polyhedron and spherical crystals were obtained as shown in Fig. 4-20(a). In the presence of only chitin without protein, individual chitin particles can be seen separately and rhombohedral shaped crystals have been deposited upon the chitin particles. Previous research also mentioned the formation of the rhombohedral crystals upon chitin matrix without matrix protein (Sugawara et al., 2006; Ping et al., 2018). However, in the presence of CaBP-ChBD, chitin particles were efficiently covered with the dumbbell shaped crystals as shown in Fig. 4-20(d-1,2). It is difficult to see the uncovered chitin particles and most of the chitin particles were covered with $CaCO_3$. It provides an evidence that fusion protein has assisted to formation of the $CaCO_3$ on the chitin matrix. With only ChBD, fewer amount of crystals have been precipitated upon the chitin matrix as shown in Fig. 4-21(b). Also, crystal morphology is mostly similar to the crystal morphology obtained with CaBP-ChBD and dumbbell and rod shape crystals are dominant. However, in the presence of only CaBP, chitin particles are like almost uncover and rhombohedral shaped crystals can be seen on the chitin matrix as similar to the case without protein (Fig. 4-22(b)).

Some of previous researches have reported the formation of the dumbbell shaped crystals, mainly in presence of double hydrophilic block copolymers, lignin, Mg^{2+} ions and other organic additives (Feng, 2011; Zhu et al., 2010). Formation of dumbbell, ellipsoidal and rod shape crystals are mainly due to the reassemble of the rhombohedral crystals and elongated into the *C* axis when the crystallization take place in the presence of low molecular weight additives (Didymus et al., 1993).

Behavior of the CaBP-ChBD and ChBD on the $CaCO_3$ formation can be explained in two ways. Basically, both of the proteins can be adsorbed into the chitin and chitin act as a template to $CaCO_3$ to nucleate and grow. However, in the case of CaBP-ChBD efficient precipitation of the $CaCO_3$ on the chitin matrix was happened due to the associated CaBP, which helped to proficient precipitation of the $CaCO_3$ on the chitin matrix. Also, CaBP-ChBD, ChBD and CaBP themselves contributed to the growth of the $CaCO_3$ by absorbing into the crystal phases. Variation of the pH mainly affect to the conformational changes of the organic additives which has significant influence on the morphology of the $CaCO_3$ crystals under the presence of organic additives. Previously, twin sphere shaped calcite crystals have been obtained due to the confirmation change of the polymer chain under the alkaline condition (Y. Yao et al., 2009). In our case, changes of the structure of the proteins mainly with CaBP-ChBD and ChBD under the alkaline condition would be a one reason for the formation of dumbbell shaped crystals since pH of the reaction mixture is around 9.

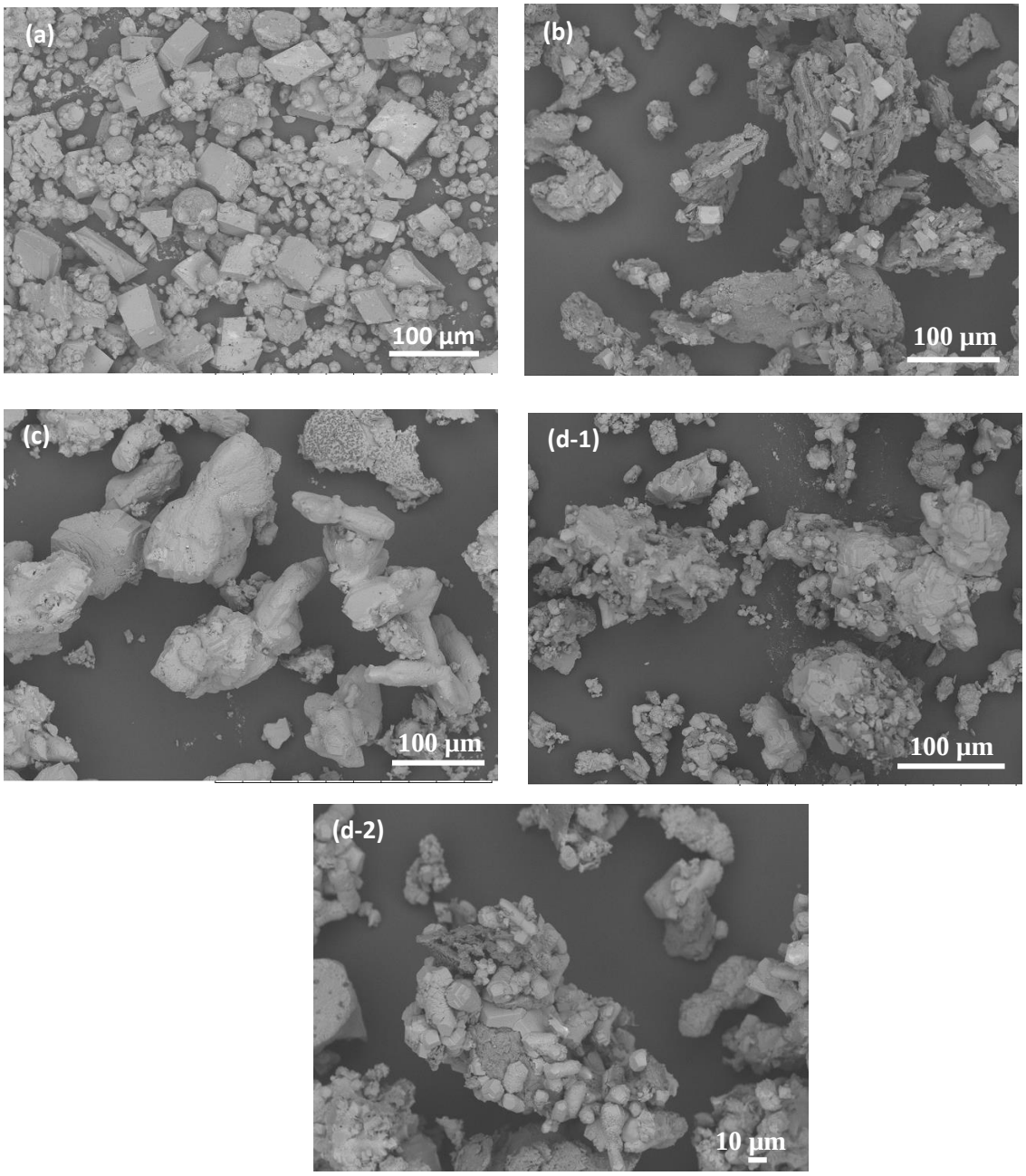

Fig. 4-20 SEM images of the $CaCO_3$ precipitate (a) S1 (b) S2 (c) S3 (d-1,2) S4

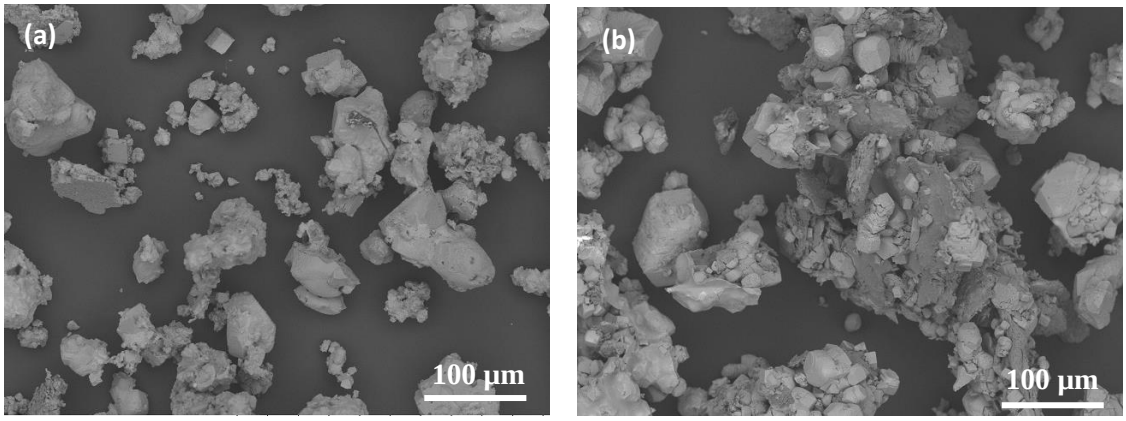

Fig. 4-21 SEM images of the $CaCO_3$ precipitate with ChBD (a) S5 (b) S6

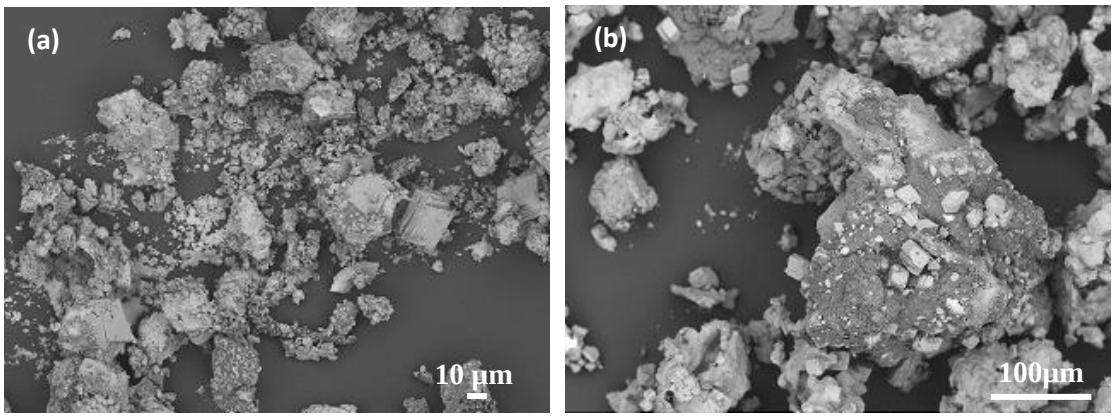

Fig. 4-22 SEM images of the $CaCO_3$ precipitate with CaBP (a) S5 (b) S6

On the other hand, carboxylic group of the amino acid protonated completely under higher pH (8-9) and form polyanionic chain where Ca^{2+} could be easily attached into the protein and create nucleation sites (Cölfen and Qi, 2001). Also, it leads to increase the supersaturation of the solution. This would be a reason for the higher nucleation and growth rate observed with the CaBP-ChBD than without. Donners et al., (2002) also reported the dumbbell shape of crystals in the presence of alanyl-alanine-derived poly (isocyanide)s, they mentioned that higher nucleation density, low spread in size and the absence of rhombohedral crystals provide evidence of its behavior as efficient nucleator. Also, they have clearly mentioned that, formation of the crystals with the shape of dumbbell is due to the development of the growth faces of crystals in addition to the end faces due to the adsorption of polymer onto these faces. Therefore, it inhibits the growth of the crystals in those directions and growth only along the *c*-axis (Feng, 2011; Sommerdijk and de With, 2009).

When the protein contains both of the positively and negatively charged amino acid residues, several kinds of electrostatic interactions are possible which can be affected for the morphology of the crystals. Basically, interaction between the protein molecules is possible due to the charged side chains. Also, positively charged amino groups are interact with the negatively charged carbonate ions and negatively charged carboxylic groups can interact with the positively charged Ca^{2+} ions (Ghatak et al., 2013). These complex nature of the interaction causes to produce several different morphologies as shown in Fig. 4-20(c) & Fig. 4-21(a). However, one research group reported that glutamic acid and lysine have low tendency to incorporate into calcite crystals (Borukhin et al., 2012). Hence, it seems like histidine and other acidic amino acids and amino acids with uncharged polar side chains have significant contribution for the morphology change.

Amino acids with uncharged polar side chains have a significant contribution to the $CaCO_3$ formation. According to the amino acid sequence of CaBP-ChBD, it contains Cysteine, Serine, and Asparagine which have considerable effect on the $CaCO_3$ crystallization. In nature, there are some mineral associated proteins which are rich with cysteine. Basic $CaCO_3$ associated proteins from the lustrin A (Chen et al., 2003), nacre of the abalone (Treccani et al., 2006), perlwapin (Treccani et al., 2006) are associated with the cysteine rich domain. Also, under the alkaline conditions, there is a high possibility to charge the carboxyl group negatively than positive charge on the amino group. Our experiments were conducted on the medium with pH=9. Hence, most of the amino acids with uncharged polar side chains have capability to charge negatively and bind to the Ca^{2+} ions which affect for the morphology of the crystals. Also, cysteine has capability to interact with the minerals through thiol bonds (S-Ca) which are stronger than the disulfide bonds (S-S) (Colin et al., 1964).

Further, $CaCO_3$ precipitation experiment was conducted by adding same concentration of CaBP and ChBD into the reaction mixture. As shown in Fig. 4-16, amount of precipitate is closer to the amount of precipitate obtained by using only ChBD. Morphology of the crystals also similar to the case of CaBP-ChBD and ChBD. Dumbbell, ellipsoidal and polyhedron shaped crystals can be seen in the precipitate as shown in the Fig. 4-23. Also, it can be seen that chitin particles were covered partially with the $CaCO_3$ crystals. All of these results reveled that, excellent ability of the CaBP-ChBD on the formation of the $CaCO_3$ is not only due to the CaBP and ChBD. Structure of the protein (CaBP-ChBD), its molecular arrangement have significant influence on the formation of the $CaCO_3$. Further experiments should be carried out to give better conclusion about the change of the secondary structure of the protein during the $CaCO_3$ formation.

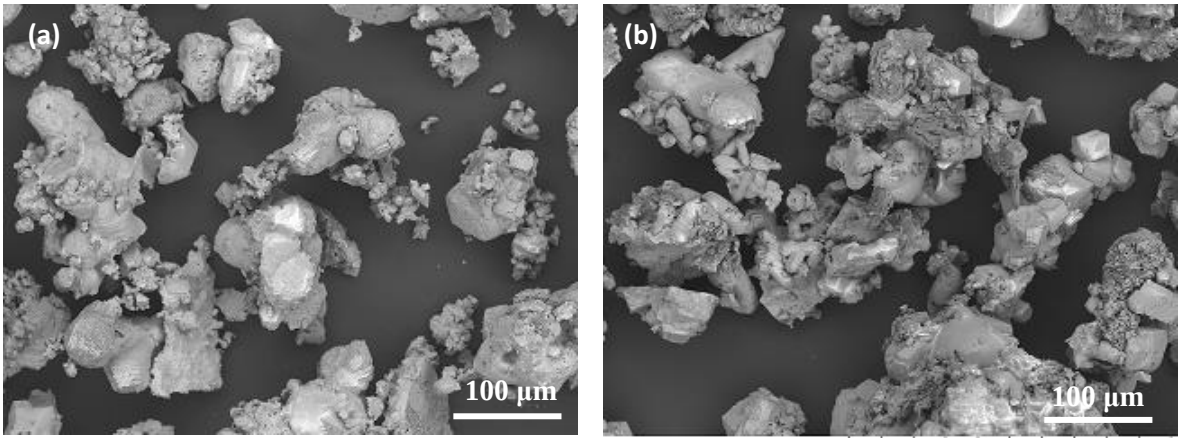

Fig. 4-23 SEM images of the $CaCO_3$ precipitate with CaBP & ChBD (a) S9 (b) S10

$CaCO_3$ precipitation with BSA

$CaCO_3$ precipitation experiments were conducted with the BSA as control experiment. BSA is a most abundant plasma protein in mammals and it is a neutral and non-reactive protein (Majorek et al., 2012). BSA is extensively used as matrix or soft template to induce the formation of calcium carbonate (C. L. Yao et al., 2009). In addition, BSA has strong affinity to variety of inorganic minerals. Hence, BSA incorporated nanomaterials have used variety of supramolecular assemblies (Yang et al., 2009).

According to the obtained results, by adding BSA into the reaction mixture little increment of the precipitate was exhibited as shown in Fig. 4-24. However, it is not significant as like with CaBP-ChBD or other proteins. Therefore, the results confirmed that superior ability of the CaBP-ChBD to form $CaCO_3$ is a unique property. Morphology of the crystals also examined by using SEM. According to the results given in Fig. 4-25(a) without chitin, distorted shaped crystal agglomerations were obtained. Surface of the crystals appeared as rough due to the adsorption of the protein into the growing crystal faces. Yang et al., (2009) have mentioned that formations of this kind of complex structures are related to the protein mediated self-assembly and they have obtained $CaCO_3$/BSA hybrid crystals. Also, BSA didn't contribute to the formation of the $CaCO_3$ crystals on the chitin matrix and uncovered chitin particles can be seen as shown in Fig. 4-25(b).

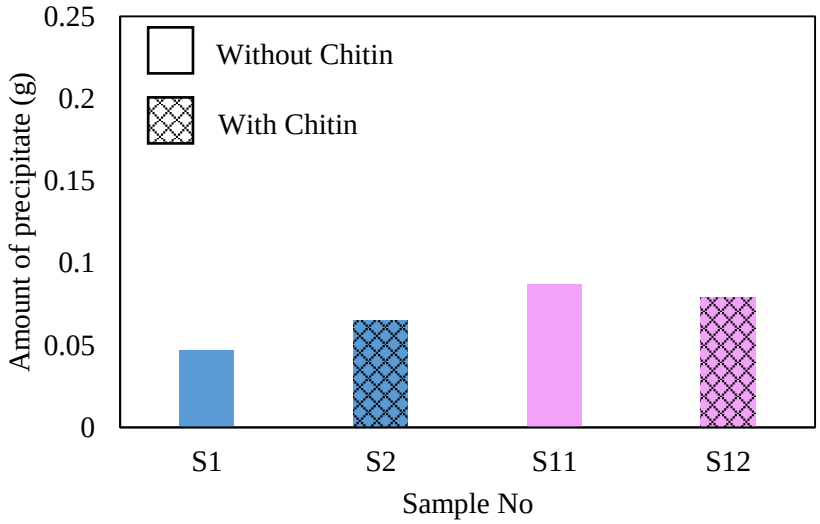

Fig. 4-24 Amount of precipitate obtained for different test cases with and without chitin or BSA

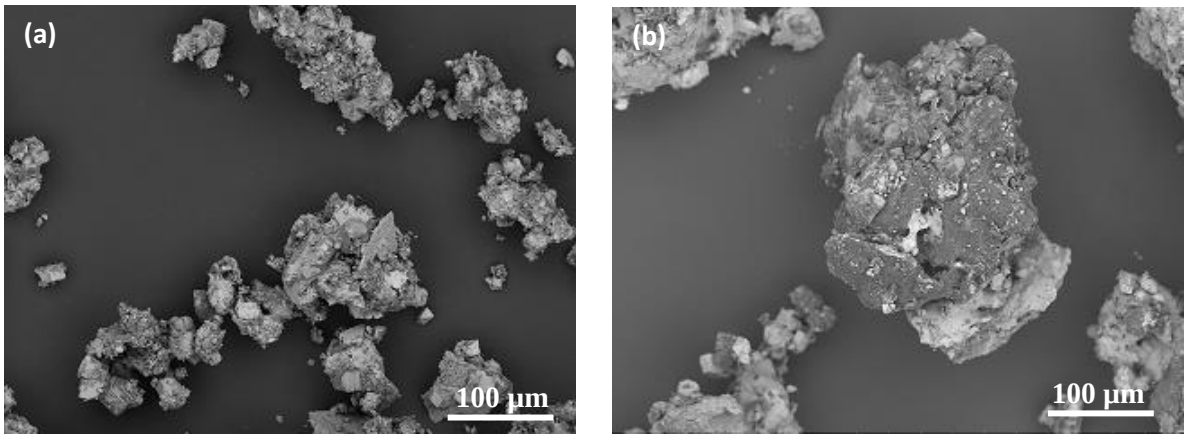

Fig. 4-25 SEM images of the $CaCO_3$ precipitate with BSA (a) S11 (b) S12

4.5. Conclusion

Novel fusion protein was generated to facilitate the organic-inorganic hybrid material formation by efficient precipitation of the $CaCO_3$ on the chitin matrix. Recombinant protein was constructed by introducing CaBP into the ChBD. Target protein (CaBP-ChBD) was successfully constructed and expressed into the *E-Coli*.

Chitin binding assay was conducted for recombinant protein (CaBP-ChBD) and the ChBD separately and found that both of the proteins have a superior ability to bind into the insoluble chitin and 80% of the protein was bound to the insoluble chitin within 3 hours. $CaCO_3$

precipitation experiments were conducted separately by hydrolysis of the urea using jack bean urease in the presence of CaBP-ChBD, ChBD and CaBP.

$CaCO_3$ formation efficiency has increased significantly in the presence of proteins than that of without proteins. However, CaBP-ChBD exhibited higher $CaCO_3$ formation efficiency than the ChBD and CaBP. By adding CaBP-ChBD into the reaction mixture $CaCO_3$ formation efficiency was increased by 55%. However, with ChBD and CaBP it was 25% and 18%. Also, in the presence of chitin and CaBP-ChBD, chitin particles were efficiently covered with the dumbbell shaped $CaCO_3$ crystals while without CaBP-ChBD, few crystals could be seen on the chitin surface. In addition, $CaCO_3$ crystals were not efficiently bound to the chitin particles in the presence of ChBD and CaBP. Incorporated amino acid residue in the CaBP-ChBD would be the reason for its superior performance in $CaCO_3$ crystallization.

Finally, developed recombinant protein could be used to facilitate efficient precipitation of the $CaCO_3$ on the chitin matrix and form organic-inorganic hybrid material which can be used for number of industrial applications.

References

Aalten, D.M.F. V, Komander, D., Synstad, B., Gasaidenes, S., Peter, M.G., Eijsink, V.G.H., 2001. Structural insights into the catalytic mechanism of a family 18 exo-chitinase. Proc. Natl. Acad. Sci. 98, 8979–8984.

Arakaki, A., Shimizu, K., Oda, M., Sakamoto, T., Nishimura, T., Kato, T., 2015. Biomineralization-inspired synthesis of functional organic/inorganic hybrid materials: Organic molecular control of self-organization of hybrids. Org. Biomol. Chem. 13, 974–989. https://doi.org/10.1039/c4ob01796j

Beier, S., Bertilsson, S., 2013. Bacterial chitin degradation-mechanisms and ecophysiological strategies. Front. Microbiol. 4, 1–12. https://doi.org/10.3389/fmicb.2013.00149

Borukhin, S., Bloch, L., Radlauer, T., Hill, A.H., Fitch, A.N., Pokroy, B., 2012. Screening the incorporation of amino acids into an inorganic crystalline host: The case of calcite. Adv. Funct. Mater. 22, 4216–4224. https://doi.org/10.1002/adfm.201201079

Briegel, C., Seto, J., 2012. Single Amino Acids as Additives Modulating $CaCO_3$ Mineralization. In Advanced Topics in Biomineralization. pp. 33–48.

Care, A., Bergquist, P.L., Sunna, A., 2015. Solid-binding peptides: Smart tools for nanobiotechnology. Trends Biotechnol. 33, 259–268. https://doi.org/10.1016/j.tibtech.2015.02.005

Chambers, A., Park, C., Baker, R.T.K., Rodriguez, N.M., Chen, P., Lin, J., Tan, K.L., Brown, S.D.M., Dresselhaus, G., 1999. Polycationic Peptides from diatom biosilica that direct silica nanosphere formation. Science.286, 1129-1132.

Chen, T., Small, D.A., Wu, L.Q., Rubloff, G.W., Ghodssi, R., Vazquez-Duhalt, R., Bentley, W.E., Payne, G.F., 2003. Nature-Inspired Creation of Protein-Polysaccharide Conjugate and Its Subsequent Assembly onto a Patterned Surface. Langmuir. 19, 9382–9386. https://doi.org/10.1021/la0347096

Cölfen, H., Qi, L., 2001. A Systematic Examination of the Morphogenesis of Calcium Carbonate in the presence of a double-hydrophilic block copolymers. Chem. Eur. J. 7, 106–116.

Colin, R., Goldfinger, P., Jeunehomme, M., 1964. Mass-spectrometric studies of the vaporization of the sulphides of calcium, strontium and barium. The dissociation energy of S2 and SO. Trans. Faraday Soc. 60, 306–316. https://doi.org/10.1039/tf9646000306

DeOliveira, D.B., Laursen, R.A., 1997. Control of calcite crystal morphology by a peptide designed to bind to a specific surface. J. Am. Chem. Soc. 119, 10627–10631.

https://doi.org/10.1021/ja972270w

Didymus, J.M., Oliver, P., Mann, S., DeVries, A.L., Hauschka, P. V., Westbroek, P., 1993. Influence of low-molecular-weight and macromolecular organic additives on the morphology of calcium carbonate. J. Chem. Soc. Faraday Trans. 89, 2891–2900. https://doi.org/10.1039/FT9938902891

Donners, J.J.J.M., Nolte, R.J.M., Sommerdijk, N.A.J.M., 2002. A shape-persistent polymeric crystallization template for $CaCO_3$. J. Am. Chem. Soc. 124, 9700–9701. https://doi.org/10.1021/ja0267573

Dorozhkin, S. V., Epple, M., 2002. Biological and Medical Significance of Calcium Phosphates. Angew. Chem. Int. Ed. 41, 3130- 3146.

Feng, Q.L., 2011. Molecular Biomineralization. https://doi.org/10.1007/978-3-642-21230-7

Gaskin, D.J.H., Starck, K., Vulfson, E.N., 2000. Identification of inorganic crystal-specific sequences using phage display combinatorial library of short peptides: A feasibility study. Biotechnol. Lett. 22, 1211–1216. https://doi.org/10.1023/A:1005603117023

Gebauer, D., Verch, A., Börner, H.G., Cölfen, H., 2009. Influence of selected artificial peptides on calcium carbonate precipitation - A quantitative studyp. Cryst. Growth Des. 9, 2398–2403. https://doi.org/10.1021/cg801292p

Ghatak, A.S., Koch, M., Guth, C., Weiss, I.M., 2013. Peptide induced crystallization of calcium carbonate on wrinkle patterned substrate: Implications for chitin formation in molluscs. Int. J. Mol. Sci. 14, 11842–11860. https://doi.org/10.3390/ijms140611842

Hashimoto, M., Ikegami, T., Seino, S., Ohuchi, N., Fukada, H., Sugiyama, J., Shirakawa, M., Watanabe, T., 2000. Expression and Characterization of the Chitin-Binding Domain of Chitinase A1 from Bacillus circulans WL-12. J. Bacteriol. 182, 3045–3054. https://doi.org/10.1128/jb.182.11.3045-3054.2000

Honda, S., Kunii, T., Nohara, K., Wakita, S., Sugahara, Y., Kawakita, M., Oyama, F., Sakaguchi, M., 2017. Characterization of a Bacillus thuringiensis chitinase that binds to cellulose and chitin. AMB Express 7. https://doi.org/10.1186/s13568-017-0352-y

Iconomidou, V.A., Chryssikos, G.D., Gionis, V., Willis, J.H., Hamodrakas, S.J., 2001. "Soft"-cuticle protein secondary structure as revealed by FT-Raman, ATR FT-IR and CD spectroscopy. Insect Biochem. Mol. Biol. 31, 877–885. https://doi.org/10.1016/S0965-1748(01)00033-9

Ikegami, T., Okada, T., Hashimoto, M., Seino, S., Watanabe, T., Shirakawa, M., 2000. Solution structure of the fibronectin type III domain from Bacillus circulans WL-12 chitinase A1. J. Biol. Chem. 275, 13654–13661. https://doi.org/10.1074/jbc.M109726200

Inoue, H., Ozaki, N., Nagasawa, H., 2001. Purification and structural determination of a phosphorylated peptide with anti-calcification and chitin binding activities in the exoskeleton of the crayfish, procambarus clarkii 65, 1840–1848.

Jackson, A.P., Vincent, J.F.V., Turner, R.M., 1990. Comparison of nacre with other ceramic composites. J. Mater. Sci. 25, 3173–3178. https://doi.org/10.1007/BF00587670

Jain, G., Pendola, M., Huang, Y.C., Gebauer, D., Evans, J.S., 2017. A Model Sea Urchin Spicule Matrix Protein, rSpSM50, Is a Hydrogelator That Modifies and Organizes the Mineralization Process. Biochemistry 56, 2663–2675. https://doi.org/10.1021/acs.biochem.7b00083

Johnson, A.K., Zawadzka, A.M., Deobald, L.A., Crawford, R.L., Paszczynski, A.J., 2008. Novel method for immobilization of enzymes to magnetic nanoparticles. J. Nanoparticle Res. 10, 1009–1025. https://doi.org/10.1007/s11051-007-9332-5

Kumagai, H., Matsunaga, R., Nishimura, T., Yamamoto, Y., Kajiyama, S., Oaki, Y., Akaiwa, K., Inoue, H., Nagasawa, H., Tsumoto, K., Kato, T., 2012. CaCO 3/Chitin hybrids: Recombinant acidic peptides based on a peptide extracted from the exoskeleton of a crayfish controls the structures of the hybrids. Faraday Discuss. 159, 483–494. https://doi.org/10.1039/c2fd20057k

Lakshminarayanan, R., Kini, R.M., Valiyaveettil, S., 2002. Investigation of the role of ansocalcin in the biomineralization in goose eggshell matrix. Proc. Natl. Acad. Sci. 99, 5155–5159. https://doi.org/10.1073/pnas.072658899

Launey, M.E., Ritchie, R.O., 2009. On the fracture toughness of advanced materials. Adv. Mater. 21, 2103–2110. https://doi.org/10.1002/adma.200803322

Lobo, M.D.P., Silva, F.D.A., Landim, P.G. de C., da Cruz, P.R., de Brito, T.L., de Medeiros, S.C., Oliveira, J.T.A., Vasconcelos, I.M., Pereira, H.D.M., Grangeiro, T.B., 2013. Expression and efficient secretion of a functional chitinase from Chromobacterium violaceum in Escherichia coli. BMC Biotechnol. 13. https://doi.org/10.1186/1472-6750-13-46

Majorek, K.A., Porebski, P.J., Dayal, A., Zimmerman, M.D., Jablonska, K., Stewart, A.J., Chruszcz, M., Minor, W., 2012. Structural and immunologic characterization of bovine, horse, and rabbit serum albumins. Mol. Immunol. 52, 174–182. https://doi.org/10.1016/j.molimm.2012.05.011

Masica, D.L., Schrier, S.B., Specht, E.A., Gray, J.J., 2010. De novo design of peptide-calcite biomineralization systems. J. Am. Chem. Soc. 132, 12252–12262. https://doi.org/10.1021/ja1001086

Nawarathna, T.H.K., Nakashima, K., Fujita, M., Takatsu, M., Kawasaki, S., 2018. Effects of Cationic Polypeptide on CaCO 3 Crystallization and Sand Solidification by Microbial-Induced Carbonate Precipitation. ACS Sustain. Chem. Eng. 6, 10315–10322. https://doi.org/10.1021/acssuschemeng.8b01658

Nayebi, N., Cetinel, S., Omar, S.I., Tuszynski, J.A., Montemagno, C., 2017. A computational method for selecting short peptide sequences for inorganic material binding. Proteins Struct. Funct. Bioinforma. 85, 2024–2035. https://doi.org/10.1002/prot.25356

Neeraja, C., Moerschbacher, B., Podile, A.R., 2010. Fusion of cellulose binding domain to the catalytic domain improves the activity and conformational stability of chitinase in Bacillus licheniformis DSM13. Bioresour. Technol. 101, 3635–3641. https://doi.org/10.1016/j.biortech.2009.12.118

Nguyen, P.Q., Botyanszki, Z., Tay, P.K.R., Joshi, N.S., 2014. Programmable biofilm-based materials from engineered curli nanofibres. Nat. Commun. 5, 1–10. https://doi.org/10.1038/ncomms5945

Njegić Džakula, B., Falini, G., Kralj, D., 2018. Crystal Growth Mechanism of Vaterite in the Systems Containing Charged Synthetic Poly(Amino Acids). Croat. Chem. Acta. 90, 689–698. https://doi.org/10.5562/cca3290

Ping, H., Wan, Y., Xie, H., Xie, J., Wang, W., Wang, H., Munir, Z.A., Fu, Z., 2018. Organized Arrangement of Calcium Carbonate Crystals, Directed by a Rationally Designed Protein. Cryst. Growth Des. 18, 3576–3583. https://doi.org/10.1021/acs.cgd.8b00365

Raikhel, N. V, Lee, H.I., 1993. Structure and function of chitin-binding proteins. Annu. Rev. Plant Physiol. Plant Mol. Biol. 44, 591–615.

Rebers, J.E., Riddiford, L.M., 1988. Structure and expression of a Manduca sexta larval cuticle gene homologous to Drosophila cuticle genes. J. Mol. Biol. 203, 411–423. https://doi.org/10.1016/0022-2836(88)90009-5

Sarikaya, M., Tamerler, C., Jen, A.K., Schulten, K., Baneyx, F., 2003. Molecular biomimetics: nanotechnology through biology 25, 577–585. https://doi.org/10.1038/nmat964

Shimizu, K., Cha, J., Stucky, G.D., Morse, D.E., 2002. Silicatein : Cathepsin L-like protein in sponge biosilica. Proc. Natl. Acad. Sci. 95, 6234–6238. https://doi.org/10.1073/pnas.95.11.6234

Sommerdijk, N.A.J.M., de With, G., 2009. ChemInform Abstract: Biomimetic $CaCO_3$ Mineralization Using Designer Molecules and Interfaces . ChemInform. 40, 4499–4550. https://doi.org/10.1002/chin.200905231

Stephen Mann, 2001. Biomineralization, oxford university press.

Stephen, W., Lia, A., 1997. Design strategies in mineralized biological materials. J. Mater. Chem. 7, 689–702.

Sudo, S., Fujikawa, T., Ohkubo, T., Sakaguchi, K., Tanaka, M., Nakashima, K., 1996. Structures of mollusc shell framework proteins. Nature.387, 563–564.

Sugawara, A., Nishimura, T., Yamamoto, Y., Inoue, H., Nagasawa, H., Kato, T., 2006. Self-organization of oriented calcium carbonate/polymer composites: Effects of a matrix peptide isolated from the exoskeleton of a crayfish. Angew. Chemie - Int. Ed. 45, 2876–2879. https://doi.org/10.1002/anie.200503800

Sun, J., Bhushan, B., 2012. Hierarchical structure and mechanical properties of nacre: A review. RSC Adv. 2, 7617–7632. https://doi.org/10.1039/c2ra20218b

Svitii, A.L., Kirchman, D.L., 1998. A chitin-binding domain in a marine bacterial chitinase and other microbial chitinases : implications for the ecology and evolution of 1,4-glycanases. Microbilogy. 144,1299-1308.

Treccani, L., Mann, K., Heinemann, F., Fritz, M., 2006. Perlwapin, an abalone nacre protein with three four-disulfide core (whey acidic protein) domains, inhibits the growth of calcium carbonate crystals. Biophys. J. 91, 2601–2608. https://doi.org/10.1529/biophysj.106.086108

Vogt, S., Kelkenberg, M., Nöll, T., Steinhoff, B., Schönherr, H., Merzendorfer, H., Nöll, G., 2018. Rapid determination of binding parameters of chitin binding domains using chitin-coated quartz crystal microbalance sensor chips. Analyst. 143, 5255–5263. https://doi.org/10.1039/c8an01453a

Yang, H., Yao, W., Yang, L., Ma, X., Wang, H., Ye, F., Wong, K., 2009. The self-assembly of CaCO3 crystals in the presence of protein. J. Cryst. Growth. 311, 2682–2688. https://doi.org/10.1016/j.jcrysgro.2009.02.049

Yao, C.L., Xu, W.H., Ding, A.M., Zhu, J.M., 2009. Sucrose/bovine serum albumin mediated biomimetie crystallization of calcium carbonate. J. Chem. Sci. 121, 89–93. https://doi.org/10.1007/s12039-009-0010-2

Yao, Y., Dong, W., Zhu, S., Yu, X., Yan, D., 2009. Novel morphology of calcium carbonate controlled by poly(L-lysine). Langmuir. 25, 13238–13243. https://doi.org/10.1021/la901913d

Zhang, Y., Zheng, F., Yang, T., Zhou, W., Liu, Y., Man, N., Zhang, L., Jin, N., Dou, Q., Zhang, Y., Li, Z., Wen, L.P., 2012. Tuning the autophagy-inducing activity of lanthanide-based nanocrystals through specific surface-coating peptides. Nat. Mater. 11, 817–826. https://doi.org/10.1038/nmat3363

Zhu, W.K., Luo, X.G., Luo, A.K., Liang, X., 2010. Synthesis and Characterization of Dumbbell Shaped Calcium Carbonate Induced by Lignin. Mater. Sci. Forum. 658, 49–52. https://doi.org/10.4028/www.scientific.net/msf.658.49

Zou, Z., Bertinetti, L., Politi, Y., Fratzl, P., Habraken, W.J.E.M., 2017. Control of Polymorph Selection in Amorphous Calcium Carbonate Crystallization by Poly(Aspartic Acid): Two Different Mechanisms. Small. 13, 1–11. https://doi.org/10.1002/smll.201603100

CHAPTER 5. CONCLUSIONS AND FUTURE PROSPECTS

In this thesis, I examined the improvement of the efficiency of the urease-based biomineralization by using biomacromolecules. Effects of the biomacromolecules, such as polypeptides, polysaccharides and proteins on the $CaCO_3$ formation and sand solidification was examined by using the microbial-induced carbonate precipitation (MICP) and enzyme-induced carbonate precipitation (EICP) methods. Also, novel fusion protein was developed to facilitate organic-matrix mediated biomineralization.

Effects of the synthetic cationic and anionic polypeptides on the $CaCO_3$ formation and the sand solidification were examined in MICP method, where poly-L-lysine and poly-glutamate were used as a cationic and an anionic polypeptide, respectively. The results revealed that, poly-L-lysine had positive effect on the $CaCO_3$ formation while no significant effect was found by poly-glutamate addition. Electrostatic interaction between positively charged poly-L-lysine and negatively charged HCO_3^- ions would lead to the enrichment of HCO_3^- ions in local regions, resulting in $CaCO_3$ crystal nucleation and growth. Also, poly-L-lysine changed the morphology of $CaCO_3$ crystals into ellipsoidal shaped calcite crystals while rhombohedral or polyhedron shaped calcite crystals were dominant without additives. Morphology change would be mainly due to the change in the conformation of poly-L-lysine chain from random coil to α-helix under alkaline condition. Poly-glutamate promoted the formation and stabilization of metastable vaterite crystals due to higher local supersaturation of Ca^{2+} ions induced by negatively charged carboxyl group in the poly-glutamate.

Sand solidification experiments were conducted with and without poly-L-lysine under different bacteria injection intervals. Higher unconfined compressive strength (UCS) was achieved by reinjection of the bacteria than that of the injection once. Reinjection of the bacteria was found to be useful to maintain higher urease activity during the experimental time for better cementation. By adding poly-L-lysine, higher UCS value was achieved than that of without poly-L-lysine. 30% of strength increment was achieved for the top of the sample by introducing poly-L-lysine than the conventional method. Positively charged poly-L-lysine could have assisted the formation of the better bridge between sand particles and cell surface, both of which are negatively charged. Also, higher $CaCO_3$ formation efficiency and the change of the morphology would be a reason for the better cementation obtained with poly-L-lysine.

Although, poly-L-lysine has better ability to perform well in both of the $CaCO_3$ formation and sand solidification, use it for field applications is not practical due to associated

higher cost. Hence, next attempt was initiated by introducing natural biopolymer as an alternative.

In Chapter 3, effects of the natural biopolymer on the $CaCO_3$ formation and the sand solidification was examined by using MICP method. Chitosan was selected for the experiments since it is a one of the most abundant natural polysaccharide. Higher amount of precipitate was obtained by adding chitosan than that of without chitosan. Precipitate with chitosan has both of precipitated $CaCO_3$ and the precipitated chitosan hydrogel. Chitosan has a capability to form its hydrogel under the alkaline condition. Hence, weak alkaline condition created by the hydrolysis of urea provide a favorable environment for the chitosan to form its hydrogel. At lower cell concentrations, good rhombohedral crystals were obtained with the individual chitosan hydrogel while at higher cell concentrations, distorted shaped calcite crystals were formed with the rough surface. Chitosan has a better capability to make complexes with certain metal ions by sorption and chelation. Ca^{2+} can absorb into the chitosan hydrogel by hard acid-hard base reaction and provide nucleation sites for $CaCO_3$ crystals to nucleate and growth. Binding of the -OH and $-NH_2$ functional groups of the chitosan on to the surface of the crystals increased the roughness of the crystal surface. Sand solidification experiments were conducted by adding chitosan under different experimental conditions. By adding chitosan, strongly cemented sand specimen could be obtained with 38% of strength increment at the top of the sample. Chitosan hydrogel would assist the formation of a better bridge between sand particles leading to better cementation. Chitosan can be used as an additive to enhance the performance of MICP process more sustainably and produce organic-inorganic green materials for certain industrial application.

In Chapter 2 and Chapter 3, we investigated the effects of biomacromolecules on the $CaCO_3$ crystallization and identified the superior ability of the biomacromolecules on the $CaCO_3$ crystallization and the change the morphology, polymorphism and physical properties. Hence, next we took an attempt to develop a genetically modified protein to facilitate organic-inorganic hybrid material formation which is described in Chapter 4. Novel fusion protein (CaBP-ChBD) was designed for efficient precipitation of $CaCO_3$ on chitin matrix by introducing calcium binding peptide (CaBP) into chitin binding domain (ChBD). Target gene for the CaBP-ChBD was successfully constructed and expressed in *E.coli*. According to the results of the chitin binding assay, 80% of the CaBP-ChBD was bound to the insoluble chitin within 3 hours. $CaCO_3$ precipitation experiments were conducted by hydrolysis of urea using extracted jack bean urease with and without addition of chitin and CaBP-ChBD. Small increment of the precipitate could be found by adding chitin while significant increment (55%)

of the precipitate was achieved by adding both of chitin and CaBP-ChBD. In the presence of the CaBP-ChBD, morphology of the crystals changed drastically into the dumbbell and ellipsoidal shape crystals while without CaBP-ChBD rhombohedral and polyhedron crystals were present. Also, with CaBP-ChBD chitin particles were completely covered with the $CaCO_3$ crystals while without CaBP-ChBD few rhombohedral particles can be seen on the chitin matrix.

In addition, we found that CaBP-ChBD has capability to upgrade the $CaCO_3$ formation efficiency even without chitin. Presence of the basic amino acid residues such as lysine, histidine and arginine in CaBP and also in the ChBD would facilitate efficient $CaCO_3$ formation. In addition, negative charge of the carboxylic groups of the glutamic and aspartic acid residues under alkaline condition would have considerable impact on the morphology of the crystal. Interestingly, we found that ChBD itself has an ability to upgrade the $CaCO_3$ formation. By adding ChBD, $CaCO_3$ formation efficiency was increased by 25%. Associated basic and the acid amino acid residues in the ChBD would be a reason for its ability to upgrade $CaCO_3$ formation. However, influence of the CaBP on the $CaCO_3$ crystallization is not significant as like CaBP-ChBD or ChBD. Only 18 % of increment could be achieved by adding CaBP.

Finally, generated recombinant protein (CaBP-ChBD) could be used to formation of organic-inorganic hybrid materials by efficient precipitation of the $CaCO_3$ on the chitin matrix which will be useful for number of industrial applications including geotechnical and biomedical engineering applications.

Future prospects

We found that cationic polypeptide has positive effect on the $CaCO_3$ crystallization while anionic polypeptide has negative effect. However, the effect would be depended on the type of the amino acid. Hence, further investigation of the effects of polypeptides by using other cationic and anionic polypeptides such as poly arginine, histidine and poly aspartic would be important.

Chitosan exhibited excellent performance in $CaCO_3$ crystallization as well as sand solidification. We have some suggestions for further improve the efficiency of the $CaCO_3$ crystallization. Generally, organic matrix play a vital role in $CaCO_3$ biomineralization. Deposition of $CaCO_3$ on the insoluble organic matrix is associated with the soluble acidic proteins or silk fibroin-like proteins. As an example in nacre, $CaCO_3$ is deposited on the chitin matrix with the assistance of silk fibroin like protein. Hence, further investigation about the

effect of the chitosan/chitin on the $CaCO_3$ crystallization by incorporating a water soluble acidic protein would be interesting. It would be helped to efficient precipitation of $CaCO_3$ on the chitin/chitosan matrix.

Also, biopolymers are biodegradable. Therefore, durability of the polymer treated soil should be investigated in term of dry and wet conditions.

Further, we developed a novel fusion protein to facilitate organic-inorganic hybrid material formation and we found that it has capability to efficient precipitation of $CaCO_3$ on the chitin matrix. We have some suggestions for further improvement. As mentioned earlier, deposition of the $CaCO_3$ on the insoluble organic matrix is mainly associated with the soluble acidic protein or silk fibroin like protein. Hence, incorporate silk fibroin like protein in between the CaBP and ChBD would be helped to efficient organic-inorganic hybrid material formation. Further, in nature biomineralization mostly associated with the aragonite crystals and it contributed to gain higher strength for the structure of the organisms. Hence, replace the CaBP with aragonite binding peptide would be produced hybrid material with higher mechanical strength. As final goal, investigate the effect of the fusion protein (CaBP-ChBD) on sand solidification by using extracted urease as well as microbial urease would be more interesting approach.

Appendix A

Effects of the poly-L-lysine on the $CaCO_3$ crystallization using jack bean urease

Effect of urease concentration on the $CaCO_3$ precipitation with and without poly-L-lysine

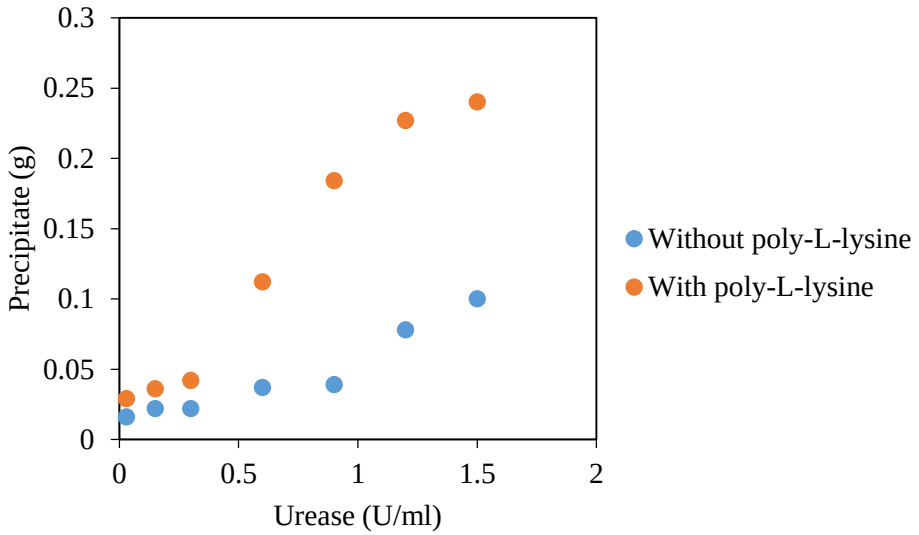

Figure 1: Variation of the amount of precipitate with the urease concentration with (10 mg/L) and without poly-L-lysine

Morphology change of the crystals with the urease concentration without poly-L-lysine

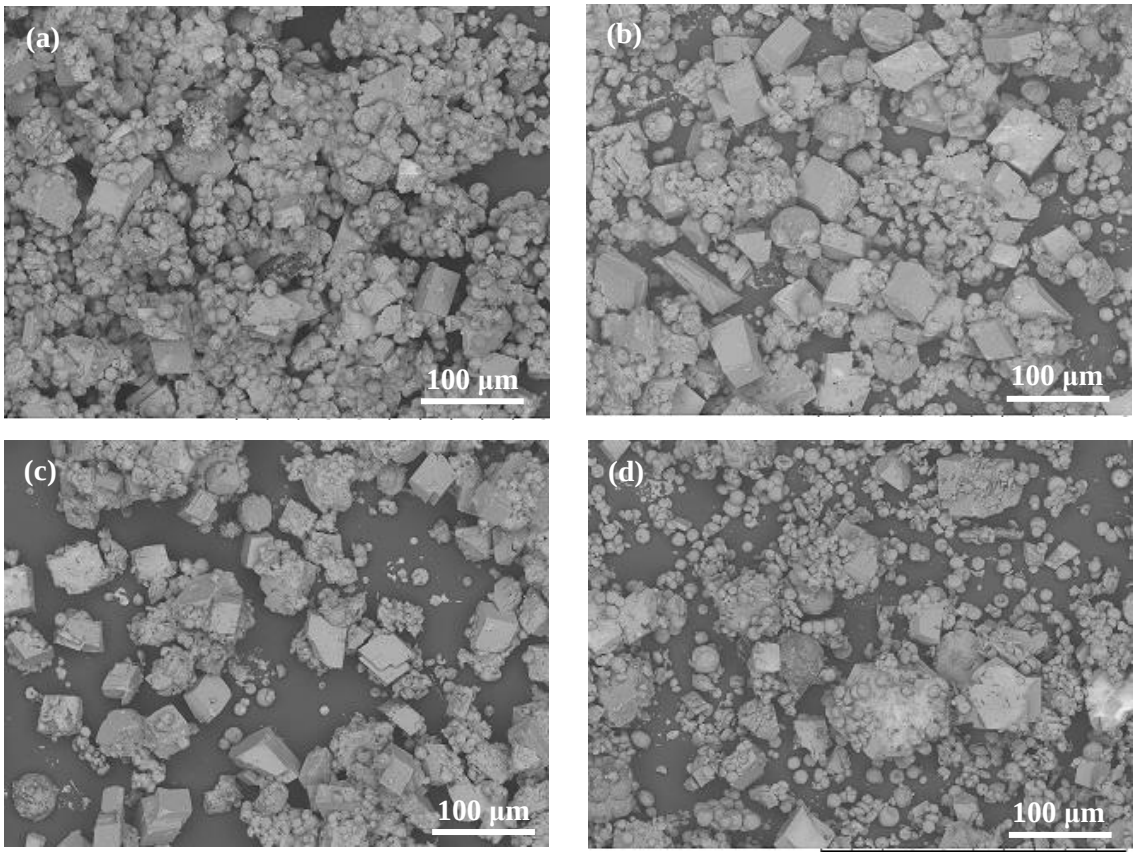

Figure 2: SEM images of $CaCO_3$ precipitates at various urease concentrations without poly-L-lysine: (a) 0.6 U/ml, (b) 0.9 U/ml, (c) 1.2 U/ml, and (d) 1.5 U/ml.

XRD Analysis

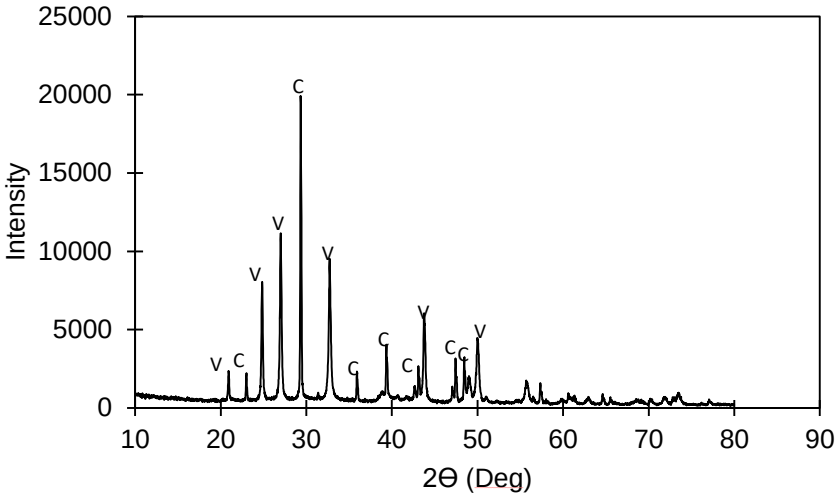

Figure 3: XRD pattern of the $CaCO_3$ precipitate obtained using jack bean

Morphology change of the crystals with the urease concentration with poly-L-lysine

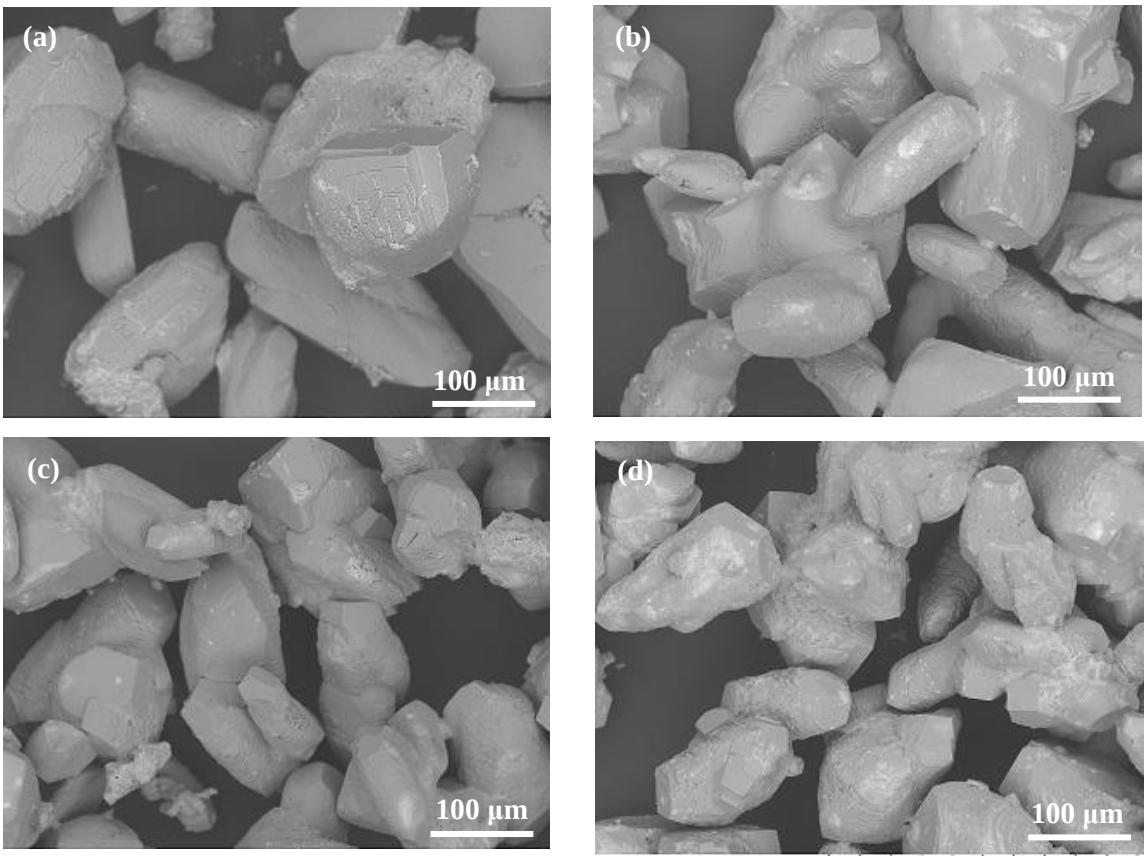

Figure 4: SEM images of $CaCO_3$ precipitates at various urease concentrations with poly-L-lysine (10 mg/l): (a) 0.6 U/ml, (b) 0.9 U/ml, (c) 1.2 U/ml, and (d) 1.5 U/ml.

Effect of the poly-L-lysine concentration on the $CaCO_3$ crystallization

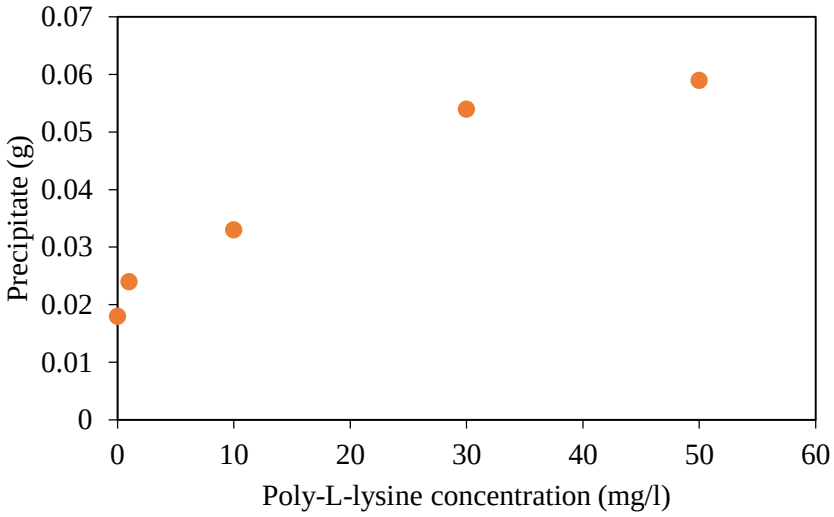

Figure 5: Variation of the amount of precipitate with the poly-L-lysine concentration (urease concentration-0.3U/ml)

Morphology change of the crystals with the poly-L-lysine concentration

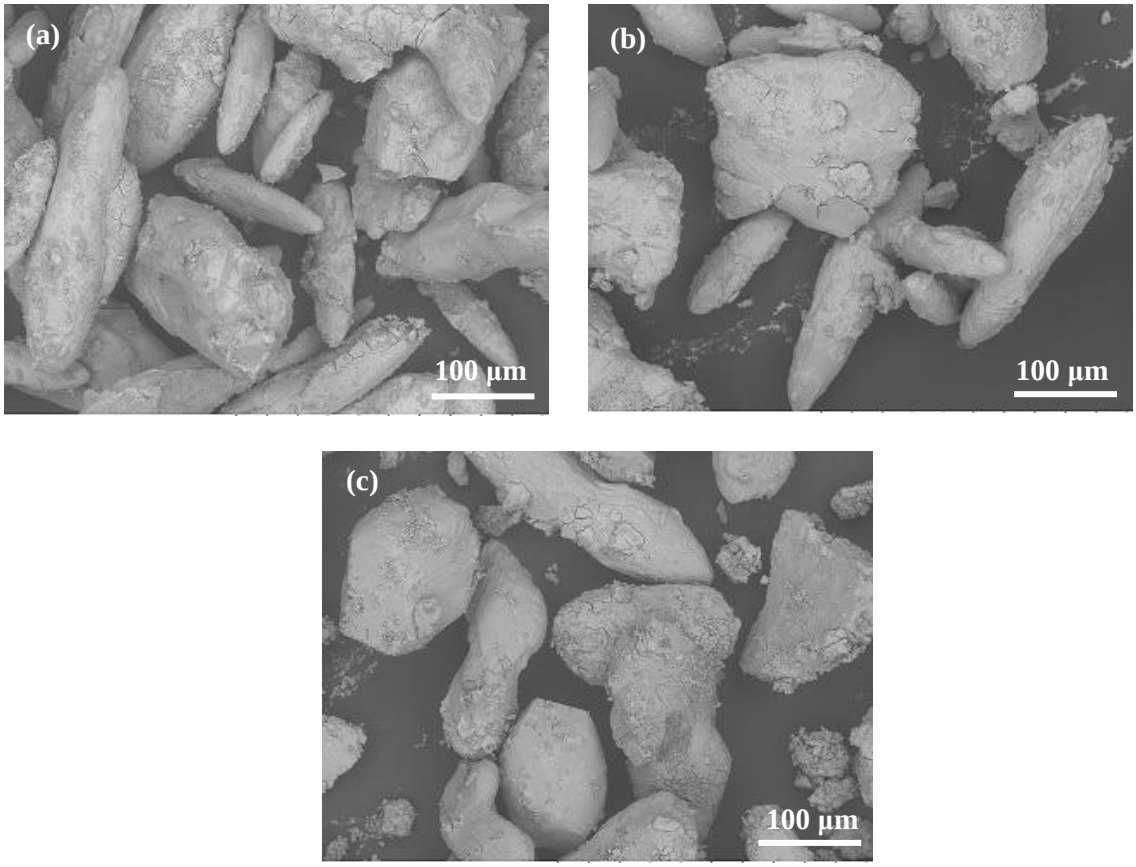

Figure 6: SEM images of $CaCO_3$ precipitates at poly-L-lysine concentrations (a) 10 mg/l, (b) 30 mg/l (c) 50 mg/l

Appendix B

Effects of the poly-glutamate on the $CaCO_3$ crystallization using jack bean urease

Effect of urease concentration on the $CaCO_3$ precipitation with and without poly-glutamate

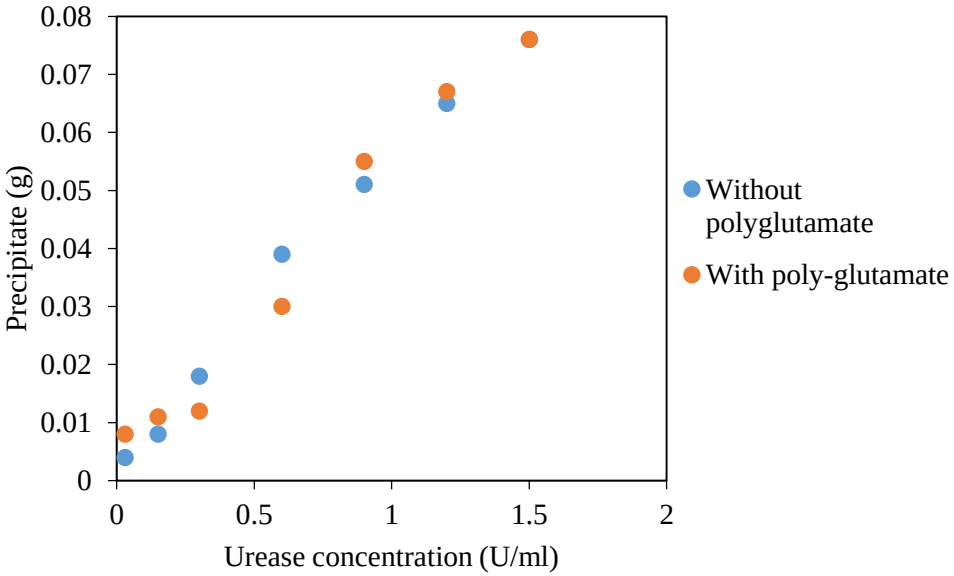

Figure 1: Variation of the amount of precipitate with the urease concentration with (10 mg/L) and without poly-glutamate

Morphology change of the crystals with the urease concentration with poly-glutamate

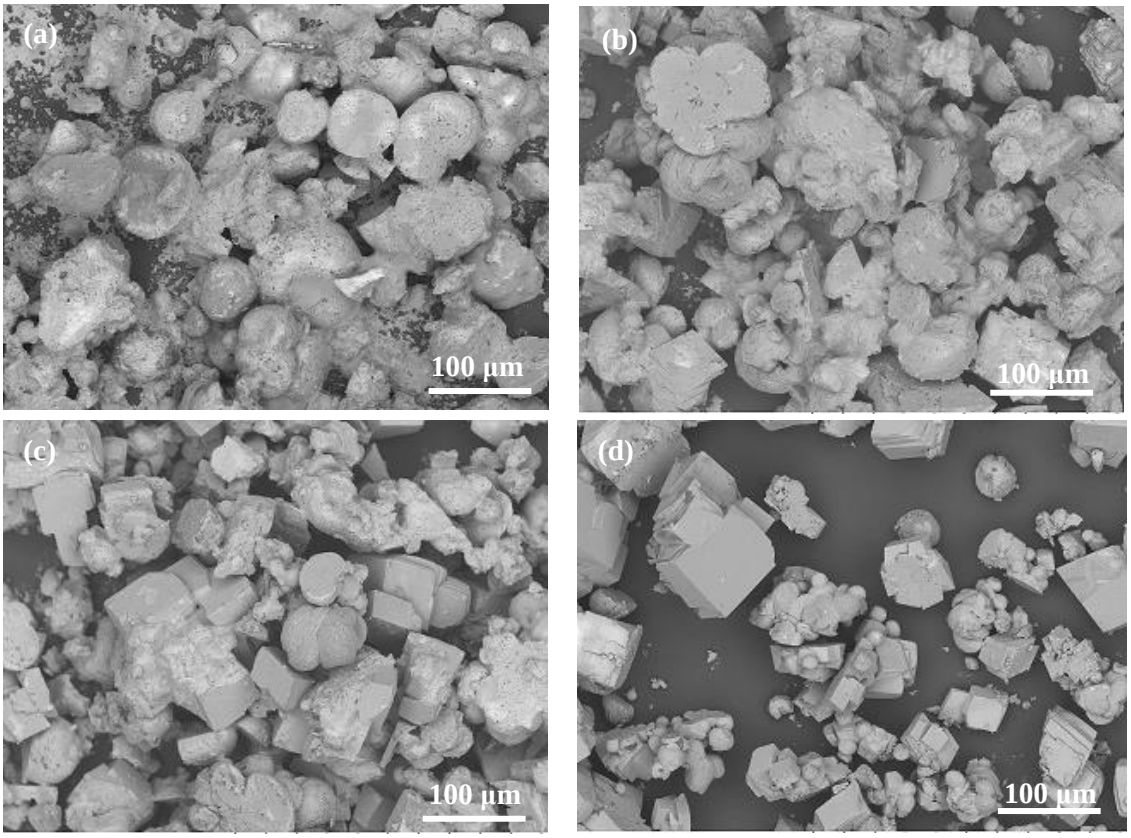

Figure 2: SEM images of $CaCO_3$ precipitates at various urease concentrations with poly-glutamate (10 mg/l): (a) 0.6 U/ml, (b) 0.9 U/ml, (c) 1.2 U/ml, and (d) 1.5 U/ml.

Effect of the poly-glutamate concentration on the $CaCO_3$ crystallization

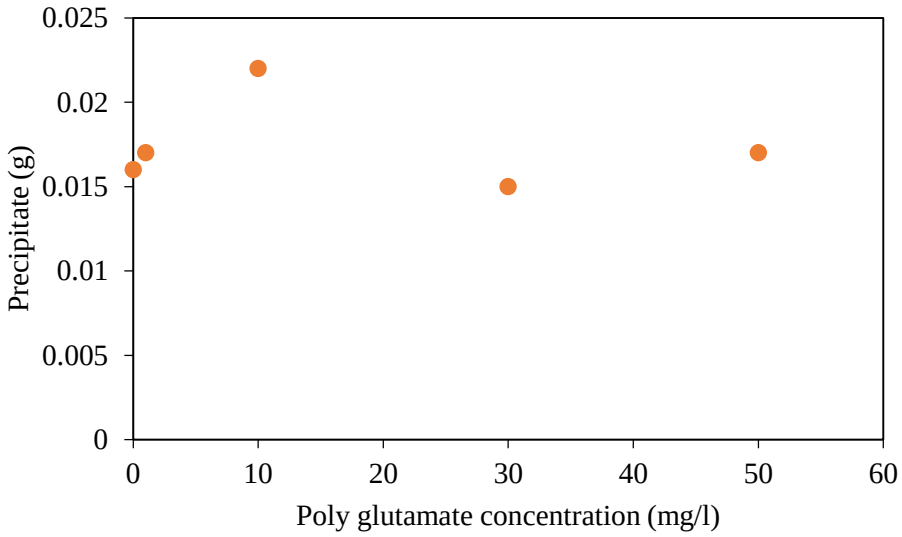

Figure 3: Variation of the amount of precipitate with the poly-glutamate concentration (urease concentration-0.3U/ml)

Appendix C

Effects of the chitosan on the $CaCO_3$ crystallization using jack bean urease

Effect of urease concentration on the $CaCO_3$ precipitation with and without chitosan

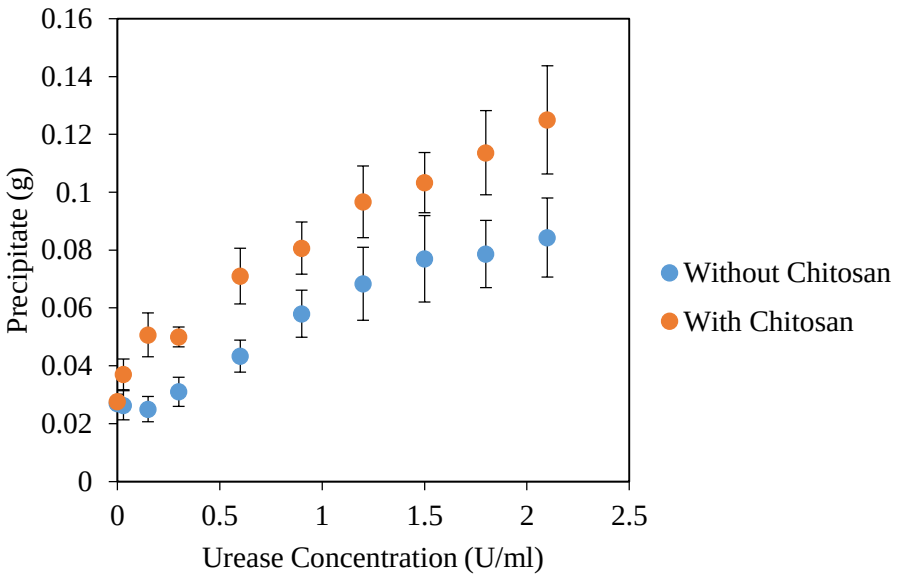

Figure 1: Variation of the amount of precipitate with the urease concentration with (0.03 %) and without chitosan

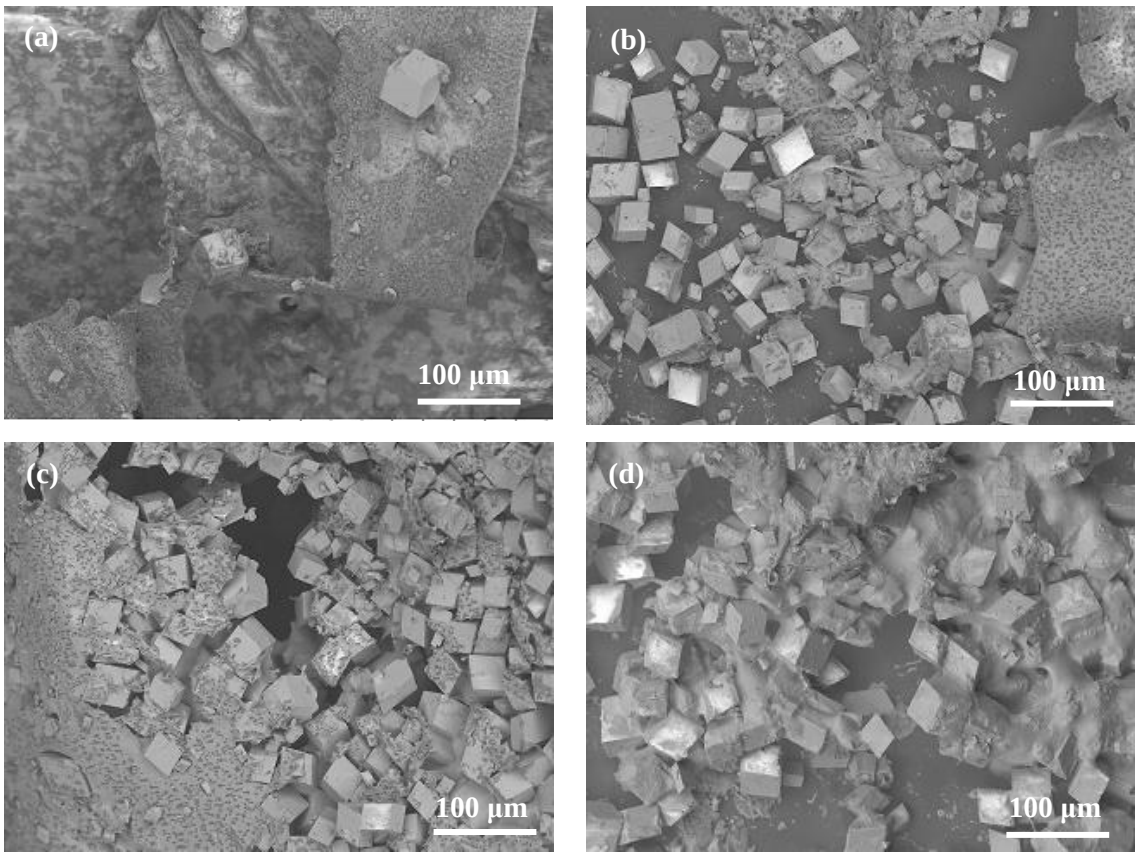

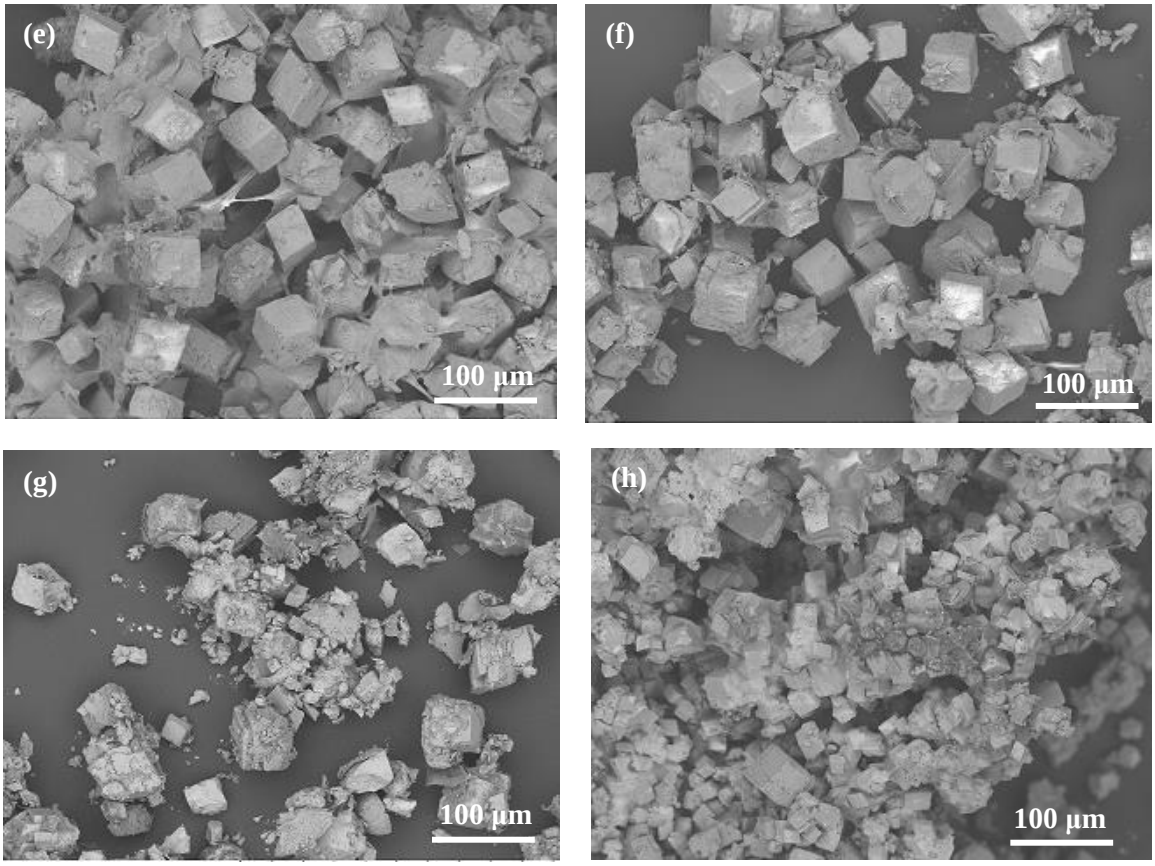

Figure 2: SEM images of $CaCO_3$ precipitates at various urease concentrations with chitosan (0.03 %): (a) 0.03, (b) 0.15 U/ml, (c) 0.3 U/ml, (d) 0.6 U/ml, (e) 0.9 U/ml, (f) 1.2 U/ml (g) 1.5 U/ml (h) 2.1 U/ml

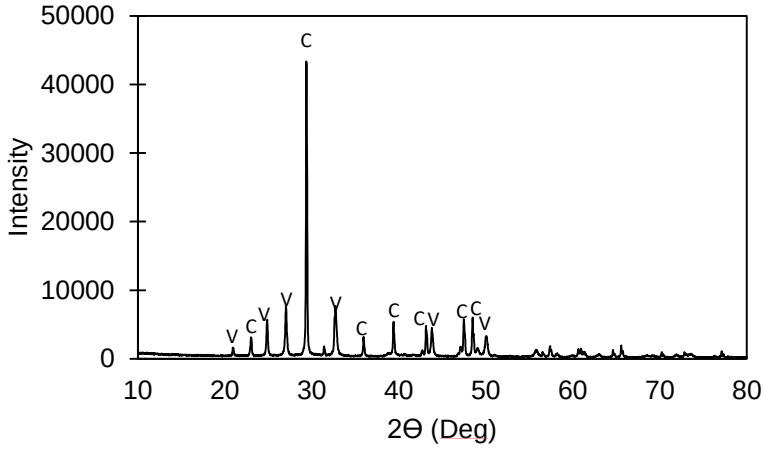

Figure 3: XRD pattern of the $CaCO_3$ precipitate obtained using jack bean urease with chitosan

Effect of the chitosan concentration on the $CaCO_3$ crystallization

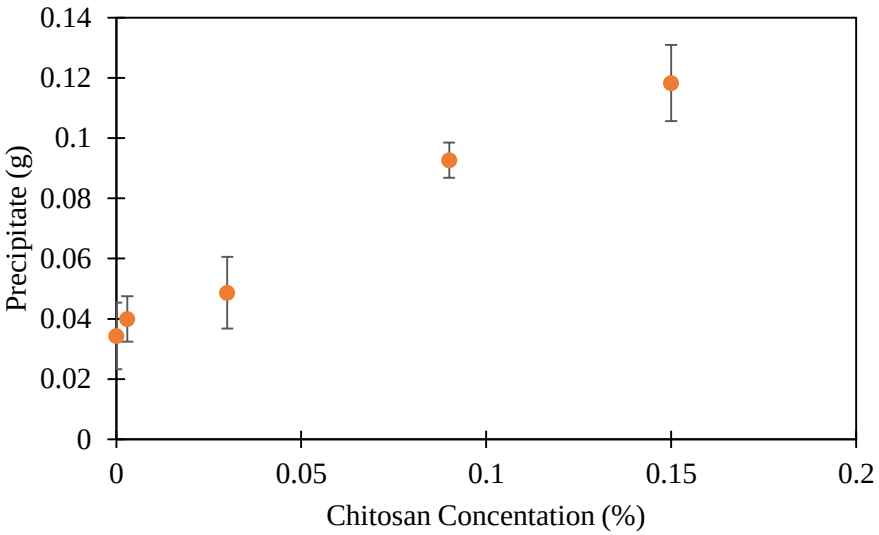

Figure 4: Variation of the amount of precipitate with the chitosan concentration (urease concentration-0.3U/ml)

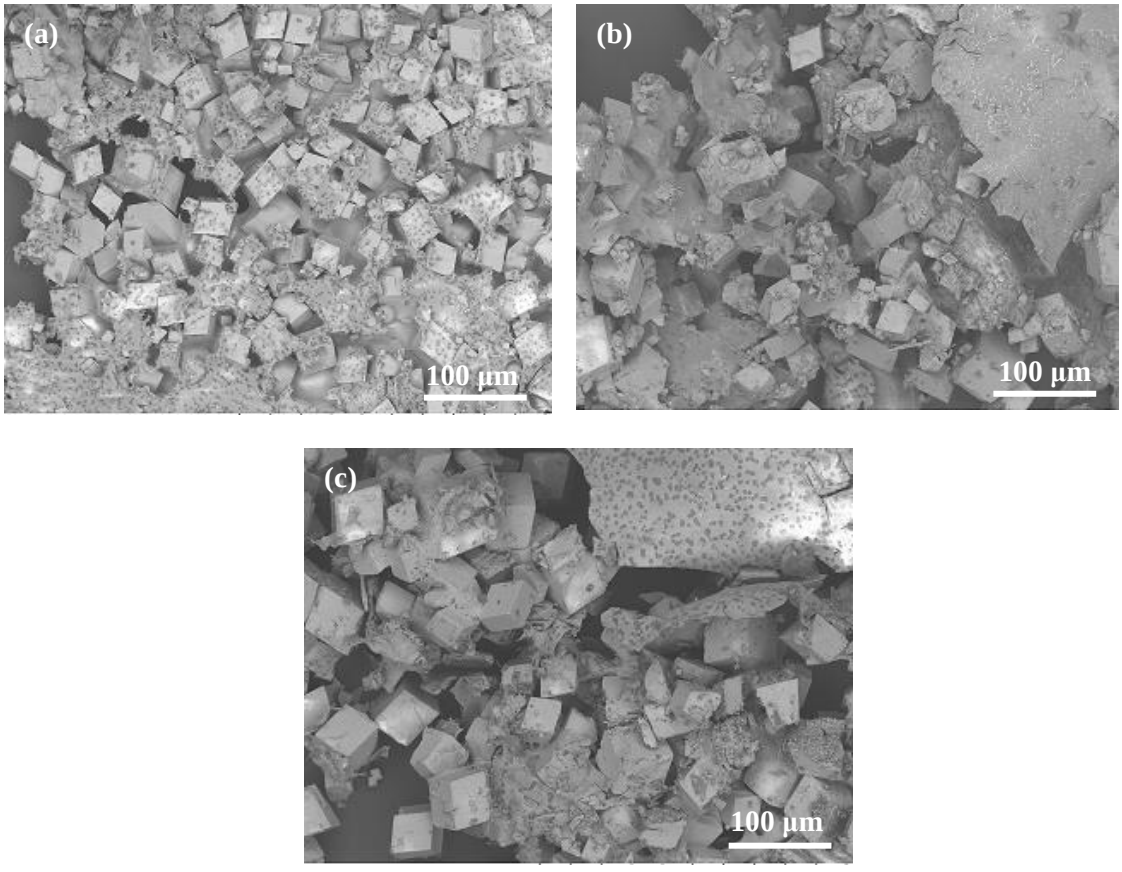

Figure 5: SEM images of $CaCO_3$ precipitates at chitosan concentrations (a) 0.03 %, (b) 0.09 %, (c) 0.15 %